University of Minnesota
ST. ANTHONY FALLS HYDRAULIC LABORATORY

Project Report No. 159

MODEL STUDIES OF THE BED REGIME OF ALLUVIAL CHANNELS AS INFLUENCED BY SUBMERGED GROINS

by

S. Dhamotharan
W. Q. Dahlin
and
J. M. Wetzel

Prepared for
ST. PAUL DISTRICT, CORPS OF ENGINEERS
Department of the Army

March 1976
Minneapolis, Minnesota

PREFACE

Existing experimental data have shown that submerged groins may be effective in controlling scour of river beds for the purpose of maintaining required water depths for navigation. A particular advantage of the submerged as compared to the unsubmerged contraction is the capability of inducing scour at the lower discharges and water depths when it is needed, and reducing scour at the higher discharges and water depths when it is not needed. Results of previous tests conducted at the St. Anthony Falls Hydraulic Laboratory with a parallel wall submerged contraction have indicated reasonable agreement between experimental data and theory. The present studies were carried out in a larger scale facility with various submerged groin geometries, including the parallel wall contraction. The basic investigation was initiated to further establish the validity of the theoretical equations and to evaluate the overall performance of the various groin configurations in providing the desired bed profile.

The study was supported by the St. Paul District, Corps of Engineers, Department of the Army under Contract No. DACW 37-75-C-0212. Mr. Helmer Johnson of the St. Paul District served as the contract monitor.

The project was instigated by the late Dr. Alvin G. Anderson, who was the principal investigator until his death early in the planning stages of the program. His concepts and details of the tests were subsequently carried out under the supervision of Mr. W. Q. Dahlin and Mr. J. M. Wetzel. Mr. Sundararajan Dhamotharan was responsible for conducting the model tests and the data analysis with the assistance of Mr. Bruce Haverly and Mr. Daniel Johnson.

ABSTRACT

Experimental studies were conducted in a straight reach of rectangular channel to determine the dynamic equilibrium depth of scour associated with submerged constrictions or groins. Tests were carried out with various groin geometries in both rigid- and movable-bed models. Velocity traverses were made over the groins and in the constricted region to establish the relationship between the ratio of discharge through the constriction to the total discharge and the relative groin submergence and geometry. Measurements of the eroded bed profile in the constricted region indicated that the equilibrium relative depth of scour was related primarily to the discharge ratio and the constriction ratio. All groin geometries tested demonstrated the capability of providing relatively large scour depths at low stages, and less scour depths at high stages for which a larger portion of the total discharge passed over the groins. Reasonable agreement with predicted relative scour depths was noted for relatively large sediment transport rates.

TABLE OF CONTENTS

LIST OF TABLES

LIST OF PHOTOS

PHOTO 18 (Ser. No. 243-85) Rigid-bed, Type A7, Run No. 36, Q = 40 lps, D_1 = 15 cm, Surface flow pattern.

PHOTO 19 (Ser. No. 243-120) Movable-bed, Type A4, Run No. 110, Q = 75 lps, D_1 = 15 cm, Surface flow pattern.

PHOTO 20 (Ser. No. 243-122) Movable-bed, Type A4, Run No. 110, Q = 75 lps, D_1 = 15 cm, Final erosion pattern.

PHOTO 21 (Ser. No. 243-117) Movable-bed, Type A4, Run No. 109, Q = 100 lps, D_1 = 20 cm, Surface flow pattern.

PHOTO 22 (Ser. No. 243-119) Movable-bed, Type A4, Run No. 109, Q = 100 lps, D_1 = 20 cm, Final erosion pattern.

PHOTO 23 (Ser. No. 243-114) Movable-bed, Type A4, Run No. 108, Q = 150 lps, D_1 = 30 cm, Surface flow pattern.

PHOTO 24 (Ser. No. 243-116) Movable-bed, Type A4, Run No. 108, Q = 150 lps, D_1 = 30 cm, Final erosion pattern.

PHOTO 25 (Ser. No. 243-123) Movable-bed, Type A4, Run No. 120, Q = 50 lps, D_1 = 9 cm, Surface flow pattern.

PHOTO 26 (Ser. No. 243-125) Movable-bed, Type A4, Run No. 120, Q = 50 lps, D_1 = 9 cm, Final erosion pattern.

PHOTO 27 (Ser. No. 243-111) Movable-bed, Type A3, Run No. 107, Q = 75 lps, D_1 = 15 cm, Surface flow pattern.

PHOTO 28 (Ser. No. 243-113) Movable-bed, Type A3, Run No. 107, Q = 75 lps, D_1 = 15 cm, Final erosion pattern.

PHOTO 29 (Ser. No. 243-131) Movable-bed, Type A5, Run No. 113, Q = 75 lps, D_1 = 15 cm, Surface flow pattern.

PHOTO 30 (Ser. No. 243-133) Movable-bed, Type A5, Run No. 113, Q = 75 lps, D_1 = 15 cm, Final erosion pattern.

PHOTO 31 (Ser. No. 243-140) Movable-bed, Type A6, Run No. 116, Q = 75 lps, D_1 = 15 cm, Surface flow pattern.

PHOTO 32 (Ser. No. 243-142) Movable-bed, Type A6, Run No. 116, Q = 75 lps, D_1 = 15 cm, Final erosion pattern.

PHOTO 33 (Ser. No. 243-149) Movable-bed, Type A7, Run No. 119, Q = 75 lps, D_1 = 15 cm, Surface flow pattern.

PHOTO 34 (Ser. No. 243-151) Movable-bed, Type A7, Run No. 119, Q = 75 lps, D_1 = 15 cm, Final erosion pattern.

PHOTO 35 (Ser. No. 243-153) Movable-bed, Type A7, Run No. 122, Q = 50 lps, D_1 = 9 cm, Surface flow pattern.

PHOTO 36 (Ser. No. 243-155) Movable-bed, Type A7, Run No. 122, Q = 50 lps, D_1 = 9 cm, Final erosion pattern.

LIST OF SYMBOLS

a	Constant dependent on U_{*1}/w
B_1	Upstream channel width
B_2	Constricted region channel width
c	Silt factor
d_{50}	Mean diameter of sediment
D_1	Upstream channel depth
D_2	Constricted region channel depth
D_3	Depth over constriction
D_m	Mean depth
D_s	Typical sediment grain diameter
f	Channel shape factor
g	Gravitational constant
G	Groin geometry factor
m	Constant dependent on critical tractive stress
n_0	Emperical constant
n_1	Manning's coefficient in upstream region
n_2	Manning's coefficient in constricted region
n_3	Manning's coefficient over constriction
P_i	Sediment factor
Q_1	Total discharge
Q_2	Discharge in constricted region
Q_3	Discharge over constriction
S_1	Upstream region bed slope
S_2	Constricted region bed slope

S_3	Slope over constriction
U_{*1}	Upstream region shear velocity
U_{*c}	Shear velocity based on τ_c
V_1	Mean velocity in upstream region
V_2	Mean velocity in constricted region
V_3	Mean velocity over constriction
w	Mean fall velocity of sediment
α	Constant
β	Constant
δ	Constant
θ	Constant dependent on τ_c/τ_1
λ	Constant
ν	Kinematic viscosity
ρ_s	Sediment density
ρ_f	Fluid density
σ	Standard deviation of sediment
τ_1	Mean upstream region shear stress
τ_2	Mean constricted region shear stress
τ_{b1}	Mean upstream region bed shear stress
τ_{b2}	Mean constricted region bed shear stress
τ_c	Critical tractive stress of sediment
ψ	Groin inclination angle

MODEL STUDIES OF THE BED REGIME OF ALLUVIAL CHANNELS AS INFLUENCED BY SUBMERGED GROINS

I. INTRODUCTION

One of the principal purposes for regulatory works in natural channels is to establish and maintain depths sufficiently great to permit barge and other traffic to be undertaken during low-water periods. Many such streams are characterized by bends with appreciable depths and connecting reaches or crossings with considerably smaller depths. Because of these smaller depths in crossings, navigation may be difficult during low-water periods. In order to maintain navigable depths throughout the navigation season, various measures, such as periodic dredging in critical areas or the conststruction of channel constrictions, have been introduced. Experience and the analysis of the transport characteristics of natural streams indicate that a single dredging operation is usually not sufficient, but that periodic dredging is necessary to maintain the channel. However, channel constrictions, whether combined with the dredging operation or not, have been effective in establishing and maintaining appropriate channel depths. Such constrictions often take the form of groins projecting out from the banks, or they may be a combination of groins and parallel works, particularly in bends, to control the flow pattern.

For an unsubmerged constriction, all the flow passes through the constriction with an increase in velocity and slope which erodes the bed to a lower elevation. At high flow rates, the resultant scour may be excessive. Anderson and Davenport [1]* have suggested that submerged constrictions would alleviate excessive scour, since for large discharges a considerable portion of the flow passes over the groins and thus does not contribute to the sediment transport capacity. Their laboratory studies for a particular parallel wall submerged constriction generally verified this conclusion. To further investigate the effectiveness of various submerged groin configurations in controlling bed erosion and to determine the validity of certain assumptions of their theoretical analysis, the present basic study was initiated. The

*Numbers in brackets refer to list of references on pages 32 and 33.

study consisted of a literature review followed by experimental tests with submerged groins in both rigid and movable bed models, and is described in the following sections.

II. LITERATURE REVIEW

Numerous experimental and analytical studies have been carried out on local erosion of sand beds around various types of flow obstructions such as bridge piers, spur dikes, etc. While data are available in the various published reports on erosion around bridge piers or similar structures, similar specific information is relatively scarce for erosion of a sand bed in the flow region constricted by groins or spurs.

The erodible bed material may be generally classified as 1) non-cohesive sediments and 2) cohesive sediments. As the term implies, non-cohesive sediments are those consisting of discrete particles, the movement of which, for given erosive forces, depends only on particle properties (e.g.) shape, size and density and on the relative position of the particle with respect to surrounding particles. Sand and gravel of stream beds or beaches that has been previously transported, or deposits laid down by wind or water may be included in this class. Cohesive sediments, on the other hand, are those for which the resistance to initial movement or erosion depends on the strength of the cohesive bond between particles. This resisting force may far outweigh the influence of the characteristics of the individual particles. This class includes soil containing clay as may be found in many residual soils. The property of cohesiveness as related to the erosion-resisting characteristics of a soil mass introduces a factor into the relationship between the erosive forces inherent in the flow and the physical properties of the soil particles that have not been evaluated. Because the forces required to erode or scour cohesive sediments are generally greater than those for non-cohesive sediments with approximately the same grain size, the rate and extent of the scour depends on this property rather than on the properties of the particles. Once the bond has been broken, the individual particles become a part of the non-cohesive population. Further deposition, scour, or transport becomes a function of the properties of these separate particles. The present study is concerned with non-cohesive sediments. Alluvial streams, which may be defined as those whose bed and banks are composed of materials such as clay, silt,

sand or gravel that has been transported by and deposited in water, typically exhibit the inherent property of meandering, with a series of bends and crossings. Bends are normally of appreciable depths followed by crossings of considerably lesser depths. Especially during low stages, the river engineer is confronted with the problem of maintaining a minimum navigation depth, particularly in the crossings. This is being accomplished now by dredging, along with some river training structures. Maintenance of navigation depth by dredging is obviously time consuming and expensive. Another current problem associated with dredging is its possible adverse effect on the environmental quality.

Channel constrictions are generally armoured rock structures projecting from the banks into the stream. Perusal of the literature reveals a variety of configurations of groin fields, such as normal to or angled upstream or downstream to the flow, L-shapes, parallel walls, or combinations of the above. These structures are also used for river training, channel stabilization, channel alignment, etc. In the following, some of the past attempts to describe the nature of flow through channel constrictions will be summarized.

The concept of increasing the depth of an alluvial stream by means of a long constriction was first introduced by Straub [2]. By combining the equation of continuity, Manning's formula, and DuBoy's sediment discharge equation, he obtained

$$\frac{D_2}{D_1} = \left(\frac{B_1}{B_2}\right)^{3/7} \left[\frac{-\left(\frac{\tau_c}{\tau_1}\right) + \left[\left(\frac{\tau_c}{\tau_1}\right)^2 + 4\left(1 - \frac{\tau_c}{\tau_1}\right)\left(\frac{B_1}{B_2}\right)\right]^{1/2}}{2(1 - \tau_c/\tau_1)}\right]^{3/7} \tag{1}$$

where D_1, D_2, B_1, and B_2 are the depths and widths of the unconstricted and constricted reaches as shown in Fig. 1. τ_1 is the average bed shear stress in the normal section and τ_c is the critical shear stress of the sediment.

As τ_c/τ_1 varies between the limits of zero and unity within the realm of dynamic equilibrium, Anderson [3] later expressed Eq. (1) as

$$\frac{D_2}{D_1} = \left(\frac{B_1}{B_2}\right)^{\theta} \qquad \frac{9}{14} \leq \theta \leq \frac{6}{7} \tag{2}$$

where θ is dependent on τ_o/τ_1.

The Kennedy formula for the non-silting, non-scouring velocity is

$$V = fc\, D_m^{\,n_o} \tag{3}$$

where f = channel shape factor
c = silt factor
D_m = mean flow depth
$n_o \approx 0.64$

Griffith [4], using the continuity equation and the above Kennedy equation, derived an expression for equilibrium depth of scour in a long constriction as

$$\frac{D_2}{D_1} = \left(\frac{B_1}{B_2}\right)^{\frac{1}{n_o+1}} \tag{4}$$

or with $n_o = 0.64$

$$\frac{D_2}{D_1} = \left(\frac{B_1}{B_2}\right)^{0.61} \tag{5}$$

Observation has indicated that n_o in Eq. (3) may vary from .44 to .73.

As part of an investigation primarily concerned with local scour around bridge piers, Laursen [5] also studied the scour associated with a long constriction. Using his own formula for sediment transportation, he developed a relation for equilibrium depth in long constrictions,

$$\frac{D_2}{D_1} = \left(\frac{B_1}{B_2}\right)^{\frac{6(2+a)}{7(3+a)}} \left(\frac{n_2}{n_1}\right)^{\frac{6a}{7(3+a)}} \tag{6}$$

bridge piers, used the following expression for bed load transport per unit width:

$$q_s = c\, q_{so}\left(\frac{\tau_1}{\tau_c} - 1\right)^{\delta}; \quad \frac{\tau_1}{\tau_c} - 1 = 0, \text{ for } \frac{\tau_1}{\tau_c} \leq 1 \tag{10}$$

where c = an empirical constant

$q_{so} = \sqrt{gRD_s^3}$

g = acceleration of gravity

R = sediment buoyancy factor = $\frac{\rho_s}{\rho_f} - 1$

D_s = grain size of bed material

ρ_s = density of bed material

ρ_f = density of fluid

δ = numerical exponent

For various values of δ, Eq. (10) reduces to well known bed load equations. For example, $\delta = 3$ results in a formula similar to that of Brown-Einstein, $\delta = 2.5$ gives the Brown-Kalinske formula, $\delta = 2$ gives an equation similar to DuBoys formula, and $\delta = 1.5$ yields an equation identical to the Meyer-Peter-Muller formula.

Using the above equation, he then derived a generalized equation for the equilibrium depth of scour,

$$\frac{D_2}{D_1} = \left(\frac{B_1}{B_2}\right)^{6/7}\left[\frac{1}{\left(\frac{B_1}{B_2}\right)^{1/\delta}\left(1 - \frac{\tau_c}{\tau_1}\right) + \frac{\tau_c}{\tau_1}}\right]^{3/7} \tag{11}$$

with $1 - \frac{\tau_c}{\tau_1} = 0$ for $\frac{\tau_c}{\tau_1} \geq 1$

or $$\frac{D_2}{D_1} = \left(\frac{B_1}{B_2}\right)^{\Theta}$$

where Θ is a variable exponent.

For very high rates of sediment transport, τ_c/τ_1 approaches zero, and for small rates of transport, τ_c/τ_1 approaches unity. It can readily be seen that for $\tau_c/\tau_1 = 1$, Θ attains an upper limit of 0.857. The lower limit for Θ at $\tau_c/\tau_1 = 0$ is dependent on δ, or as previously mentioned, on the particular bed load formula used. The variation of Θ as a function of τ_c/τ_1 is shown in Fig. 2 for the various bed load formulas.

All of the above equations for unsubmerged contractions indicate that for a given constriction ratio, the depth in the constriction, D_2, is essentially proportional to the normal depth, D_1, in the unconstricted region. Thus, as the discharge increases with a corresponding increase in D_1, D_2 also increases but at a faster rate which implies a continual lowering of the bed elevation. Excessive depths of scour may occur during high stages when large depths are not required for navigation purposes. This may lead to various problems such as increased deposition of sediment downstream and excessive local scour around groins which results in expensive structures.

To alleviate some of these problems, Anderson and Davenport [1] suggested that constrictions be designed so that they are submerged beyond a certain river stage. At this point no longer does all the flow pass through the constriction. Straub's Eq. (1) was then modified to account for the redistribution of flow as

$$\frac{D_2}{D_1} = \left(\frac{Q_2}{Q_1}\right)^{6/7} \left(\frac{B_1}{B_2}\right)^{3/7} \left[\frac{-\frac{\tau_c}{\tau_1} + \left[\left(\frac{\tau_c}{\tau_1}\right)^2 + 4\frac{B_1}{B_2}\left(1 - \frac{\tau_c}{\tau_1}\right)\right]^{1/2}}{2(1 - \tau_c/\tau_1)} \right]^{3/7} \tag{12}$$

or, by rewriting the equation in a form similar to Eq. 2,

$$\frac{D_2}{D_1} = \left(\frac{Q_2}{Q_1}\right)^{6/7} \left(\frac{B_1}{B_2}\right)^{\Theta} \tag{13}$$

and for $\tau_c/\tau_1 \to 0$, $\Theta = 0.64$

The above method of analysis relating to submerged constrictions has been postulated to offer the following potential advantages:

1. It will aid in the design of groins and dikes built to accomplish prescribed control functions.
2. The increased depths required for navigation during low water periods can be obtained without seriously influencing the flow at high or flood discharges.
3. Scour within the constriction during highwater periods will be reduced, with a consequent saving in quantity of material required for groin construction.
4. The original bed regime will suffer only minor readjustment.
5. The application of such a groin system will reduce the amount of dredging necessary to maintain navigation depths during low water periods.

Numerous model studies pertaining to river control structures have been conducted at various laboratories. Investigations with hydraulic models of natural streams have revealed some of the basic factors affecting the development of channel configurations and have pointed out some of the characteristics of structures affecting their performance in these streams. Most studies of this type have been concerned mainly with specific problems in specific reaches, and were not sufficiently broad in scope to permit the development of basic information applicable to streams in general. The Task Committee on Channel Stabilization (8), while sharing the views of the river engineers charged with the responsibility of river control that the solution to problems remaining unsolved must be sought principally in the river or stream under study, has rightly pointed out that laboratory studies have made material contributions to the solution of such problems in the past and engineers should not overlook these valuable aids when attacking river control problems in the future. Although caution should be exercised in accepting quantitive results, the trends indicated in the models will provide valuable information that can not be derived either from existing theory or from the precedent of past experience.

Franco and McKellar [9], in their model studies for a specific reach of the Arkansas River, reported that low spur groins would be effective in increasing depths over crossings but could produce considerable backwater effect

and shoaling upstream of the groins. Longitudinal groins would also be effective to some extent in deepening the channel over the crossings.

In another study, Franco [10] has concluded that 1) there is a greater tendency for dikes angled downstream to be flanked near the bank end than dikes angled upstream, and 2) level crest dikes should be placed normal to the flow or angled downstream.

Linder [11] et. al. have carried out laboratory investigations of L-type groins. Their conclusions were:

1. A minimum of 50 percent of the opening between spur dikes should be enclosed by L-type extensions.
2. Very little benefit was derived by extending the constriction above the water surface.
3. Dike spacing is an independent design consideration for each bend and although greatly influenced by the bend curvature, individual dike spacings are determined from the interrelationship of the upstream and downstream control requirements necessary to develop an integrated channel control network. This results in variable dike spacing within a control system as well as between bends.

The Central Water and Power Research Station [12, 13], after some preliminary study, has reported that 1) from the point of view of the extent of the scour hole and maximum scour near the nose, a downstream angled spur is better than one angled upstream, 2) there will be a limiting extent of scour in each case, and 3) the rate of scour will decrease with increase in flow section.

The following general conclusions can be drawn from the results of the literature search:

1. The constriction ratio, B_1/B_2, is one of the most important variables.
2. Groins angled downstream to the flow are better than those angled upstream.
3. For L-type groins, 50 percent closure of the longitudinal distance between two groins by an L-type extension is the most efficient.
4. The spacing between two groins and their angle of inclination to the flow are mostly dependent on the individual site conditions and requirements.

5. The hydraulic conditions imposed on the system affect the equilibrium depth scour. This is reflected by the shear ratio in Straub's formula, the 'a' factor in Laursen's formula, the exponent Θ in Anderson's modification of Straub's formula, and bed shear ratio in Komura's formula.

6. The characteristics of the sediment also affect the depth of scour. These characteristics include a representative grain diameter, specific gravity, particle shape and standard deviation and are usually combined into one variable τ_c, the critical shear stress.

7. For submerged groins with a given constriction ratio, the equilibrium depth of scour ratio, D_2/D_1, can be varied by changing the extent to which the constriction is submerged.

8. When properly trained and fixed in place, the stream can be relied on to scour a channel that will maintain the proper depth for navigation.

III. APPLICATION TO PRESENT STUDY

There are generally three factors which may lead to a change of bed elevation in the region of any type of river control structures, which require consideration during design.

1. There may be progressive aggradation or degradation of bed levels associated with a change in river regime.

2. There may be temporary erosion associated with changes in river stage, or with shifting of the deep water channel.

3. The presence of the constriction structure may cause erosion.

Since the three causes of scour result from different phenomena, it is, to the best knowledge of the authors, difficult to find a single solution to estimate the bed erosion due to their combined effect.

The hydraulic design of unsubmerged constrictions, which is based upon the idea of forcing the entire flow through a constricted width so as to increase the shear stress in the constricted region to cause erosion of the bed to a lower prescribed elevation, has been well established through analysis and model experiments. However, higher discharges caused problems not only in the

constricted reach by excessive scour but also by shifting the problem region downstream by excessive deposition of sediments. The concept of designing constrictions so that they are submerged beyond a certain river stage was first presented by Anderson and Davenport [1]. Presumably, this method of design would prevent excessive scour at high stages but still maintain a navigable depth at low stages.

The equations proposed by Anderson and Davenport have been previously presented, Eqs. (12) and (13). Following a similar analysis to account for the part of the flow that passes over the constriction, Gill's Eq. (11) can be modified for submerged groins as

$$\frac{D_2}{D_1} = \left(\frac{Q_2}{Q_1}\right)^{6/7} \left(\frac{B_1}{B_2}\right)^{6/7} \left[\frac{1}{\left(\frac{B_1}{B_2}\right)^{1/\delta}\left(1 - \frac{\gamma_c}{\gamma_1}\right) + \frac{\gamma_c}{\gamma_1}}\right]^{3/7} \tag{14}$$

or

$$\frac{D_2}{D_1} = \left(\frac{Q_2}{Q_1}\right)^{6/7} \left(\frac{B_1}{B_2}\right)^{\theta} \tag{15}$$

By considering various values of δ, the influence of the particular bed load formula on the calculated scour depth can be seen. This comparison for $\gamma_c/\gamma_1 \to 0$ and $B_1/B_2 = 1.51$ is shown in Fig. 3 along with Anderson's Eq. (13).

The scour depth relationship derived by Griffith, Laursen, and Komura, Eqs. (5), (6), and (9), respectively, can be modified to include the discharge ratio in a similar manner. These results are plotted in Fig. 4 for $B_1/B_2 = 1.51$, again including Anderson's Eq. (13). The slope of the modified Griffith curve is considerably different from the others.

It is now necessary to derive an expression for the ratio of the discharge transporting sediment through the constriction, Q_2, to the total discharge, Q_1. Applying the continuity equation to the two regions, the flow through the constriction is

$$Q_2 = B_2 D_2 V_2$$

and the flow over the constriction is

$$Q_3 = (B_1 - B_2)D_3V_3$$

Since $Q_1 = Q_2 + Q_3$,

$$\frac{Q_2}{Q_1} = \frac{B_2D_2V_2}{B_2D_2V_2 + (B_1 - B_2)D_3V_3} \tag{16}$$

Assuming that the mean flow velocity, V_2, through the constriction is essentially equal to the mean flow velocity over the constriction, V_3,

$$\frac{Q_2}{Q_1} = \frac{1}{1 + \frac{D_3}{D_2}\left(\frac{B_1}{B_2} - 1\right)} \tag{17}$$

where D_3 is the flow depth over the constriction. The variation of the discharge ratio as a function of D_3/D_2 is shown in Fig. 5 for several values of B_1/B_2.

Utilizing Eqs. (13 and 17), the depth in the constricted section for submerged groins has been computed for a hypothetical case in Ref. [1]. The new bed regime for increasing discharges is plotted in Fig. 6. The bed regime for the unsubmerged groins is also shown. For the submerged groins, the bed elevation in the constricted region decreases to a minimum and then returns to the original bed elevation at the higher discharges. This reduces the amount of scour that would have occurred for the higher stages but at the same time maintains the necessary depth in the constricted region for the lower discharges.

IV. GENERAL MODEL CONSIDERATIONS

To complement the previous analytical relationships for scour depth in the constricted region and to aid the design of model studies, the problem also can be examined by dimensional analysis. In this method, it is customary to consider all the significant variables, and then reduce the number of variables by combining them in dimensionless parameters. Thus, the depth of flow, D_2, in the constricted region is

$$D_2 = f(D_1, D_3, B_1, B_2, Q_1, Q_2, S_1, S_2, V_1, V_2, G, \rho_s, \rho_f, D_s, \nu, \tau_1, \tau_2, g, P_i) \qquad (18)$$

where the previously undefined variables are

- S - slope of water surface
- G - factor related to groin geometry
- ρ_f - fluid density
- ρ_s - sediment density
- ν - fluid kinematic viscosity
- D_s - sediment size
- P_i - sediment shape, size distribution, and porosity factor

The variable G includes the angle of inclination of the groins to the stream, height, spacing, and type such as normal, L-type, or parallel, level or sloping crest, L-type extension length, etc. Here the variable G will be considered a dimensionless number which will be different for each groin geometry, since the disturbance to the flow by each geometry is different.

After combining the above variables into dimensionless groups with the subscripts 1 and 2 referring to the upstream and constricted regions respectively,

$$D_2/D_1 \text{ or } D_3/D_2 = f(B_1/B_2, Q_2/Q_1, S_1, S_2, R_1, Re_1, Re_2, F_1, F_2, \tau_1^*, \tau_2^*, \tilde{q}_1, \tilde{q}_2, P_i, G) \qquad (19)$$

where

$$R = \frac{\rho_s}{\rho_f} - 1$$

$Re_{1,2}$ = Reynolds number

$F_{1,2}$ = Froude number

$\gamma^*_{1,2}$ = Shields shear stress = $\frac{\gamma_{1,2}}{\rho_f R g D_s}$

$\tilde{q}_{1,2} = \frac{Q_{1,2}}{B_{1,2}\sqrt{RgD_s}\, D_s}$

It is now necessary to examine these parameters in an attempt to establish their relative significance. It can be assumed that Re_1, Re_2, R, and P_i are of secondary importance for most river flows. As the discharges and sediment size have been included in other terms, $\tilde{q}$, can be omitted. The slopes, S_1 and S_2, are related to the bed shear stress, and thus are implicit in the Shield's shear stress γ^*.

Thus,

$$\frac{D_2}{D_1} \text{or} \frac{D_3}{D_2} = f\left(\frac{B_1}{B_2}, \frac{Q_2}{Q_1}, F, \gamma^*, G\right) \tag{20}$$

The Froude number, F, is related to the influence of gravity on the open channel flow phenomena. Furthermore, for an unobstructed channel with an alluvial bed, Garde [14] has shown that once bed ripples grow into dunes, the height and wave length of the dunes is a function of the Froude number and a dimensionless function of the average bed shear stress. Shear stress is the basic parameter which causes sediment movement and the dimensionless Shield's shear stress also includes basic characteristics of the sediment. The parameter G has been discussed previously.

As has been pointed out by many investigators, the hydraulic model is not proposed as a "cure-all" for sedimentation problems, nor does its use preclude the need for extensive field investigations in evolving plans for their solutions. On the other hand, the sedimentation model, due to uncertainties which still exist as to the mechanics and principles of sedimentation in a prototype system, can be a useful tool to provide information not obtainable by other means. The need for experimentation is basically fostered by the fact that such problems cannot be resolved by the existing theories of sedimentation and

river hydraulics alone. Hence, the model, though it possesses some inherent limitations, continues to be a most useful expedient if the results obtained are interpreted judiciously.

In the study described here, no attempt was made to model any particular reach or specific river. It was considered to be a basic model study to investigate the fundamental relationship of distribution of flow and velocity through the constriction and over the groin field under various conditions, and its effect on the bed configuration of the non-cohesive sediments.

Fixed-bed model studies [8, 15] have long been used to predict the effect of proposed channel stabilization works on stage, velocity, and discharge of the streams. In the present model studies, a fixed-bed model was used to determine the flow and velocity distribution for the flow through the constriction and over the groin field.

Movable-bed model studies can be conducted based either on a dynamic equilibrium theory or a static equilibrium theory. The dynamic equilibrium theory requires that the sediment load passing through a cross section of the upstream end be equal to that of all points along the channel. The static equilibrium theory requires that the critical shear stress on the bed be constant at all points along the channel and no upstream sediment transport rate need exist. Since most field installations of contraction structures are in flows with considerable sediment transport, the model experiments were conducted in the dynamic equilibrium state. It was thus necessary to use a flume in which a constant sediment discharge is attained after a certain adjustment process equalizes the water surface and bed slopes.

In a typical sediment transport experiment, the major variables are the water discharge Q, mean velocity V, mean depth D, channel width B, energy gradient S (slope for uniform flow), rate of sediment transport Q_s, bed roughness n, and sediment characteristics (size, size distribution, shape and density). For the present study the independent variables are those variables determined before beginning a run--the mean depth upstream of the groin field, D_1, channel width B_1, and sediment characteristics. The dependent variables are those whose values were unknown until after the experiment--the mean velocity V, slope and bed roughness, and sediment transport rate. In laboratory studies with movable beds, it is practically impossible to set up an "ideal" experiment in which all variables are independant except one. Proper quantities of sand must be introduced at the upstream

end so that there is no net gain or loss of sand in the flume with time so as to obtain an equilibrium state. Although it is still a controversial question whether an equilibrium condition of scour is ever reached or not, (a question which is beyond the scope of this study) it is assumed that such a condition does exist. In this study it was assumed that a condition of equilibrium was reached in which the flow ceased to cause further erosion of its bed, although sedimentary material was continuously transported by the stream.

The selection of groin geometry was based mostly on the knowledge gained from the literature review. Three basic geometries were considered for investigation: 1) normal type, which includes groins perpendicular to the banks and inclined at an angle to the banks, 2) L-shaped, and 3) parallel walls. The variables for groin geometry are length, height, spacing, and angle of inclination to the banks. It is obvious that countless combinations with these variables and types can be made. The constraint on time and funds available for the tests has necessarily limited the number of combinations. A summary of the groin geometries selected for study is given in Table I and Fig. 7.

Since it has been reported in many studies that spacing between groins is dependent on the particular site conditions, only one spacing, which has been selected to be twice the perpendicular length of the groins, (i.e.) half the width of the constriction, was used for groins perpendicular to the banks. As groins angled downstream were reported to be more efficient than those pointed upstream, only groins angled downstream at 60° to the banks were tested. For the L-shaped groins, the above mentioned two types of groins were used with an extension in the downstream direction for 50 percent closure of the spacing between the groins, which has been previously demonstrated to be the optimum closure conditions. Five groins on each side of the flume were symmetrically fixed with respect to the centre of the channel. The number of groins was selected after consideration of the available length of the flume, groin spacing, inlet and outlet conditions and development of flow in the groins region. The third type, namely the parallel type, was of the same longitudinal length as all of the five groins of the above mentioned types, with a 1:2 tapered section on either end.

The submergence ratio D_3/D_2 was one of the most important parameters in this study. Various submergence ratios were obtained by changing the height of groins, H, or by changing the depth of flow, D_2, which is a function of the upstream depth of flow D_1. Since the maximum flow depth that could be obtained in the flumes was 35 cm, and in order to cover a good range of submergence ratio, a constant groin height of 10 cm was selected, varying the depth of flow for various discharges. However, tests were also conducted with a 15 cm height of groins under type A1 and A2 in the rigid-bed model.

Another important controlling parameter in this study was the constriction ratio B_1/B_2. When there is no constriction, $B_1/B_2 = 1$ and the ratio can be theoretically anything above 1. Keeping in mind the required navigation width, economy of construction, etc., it was decided to conduct the majority of tests by constricting the flow to 2/3 of the width of the flume, (i.e.) for a constriction ratio of 1.5. However, tests were also conducted for a constriction ratio of 2.0 with type A2 in the rigid bed model. Model tests with groin types A3 through A7 were conducted in both the rigid and movable bed models. Discharges and depths of flow were selected so as to keep the Froude number below 0.5 to avoid formation of antidunes and/or standing waves, and also to approximate the values generally encountered in the prototype.

It was assumed that there will be no side wall effects in the present studies using a 1.83 m wide channel. Support for this is derived from Williams [16] who has concluded that narrow flume widths affect some variables significantly, but in a channel 2 ft wide, side wall effects very nearly or completely disappeared.

V. EXPERIMENTAL APPARATUS AND PROCEDURE

A. Test Facility and Models

Two identical non-recirculating flumes were used for the study, one for the rigid-bed model and another for the movable-bed model. The two flumes were located on the River Mezzanine floor of the Laboratory as shown in Fig. 8 and Photos 1 through 4. Both of the flumes were 61 cm deep, 1.83 m wide, and 10.36 m long, with a clear space of 1.2 m separating the two parallel units. Each flume had a movable carriage supported on rails to facilitate the positioning of measuring instruments with respect to three co-ordinate directions.

River water for the models was pumped from the Laboratory supply channel into an overhead 30 cm supply line to the model areas. A vertical 20 cm line conveyed the flow down to each of the flumes through a 16.5 cm orifice meter and a control valve (Photo 1). Each meter was calibrated up to 165 lps. A mercury manometer for high discharges and meriam No. 3 manometer for low discharges was connected across each of the orifices for measurement of the inlet flow discharges. Both models could be operated simultaneously at lower discharges (Photo 4).

A T-manifold was installed in each model to distribute the flow across the channel. With the addition of a wire mesh screen and ramp downstream of the manifold, a satisfactory flow distribution was achieved across the width of the flumes. The flow depth in the flumes was controlled by a screw-type overflow weir gate at the downstream end, and the depth could be set to an accuracy of a fraction of a centimeter.

For the rigid-bed model, the bottom was constructed of 19.3 cm high concrete blocks. The concrete surface was painted and sand evenly spread over it to provide a uniformly rough bed surface (Photo 2).

For the movable bed material, Bay City sand was used (Photo 3). The sand, with specific gravity of 2.65, was of fairly uniform size with a median diameter, d_{50}, of 0.33 mm. Its size distribution is shown in Fig. 9. It has a standard deviation of 1.54.

The groins were fabricated of 1.5 mm thick steel plates. The first groin was always located 2 m downstream from the inlet. Five groins on each side were fixed at a spacing of 61 cm (Photo 2). Groins were bolted to the concrete bed in the rigid-bed model and to the side walls in the movable-bed model.

B. Instrumentation

To determine the distribution of flow through the constriction and over the groin-field, velocity traverses were made across and along the flumes. An Ott-propeller type velocity meter was used for measuring velocities above 15 cm/sec as shown in Photo 5 and a pygmy cup type meter for lower velocities. Attempts were made to use a Delft-meter in the rigid-bed model for velocity measurements, but due to the frequent presence of fine material carried in the water, the Delft-meter could not be used successfully. At the start of the testing program, extensive velocity traverses were made at several stations

along the model to check the inflow distribution and development of flow through the groins. After analysing the results, it was established that a traverse between groins 3 and 4 would be adequate to determine the flow distributions. Velocity measurements were taken on a grid-pattern, i.e. in both a lateral and vertical direction.

An electrical point gauge was used to measure the flow depths in the rigid-bed model. An optical automatic probe coupled to electronic equipment for recording the data on cassette tape has been developed previously in the Laboratory and also was available for this project. This optical probe, shown in Photos 5 through 7, was used to measure the bed profile (Photo 7) and water surface profile (Photo 6) in the movable-bed model. The Laboratory Raytheon 703 computer was used to process the data recorded on the cassette tape. Limited data were also taken manually by point gauge.

In the movable-bed model a slot-type sediment sampler was used to collect samples at the downstream end, as shown in Photo 8. A cylindrical container with a conical bottom fixed over a pre-calibrated, graduated tube was used to measure the sediment discharge (Photo 9). The tube has been calibrated for the volume of sand in terms of its dry weight. Knowing the approximate quantity of sediment being transported by the flow, the same amount of sand was supplied at the upstream end of the model using a calibrated, vibrating sand feeder. The sand discharged from this feeder was distributed across the full width of the flume by means of a fan-shaped trough. These devices are shown in Photos 6 and 10.

C. Experimental Procedure

1. Rigid-Bed Model
   a) Groins were fixed in position (Photo 2).
   b) Bed surface data were taken.
   c) The required discharge was set using the control valve and the orifice manometers.
   d) The required depth was set using the screw-type weir tail gate.
   e) After the desired flow conditions were established, velocity traverses were made.

f) From the current meter data and the meter calibration, the velocity at each point of measurement was determined. The area around each of these points extending halfway to the nearest adjacent point in each direction (or to a boundary) was determined. These increments of area were then multiplied by the velocity as measured within the area to give an increment of discharge passing through that section. The increments of discharge were then summed to obtain the values of the flow through the constriction Q_2 and the total flow Q_1. The velocity traverse was taken so as to separate the flow through the constriction, Q_2, from the total computed or measured flow Q_1.

e) Photos were taken to show the flow pattern in the constricted and unconstricted region, using confetti on the water surface as shown in Photos 11 through 18 for various geometrics and flow conditions. All photos were taken with the same camera position and shutter speed.

h) Water temperature was measured.

2. Movable-Bed Model

a) Groins were fixed in position.

b) The sand bed surface was screeded using an adjustable screw-type screed (Photo 3).

c) Bed surface data were taken using both the point gauge and the optical probe (Photo 7).

d) The model was slowly flooded with water from the downstream end. This back flooding prevented the initial flow from cutting into the shaped bed.

e) Flow was admitted through the upstream end of the flume and the water surface was allowed to rise higher than desired.

f) The required discharge was set.

g) The required depth was set by lowering the weir tail gate.

h) Sand was fed from the upstream end using the sand feed device at some approximate rate (Photo 10).

i) The water surface profile was measured using both the point gauge and the optical probe (Photo 6).

j) At regular intervals, the sediment coming out of the flume was measured using the sediment sampler and the same amount placed in the sand feeder. In some instances the sediment discharge was very low and difficult to measure.

k) The test was continued until an equilibrium condition was reached. In each run a certain time was required for the ripple formation to cover the bed. Ripples and dunes started forming first in the groin region and in the region downstream of the groins and then in the region upstream of the groins. It was observed that equilibrium conditions were obtained some time after complete formation of ripples and dunes in the flume.

l) Once the equilibrium condition was reached, velocity traverses were taken to compute Q_2 and Q_1 as previously discussed for the rigid-bed model. The change in the bed configuration was thus taken into account in the flow computations.

m) The final water surface profile was taken using both point gauge and optical probe.

n) Detailed bed profile data were taken using the optical probe.

o) Photos were taken for the flow distribution using confetti on the water surface and of the erosion pattern after the test as shown in Photos 19 through 36 for various geometries and flow conditions.

p) Flow was stopped and as soon as the water drained out of the flume, limited bed profile data were taken using a point gauge.

q) Water temperature was measured.

VI. DISCUSSION OF RESULTS

A. Effect of Groin Submergence on Discharge Ratio

The first part of the experimental program was concerned with the distribution of discharge over and through the constriction for the various groin geometries. The flow distribution was determined by taking velocity measurements at various sections along the longitudinal axis of the channel for both the rigid- and movable-bed models. Typical results of the velocity surveys are shown in Figs. 10 and 11 plotted as velocity contours. The solid dots indicate the positions at which velocity measurements were made. From these

measurements, the flow passing through the constricted region, Q_2, and the flow over the groins, Q_3, was calculated. The sum of these two discharges was compared with the total discharge as measured with the supply line orifice meter. This comparison indicated an agreement to within $\pm$ 6 percent, verifying that the measurements were reasonably accurate. In addition to the physical velocity measurements, confetti was scattered on the water surface and photos were taken. Some of these results are shown in Photos 11 through 18 and a comparison of the length of the confetti traces gives an indication of the relative surface velocities in various sections.

The experimental data for the discharge ratio, Q_2/Q_1, and the theoretical equation, Eq. (17), are plotted in Figs. 12 to 15 for both the rigid- and movable- bed models. (The data have been tabulated in the Appendix.) It can be seen that for types A3, A4, and A7 the data for both rigid- and movable-bed models are essentially the same, indicating similar flow characteristics in the two models. Presumably, the change in bed roughness for these groin types in the movable-bed model between the normal and groin regions is not appreciable. However, for the L-type groins A5 and A6, the movable-bed data always fell below the data for the rigid-bed. This discrepancy is assumed to be an indication of an appreciable change in bed roughness.

Observations of the final scour pattern were made to possibly explain this behavior. With types A3 and A4, the eroded bed material in the groin region was partly redeposited in the lower velocity region behind the groins and partly carried downstream. With type A7, since the entire groin region was obstructed by longitudinal walls, the eroded material was essentially moved downstream. Also, in this case, the tapered upstream ends of the walls resulted in a rather smooth transition of the flow into the constriction. It was observed that with types A5 and A6 the eroded material was deposited as shoals in the groin region near the downstream end of the extension walls. These extensions greatly obstructed the deposition between the groins themselves. Hence, the bed roughness was increased and the effective area between the groins was decreased causing reduced values of the discharge ratio.

An attempt was made to account for the change in bed roughness by using Manning's equation and assuming that the hydraulic radius was equal to the flow depth. The discharge ratio was then expressed as

$$\frac{Q_2}{Q_1} = \left[1 + \left(\frac{n_2}{n_3}\right)\left(\frac{S_3}{S_2}\right)^{1/2}\left(\frac{B_1}{B_2} - 1\right)\left(\frac{D_3}{D_2}\right)^{5/3}\right]^{-1} \qquad (21)$$

where n_2 and n_3 are the Manning's roughness coefficients in the constricted region and the region over the constriction, and S_2 and S_3 are the respective slopes of the water surface.

As the roughness coefficients were not known, the factor $\frac{n_2}{n_3}\left(\frac{S_3}{S_2}\right)^{1/2}$ was assumed to vary from 1 to 3 to account for considerable differences in both roughness and slope in the two sections. A plot of Eq. (21) with the above assumption is shown in Fig. 16 along with the experimental data for the various groin types in the movable-bed model. No trends can definitely be observed, but the curves for roughness factors of 1 and 3 appear to bracket the data. It thus seems that in view of the arbitrariness involved in the use of Eq. (21) and the expectation that the prototype would not experience any appreciable change in roughness, any further attempts to account for roughness effects were abandoned.

Although the different groin geometries created somewhat different flow characteristics in the constricted region, the general trend of the variation of discharge ratio with submergence ratio was the same. Thus, the data for all geometries in the rigid-bed model are combined in Fig. 17, and the data for the movable-bed model are combined in Fig. 18. The scatter of the data is not considered excessive for a first approximation. It should be noted in Fig. 18 than an additional set of data are shown. These data from Ref. [17] are for a parallel walled contraction and are included to show the effect of a different constriction ratio. The general trend is the same in that for larger values of D_3/D_2, the experimental data fall slightly below the theoretical curve.

At this point, a statement should be made regarding the accuracy of the assumption $V_2 = V_3$ in the derivation of Eq. (17). Considering all the data for the various groin geometries, the experimental measurements indicated that in some cases V_2 and V_3 were considerably different. The range for V_3/V_2 in the rigid-bed model was between 0.41 and 1.23, and between 0.72 and 1.4 for the movable-bed model. However, the percentage error in velocity ratio does not result in the same error in the discharge ratio. The measured

discharge ratios were compared to the calculated values at the same D_3/D_2 for all groin geometries, and it was found that for the rigid-bed model, the standard deviation was 0.04 with an error of 4.6 percent. A similar analysis of the data for the movable-bed model indicated a standard deviation of 0.04 and an error of 5.2 percent. On this basis it was assumed that the assumption of $V_2 = V_3$ was reasonably valid.

B. Effect of Discharge Ratio on Depth Ratio

One of the objectives of this study was to provide experimental verification for the theory of dynamic equilibrium scour depth in submerged constrictions. With this in view, the tests were carried out at relatively high sediment discharge rates.

The equilibrium depth, D_2, was determined from longitudinal profiles taken along the centerline of the channel. It represents an average depth over a certain reach, which varied slightly with the particular groin geometry. Typical longitudinal bed profiles and selected cross-sections at which velocity traverses were made for each configuration are shown in Figs. 19 through 26. The broken reference line is the original bed elevation. The bed elevations measured at specific locations have been connected by straight lines in these plots, and thus do not completely represent the bed profile although the variations in depth can readily be seen. The first groin is located at the 200 cm mark in the longitudinal profiles.

The experimental data for the average depth ratio are plotted in Fig. 27 for all geometries, including the data from Ref. (17) for a parallel walled constriction at a higher constriction ratio. The data have been plotted with logarithmic coordinates so that the exponent on the discharge ratio could readily be obtained. Considerable scatter of the data is noted, although this is generally expected in studies related to sediment transport. The data points for types A5 and A6 at a discharge ratio of 0.83 and B_1/B_2 of 1.51 lie well outside the general grouping of points. This discrepancy, as previously discussed for the L-type groins, is probably associated with the variation of roughness and reduced area of flow in the constricted region.

A best fit line through the experimental data was found by the method of least squares. The equation based on the data for $B_1/B_2 = 1.51$ was

$$\frac{D_2}{D_1} = 1.37\left(\frac{Q_2}{Q_1}\right)^{0.8} = \left(\frac{Q_2}{Q_1}\right)^{0.8}\left(\frac{B_1}{B_2}\right)^{0.75} \tag{22}$$

The data from Ref. (17) for $B_1/B_2 = 2$ was similarily analysed and the equation was

$$\frac{D_2}{D_1} = 1.62\left(\frac{Q_2}{Q_1}\right)^{0.86} = \left(\frac{Q_2}{Q_1}\right)^{0.86}\left(\frac{B_1}{B_2}\right)^{0.7} \tag{23}$$

It has previously been shown in Section III that the exponent of the discharge ratio should be 6/7 or 0.857. The above two equations provide evidence that this exponent is essentially correct. Furthermore, in Fig. 2 it was shown that for large transport rates, i.e. $\tau_c/\tau_1 \to 0$, the value of θ or the exponent of B_1/B_2 for the Brown-Einstein bed load formula was 0.714. This bed load formula was based on experiments including sediment median sizes ranging from 0.3 to 7 mm. The data shown in Fig. 27 tend to support the use of the Brown-Einstein formula for calculation in view of the relatively good agreement of the exponents on the constriction ratio.

It was stated earlier in Section IV that from dimensional analysis the depth ratio, D_2/D_1, would also be a function of the Froude number, F, and the Shield's shear stress, τ^*. Analysis of the data available indicated a secondary relationship between the depth ratio and the Froude number, but the data were not sufficient to firmly establish the effect.

Some estimates of the bed shear stresses were made for a particular groin geometry, type A4. These shear stresses were determined from the water surface profiles both in the region upstream of the groins and in the constricted region. It is extremely difficult to arrive at shear stress in this manner with much degree of confidence. However, the bed shear stresses reduced to the form of the Shield's shear stress have been plotted in Fig. 28 to show the general trends for the two regions. This plot shows that the shear stress in the contracted region increases with D_2/D_1 and the shear stress in the unconstricted region decreases. Or alternatively for large

discharges and large D_1, the shear stress in the constricted region is lowered and less scour of the bed will occur. The trends shown by the data verify the basic concept of the submerged groins.

Due to the limited data available for a given groin geometry and the time restraints of the present study, no attempt has been made to quantify any relationship between D_2/D_1 and γ^* at this time. Additional extensive model studies designed to arrive at such a relationship are required.

In summary, it is thus suggested that the following two equations be used to predict the dynamic equilibrium depth, D_2, in the constricted region with reasonable confidence:

$$\frac{Q_2}{Q_1} = \frac{1}{1 + \left(\frac{B_1}{B_2} - 1\right)\frac{D_3}{D_2}} \tag{17}$$

and

$$\frac{D_2}{D_1} = \left(\frac{Q_2}{Q_1}\right)^{6/7} \left(\frac{B_1}{B_2}\right)^{\theta} \tag{24}$$

for

$$0 < \frac{\tau_c}{\tau_1} \leq 1$$

$$\frac{5}{7} < \theta \leq \frac{6}{7}$$

For calculation purposes, it may be more convenient to combine the above equations to eliminate the discharge ratio, and to use D_3/D_1 instead of D_3/D_2 in Eq. (17). If Eq. (24) is written as

$$\frac{D_2}{D_1} = \left(\frac{Q_2}{Q_1}\right)^{\lambda} \left(\frac{B_1}{B_2}\right)^{\theta}$$

and combined with Eq. (17), we have

$$\frac{D_3}{D_1} = \frac{\frac{D_2}{D_1}\left[\left(\frac{D_2}{D_1}\right)^{-1/\lambda}\left(\frac{B_1}{B_2}\right)^{\theta/\lambda} - 1\right]}{\frac{B_1}{B_2} - 1} \tag{25}$$

in some prototype situations, the possibility of sediment deposition between groins may be greater for types A5, A6, and A7 than for types A3 and A4. Also, shoaling may not occur in the groin region for types A5 and A6. The L-type groin geometries may be effective in bends and curves, although this was not investigated.

In an attempt to evaluate the efficiency of a particular groin geometry, an analysis was made of the cross-sectional bed profiles. The depth, D_2, was previously defined as the depth in the constricted region and was obtained by averaging depths measured along the longitudinal centerline of the channel. Another depth, D_{2L}, is now defined as the depth in the constricted region obtained by averaging the depths in the lateral direction of the channel at a section between groins 3 and 4 (see Fig. 8). Ideally, these two depths should be the same. However, D_{2L} was always less than D_2 due to changes in the flow characteristics in the groin region.

A deviation factor, DF, is then defined as

$$DF = \frac{(D_2 - D_{2L}) \times 100}{D_2}$$

which indicates the percentage deviation of the two depths. This factor varies with each groin geometry in accordance with the previous discussion. A small value of DF implies uniformity in depth and is regarded as an indication of an efficient groin geometry. These values for the various groin geometries tested are tabulated in Table II.

The deviation factor is most important for low flows since that is the condition for which the additional depth or lower bed elevation is required. From an evaluation of the numerical values of Table II, it is concluded that groin type A4 is somewhat better than the others in providing a uniform depth across the channel. Although type A7 also exhibits good efficiency, the excessive cost of construction would make the use of this type less attractive in the field.

VII. CONCLUSIONS

The following conclusions may be drawn from the experimental data taken for various geometries of submerged groins in a straight reach of channel:

1. The experimental data verified the basic concept of submerged groins in controlling depth of scour in the constricted region. For low stages, the bed elevation was lowered in the constriction and for high stages and consequent submergence of the groin, the bed elevation approached the original bed elevation without the constriction.

2. The ratio of the discharge through the constriction to the total discharge was found to be primarily a function of the constriction geometry. Some evidence of roughness effects were observed, although the effects were not clearly defined. Therefore, the discharge ratio, for small changes in roughness, can be determined from

$$\frac{Q_2}{Q_1} = \frac{1}{1 + \left(\frac{B_1}{B_2} - 1\right)\frac{D_3}{D_2}}$$

3. The dynamic equilibrium depth of scour, D_2, can be predicted as a first approximation with reasonable confidence with the equation based on the Brown-Einstein bed load formula,

$$\frac{D_2}{D_1} = \left(\frac{Q_2}{Q_1}\right)^{6/7}\left(\frac{B_1}{B_2}\right)^{\Theta}$$

with $\Theta = 0.714$ for $\tau_c/\tau_1 \ll 1$.

By using the discharge ratio in item 2, the equation can be rewritten in terms of the groin submergence and scour depth as

$$\frac{D_3}{D_1} = \frac{\frac{D_2}{D_1}\left[\left(\frac{D_2}{D_1}\right)^{-1.167}\left(\frac{B_1}{B_2}\right)^{0.833} - 1\right]}{\frac{B_1}{B_2} - 1}$$

4. The equilibrium scour depth ratio, D_2/D_1, was also found to be related to Shield's shear stress. Additional model studies and analysis are required to adequately define the relationship. Such studies should result in more complete basic knowledge of the scour phenomena.

5. The final selection of a groin configuration to be used is dependent on factors other than just the ability of attaining a prescribed scour depth in the constricted region. For example, consideration should be given to uniformity of scour depth across the entire width of the constriction as well as local scour around the tips of the groins. Of the groin types tested, it appeared that the downstream angled groin (type A4) was the most efficient in this regard. Parallel wall constrictions (type A7) were also efficient, but construction costs may be excessive in the prototype.

6. Selection of the groin type and longitudinal spacing of the groins is also dependent on conditions existing in the prototype, such as bends, etc. These conditions may require additional model studies to access the overall performance of submerged groins in such an application.

LIST OF REFERENCES

[1] Anderson, A.G., and Davenport, J.T., "The Use of Submerged Groins for the Regulation of Alluvial Streams", Symposium on Current Problems in River Training and Sediment Movement, Hungarian Academy of Science, Budapest, Hungary, 1968.

[2] Straub, Lorenz G., "Effect of Channel Contraction Works Upon the Regimes of Movable Bed Streams", Trans. Am. Geo. Phy. Union, Pt II, June 1934, pp 454-463.

[3] Anderson, A.G., "Sediment Transportation Mechanics: Erosion of Sediment", Progress Report Task Committee on Preparation of Sedimentation Manual, Journal Hyd. Div., ASCE, Vol. 88, No. HY4, July 1962, pp 109-127. Closing discussion, Journal Hyd. Div., ASCE, Vol. 89, No. HY6, Nov. 1963, pp 237-267.

[4] Griffith, W.M., "A Theory of Silt Transportation", Transactions, ASCE, Vol. 104, 1939, pp 1733-1737.

[5] Laursen, Emmet M, "Scour at Bridge Crossings", Transactions, ASCE, Vol. 127, Part I, Proc. paper No. 3294, 1962, pp 168-171.

[6] Komura, Saburo, "Equilibrium Depth of Scour in Long Constrictions", Journal of the Hyd. Div., ASCE, Vol. 92, No. HY5, Sept. 1966, pp 17-37.

[7] Gill, M.A., "Erosion of Sand Beds Around Spur Dikes", Journal of Hyd. Div., ASCE, Vol. 98, No. HY9, Sept. 1972, pp 1587-1601.

[8] "Progress Report, Task Committee on Channel Stabilization Works - Committee on Regulation and Stabilization of Rivers", Journal WW and Harbor Div., ASCE, Vol 91, No. WW-1, Feb. 1965, pp 7-37.

[9] Franco, J.J. and McKellar, C.D. Jr., "Development and Maintenance of Navigation Channel Arkansas River, Arkansas and Oklahoma - Hydraulic Model Investigation", Tech. Report No. 2-608, Aug. 1962. U.S. Army Engineers, Waterways Experiment Station, C of E, Vicksburg, Miss.

[10] Franco, J.J., "Research for River Regulation Dike Design", Journal WW and Harbor Div., ASCE Vol. 93,No. WW3, Aug. 1967, pp 71-87.

[11] Linder, W.M., Christian, H.E., and Mellema, W.J., "Missouri River Design Study - Lab. Investigation of L-Head Channel Control Structures", Report by U.S. Army Engineers Dist. Omaha and Kansas City, June 1964.

[12] Central Water Power Irrigation and Navigation Commission, Poona, India, Annual Report 1949.

[13] Central Water and Power Research Station, Poona, India, "Basic Research on Spurs", Annual Research Memoir, 1962.

[14] Garde, R.J., Subramanya, K., and Nambudripad, K.K., "Study of Scour Around Spur - Dikes", Journal Hyd. Div., ASCE, Vol. 87, No. HY6, Nov. 1961, pp 23-37.

LIST OF REFERENCES (cont.)

[15] Suga, Kyozo, "Some Notes on Hydraulic Model Tests of River Channels", I.A.H.R. International Symposium on River Mechanics, Jan. 1973, pp 109-120.

[16] Williams, G. P., "Sediment Transport in Alluvial Channels - Flume Width and Water Depth Effects in Sediment Transport Experiments", USGS Prof. paper No. 562, 1970, pp H1-H37.

[17] Davenport, J.T., "The Effect of Submerged Long Constrictions on the Dynamic Equilibrium Depth of Scour in Open Channels", Thesis submitted to the Graduate School, Univ. of Minn. for the degree M.S./C.E./July 1968.

TABLE I - DESCRIPTION OF GROIN GEOMETRY

Basic Type	Type No.	Length[1] L cm	Angle to the wall	Spacing cm	Height H cm	Constriction Ratio B_1/B_2	Remarks
Normal	A1	30.5	90°	61	15	1.5	Rigid bed only
Normal	A2	45.75	90°	61	15	2.0	Rigid bed only
Normal	A3	30.5	90°	61	10	1.5	Both rigid & movable beds
Normal	A4	30.5	60°	61	10	1.5	- " -
L-shape[2]	A5	30.5	90°	61	10	1.5	- " -
L-shape[2]	A6	30.5	60°	61	10	1.5	- " -
Parallel[3] wall	A7	30.5	0°	--	10	1.5	- " -

1. Length L is defined as the length to which the groins extend into the flow perpendicular to the walls.
2. Extension length of 30.5 cm parallel to the flow.
3. Effective longitudinal length of 244 cm, with 1:2 taper on either end.

TABLE II

COMPARISON OF AVERAGE LONGITUDINAL AND LATERAL SCOUR DEPTHS

Type	Run No.	D_2 cm	D_{2L} cm	$\frac{D_2-D_{2L}}{D_2}$, %
A3	105	31.77	30.71	3.33
	106	22.4	21.96	1.96
	107	18.81	16.27	13.50
A4	108	30.328	29.34	3.26
	109	22.288	20.63	7.45
	110	17.87	17.07	4.48
	120	12.91	11.53	10.69
A5	111	30.31	30.11	.66
	112	21.822	18.865	13.56
	113	18.42	15.003	18.57
A6	114	30.01	28.59	4.73
	115	21.77	18.64	14.38
	116	17.78	15.89	10.63
A7	117	29.04	28.98	.2
	118	19.52	19.47	.2
	119	15.96	14.78	7.39

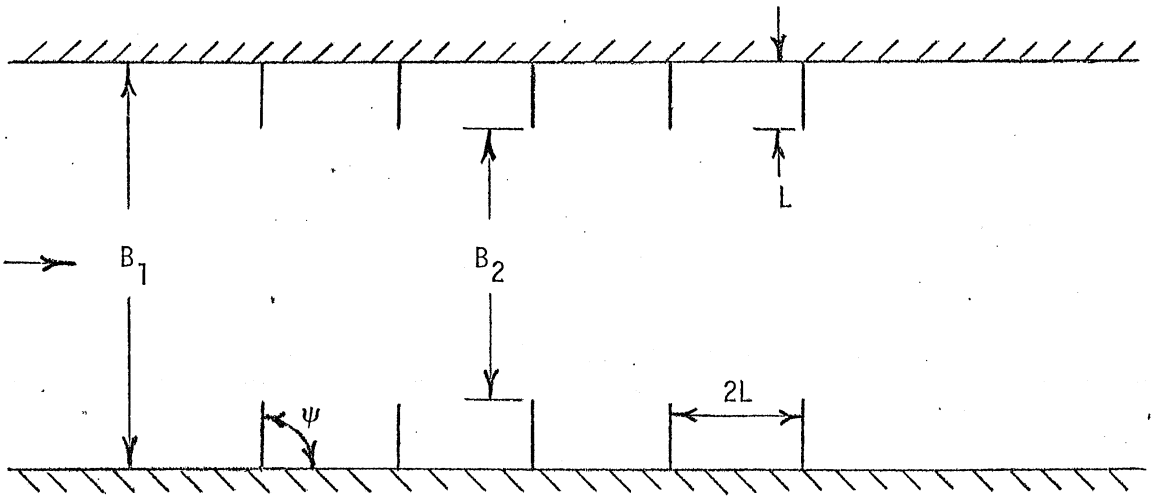

Plan

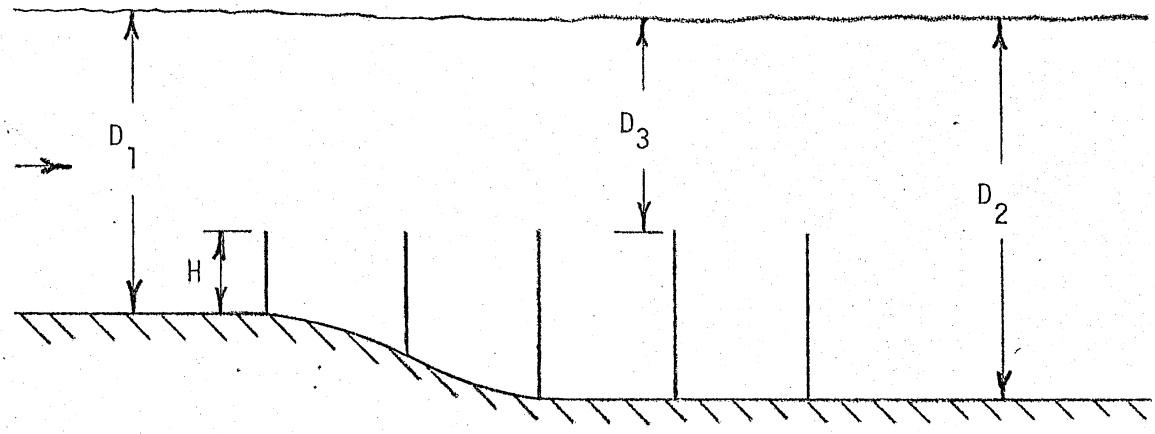

Elevation

Fig. 1 - Definition Sketch for Submerged Groins

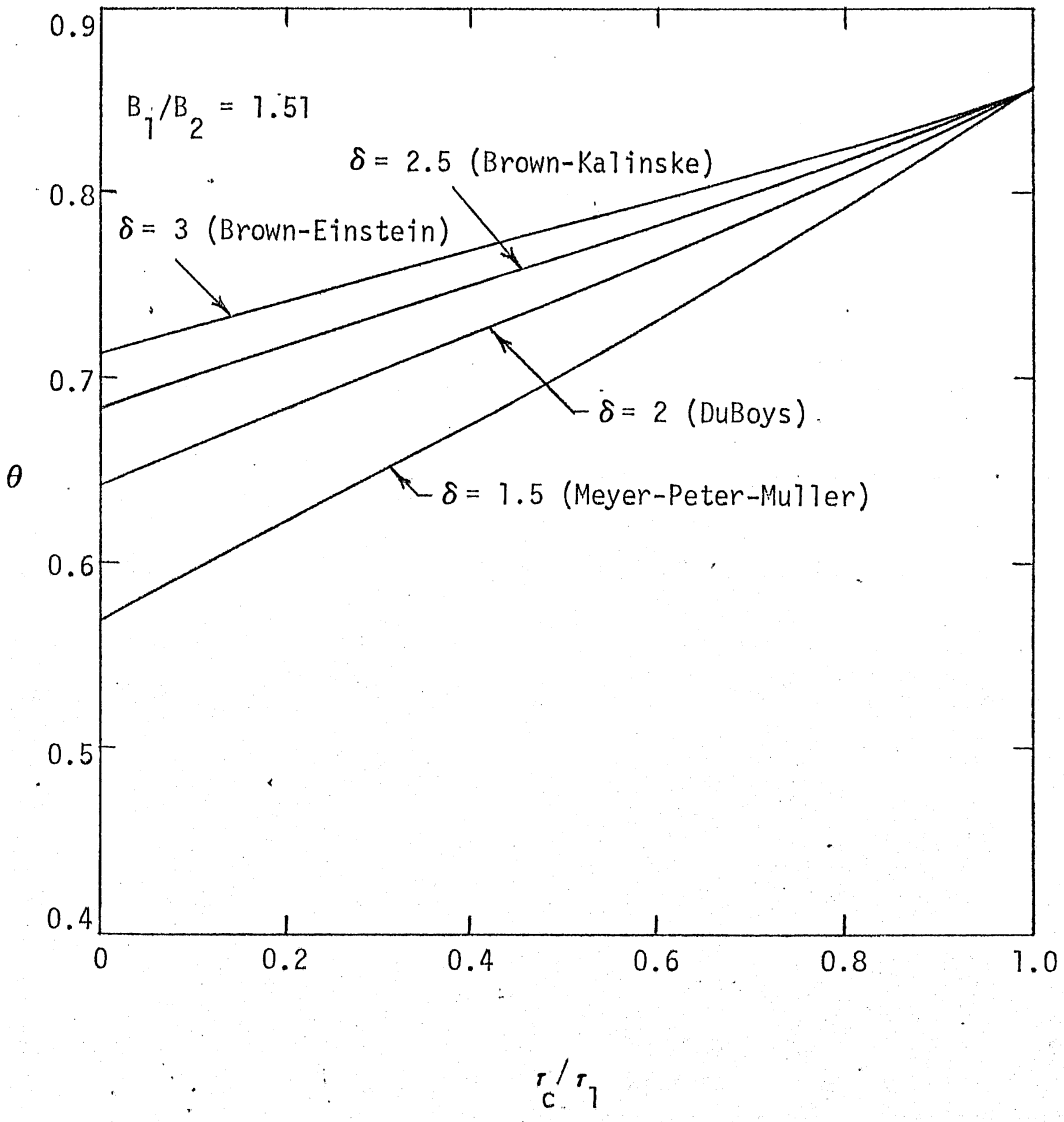

Fig. 2 - Variation of Exponent θ with Relative Transport Rate and Bed Load Formulas

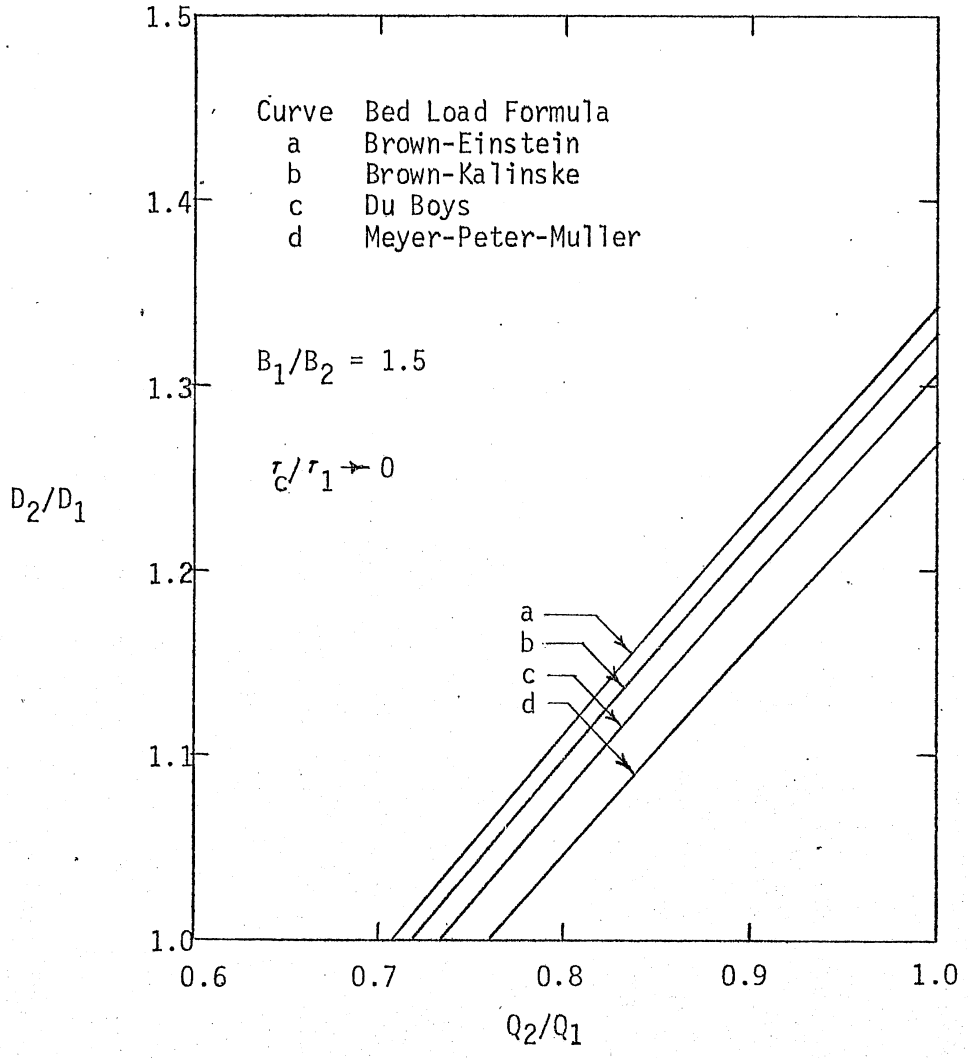

Fig. 3 - Relative Depth in Submerged Contraction for Various Bed Load Formulas.

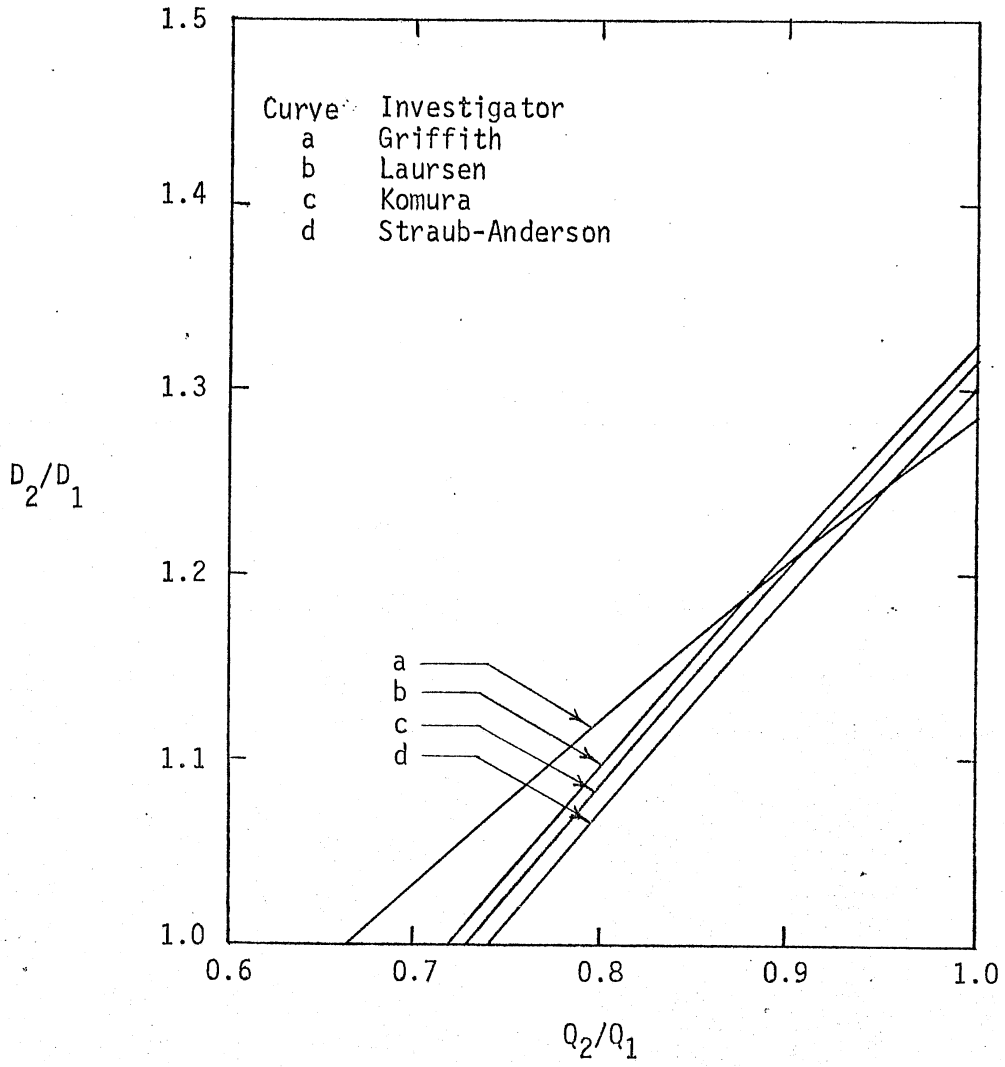

Fig. 4 - Comparison of Various Equations for Relative Depth in Submerged Contraction.

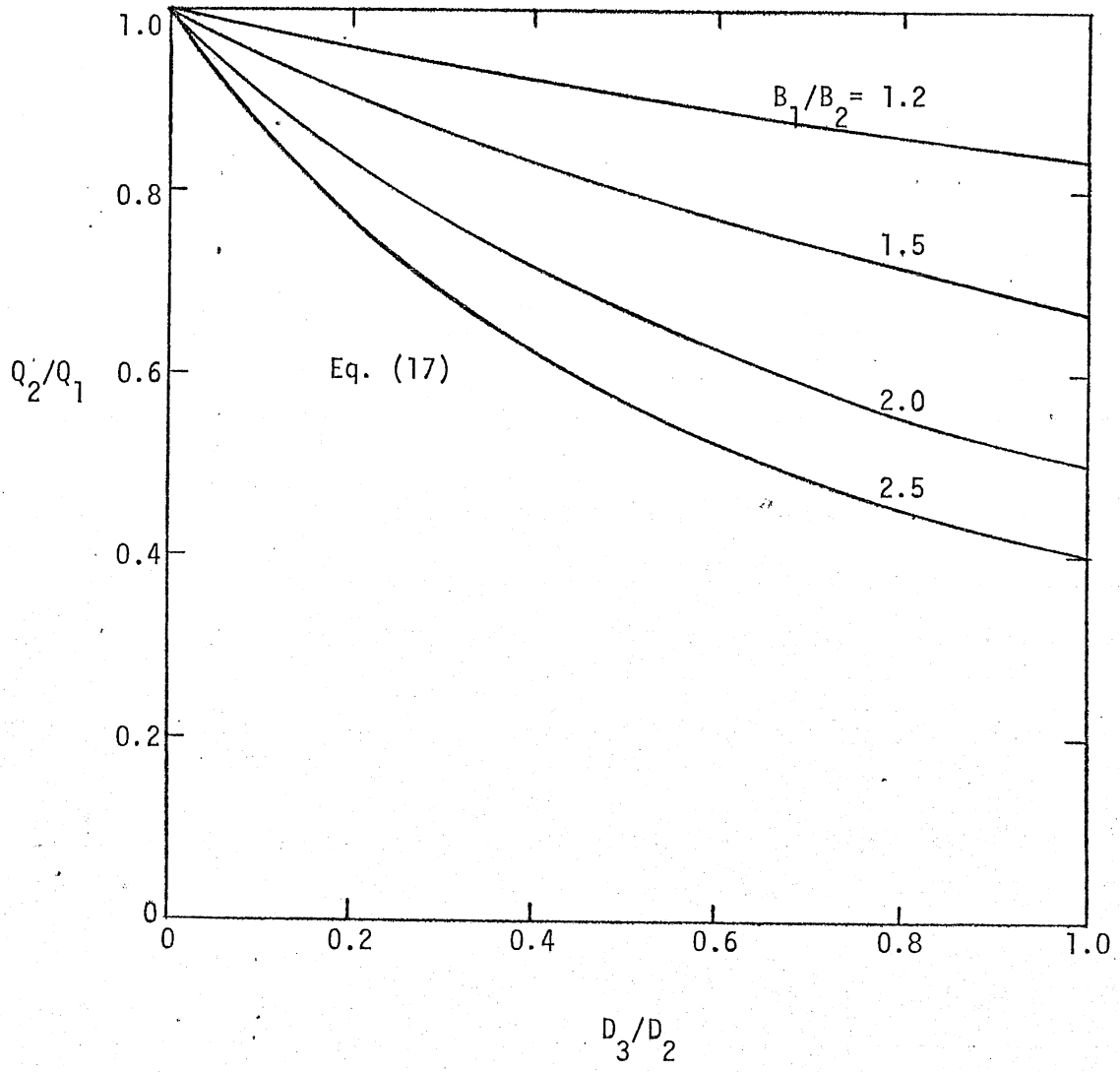

Fig. 5 - Relative Discharge through Contraction as a Function of Relative Contraction Submergence

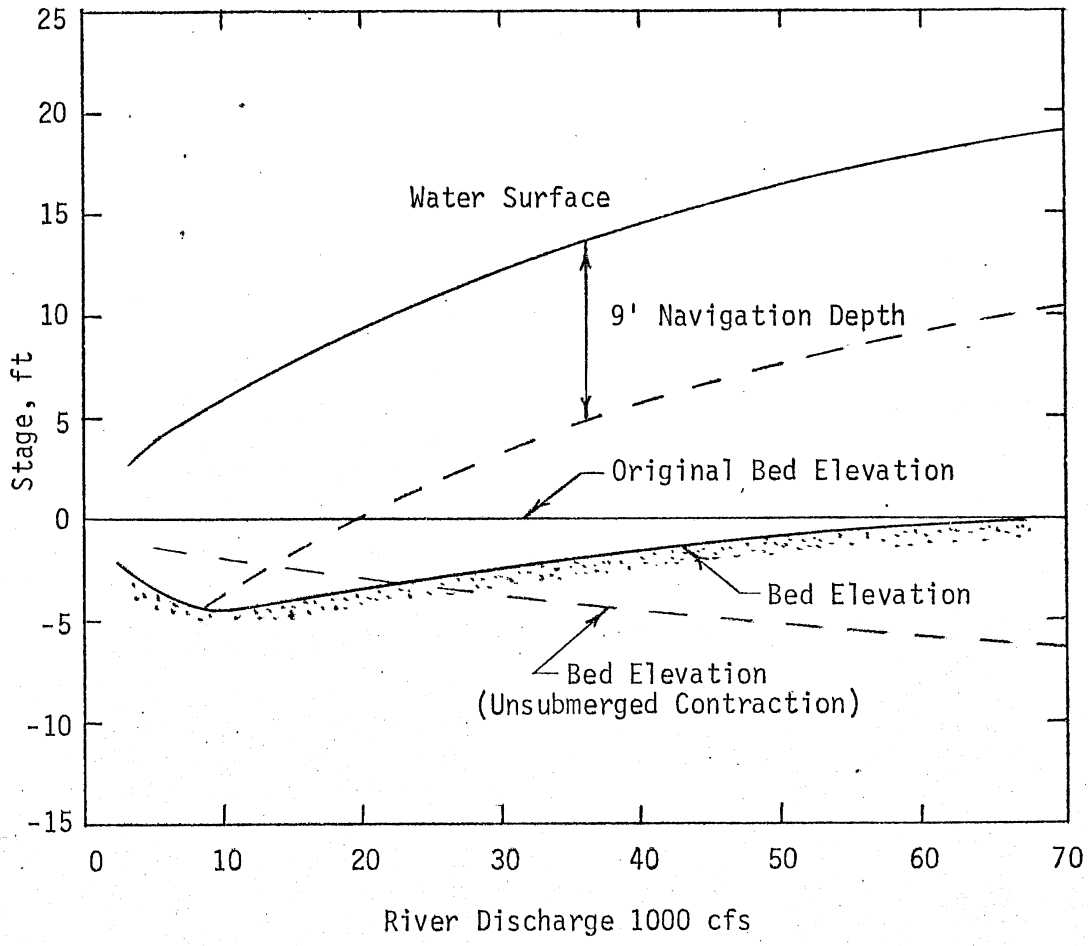

Fig. 6 - Bed Elevation in Constricted Section for Various Discharges-Submerged Contraction (from Ref. [1]).

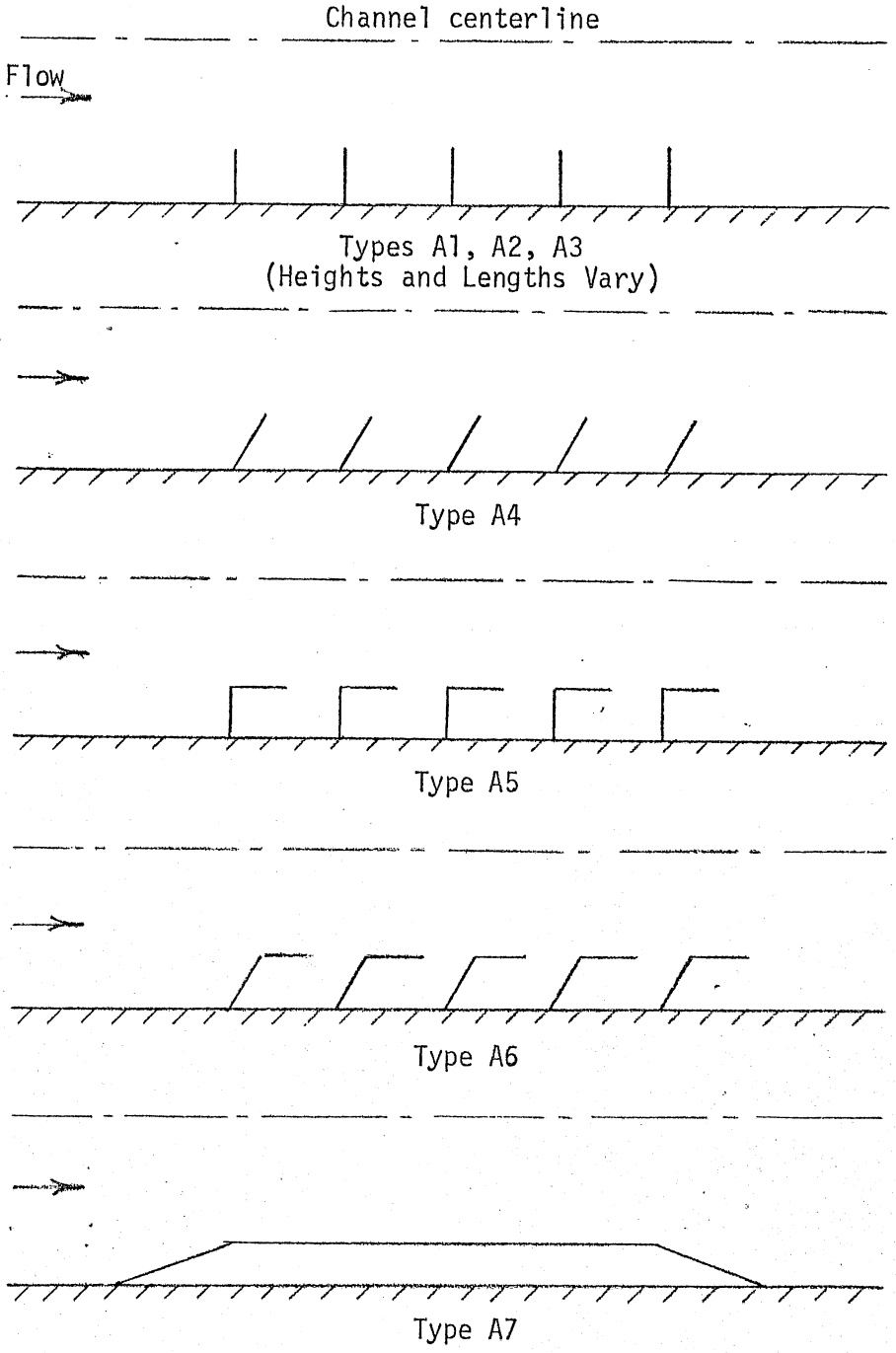

All geometries symmetrical about centerline.
See Table I for dimensions.

Fig. 7 - Plan View of Groin Geometries

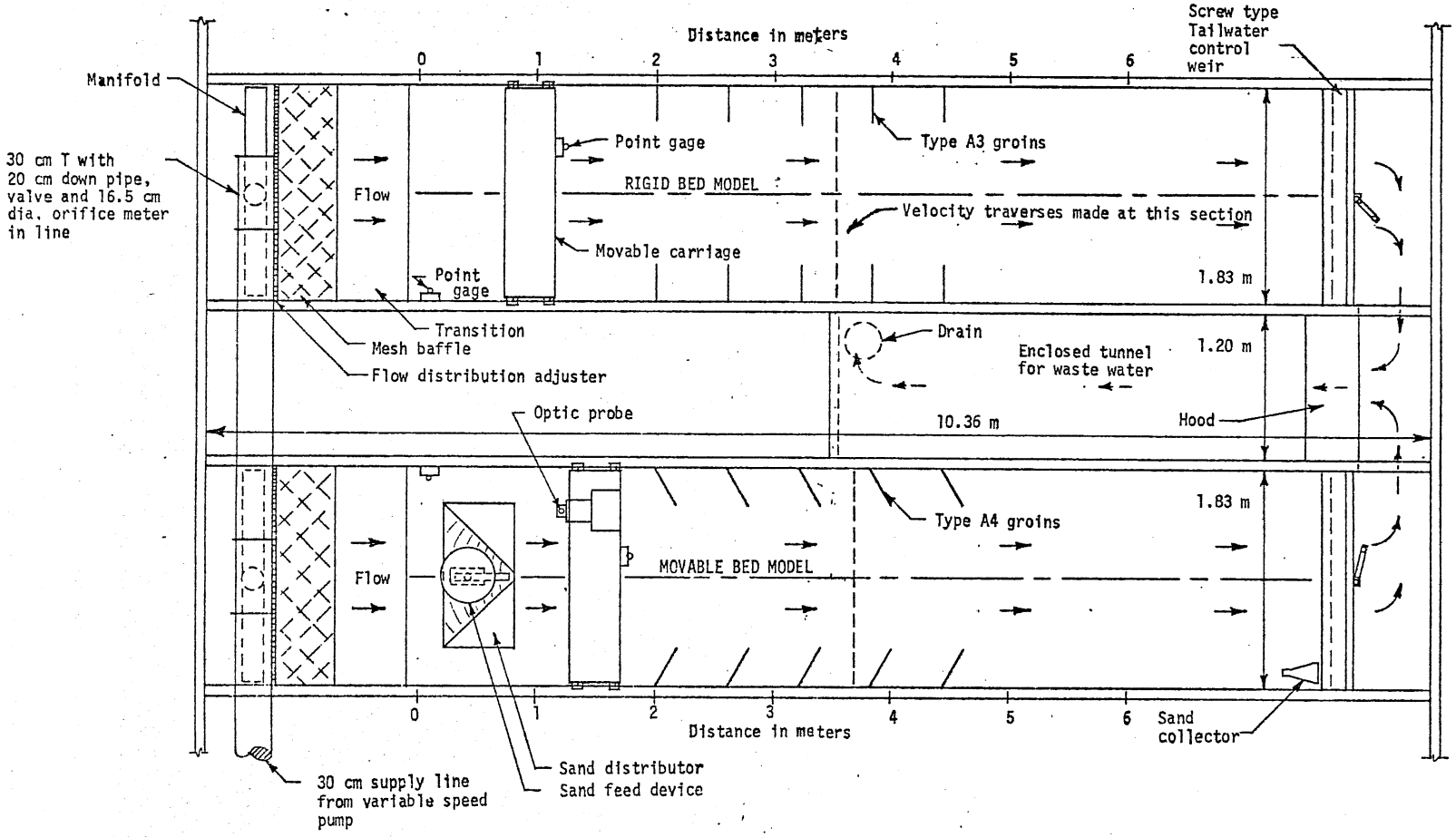

Fig. 8 - Overall Model Layout

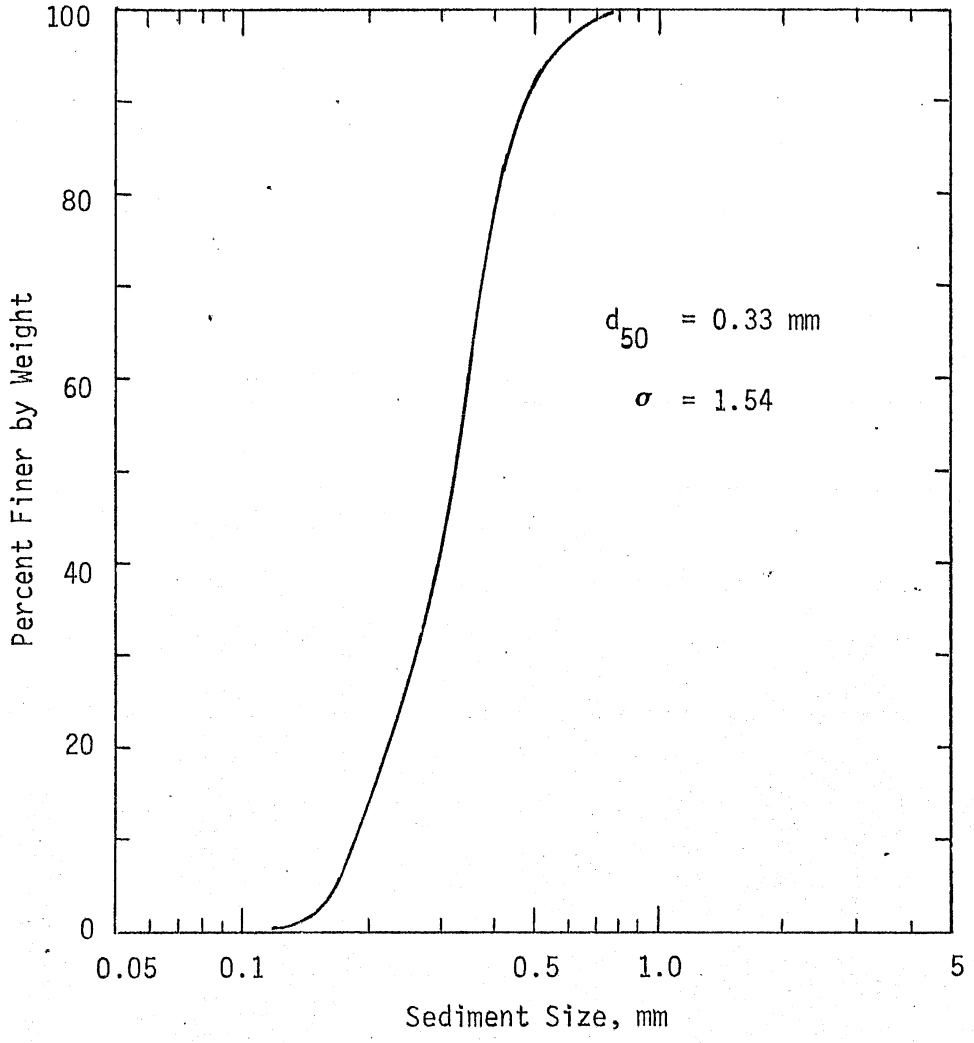

Fig. 9 - Size Distribution of Bed Material

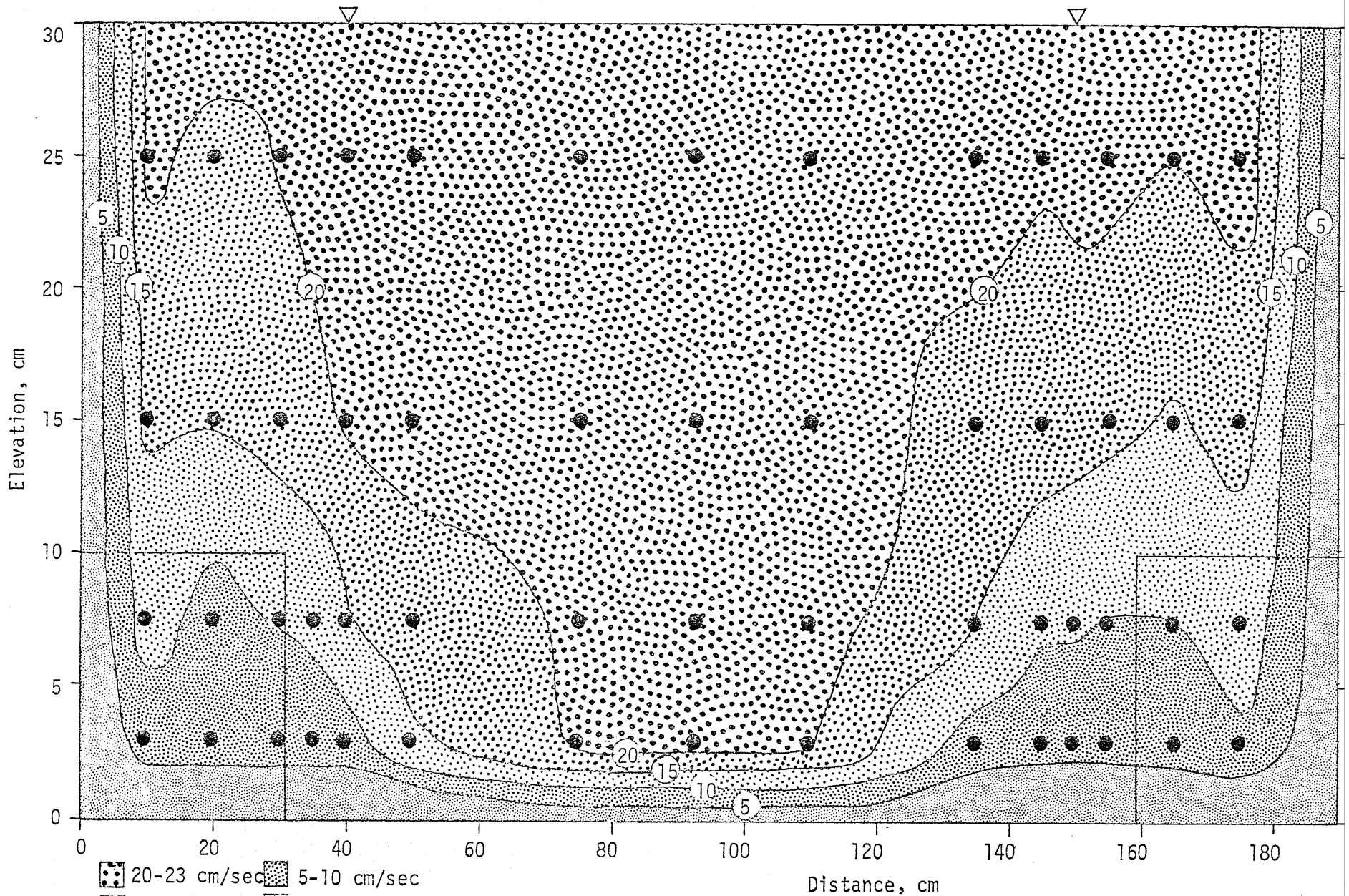

Fig. 10 - Typical Velocity Distribution at x = 370 cm, Rigid Bed Model Type A4, Run No. 26, Q = 100 lps, D_1 = 30 cm

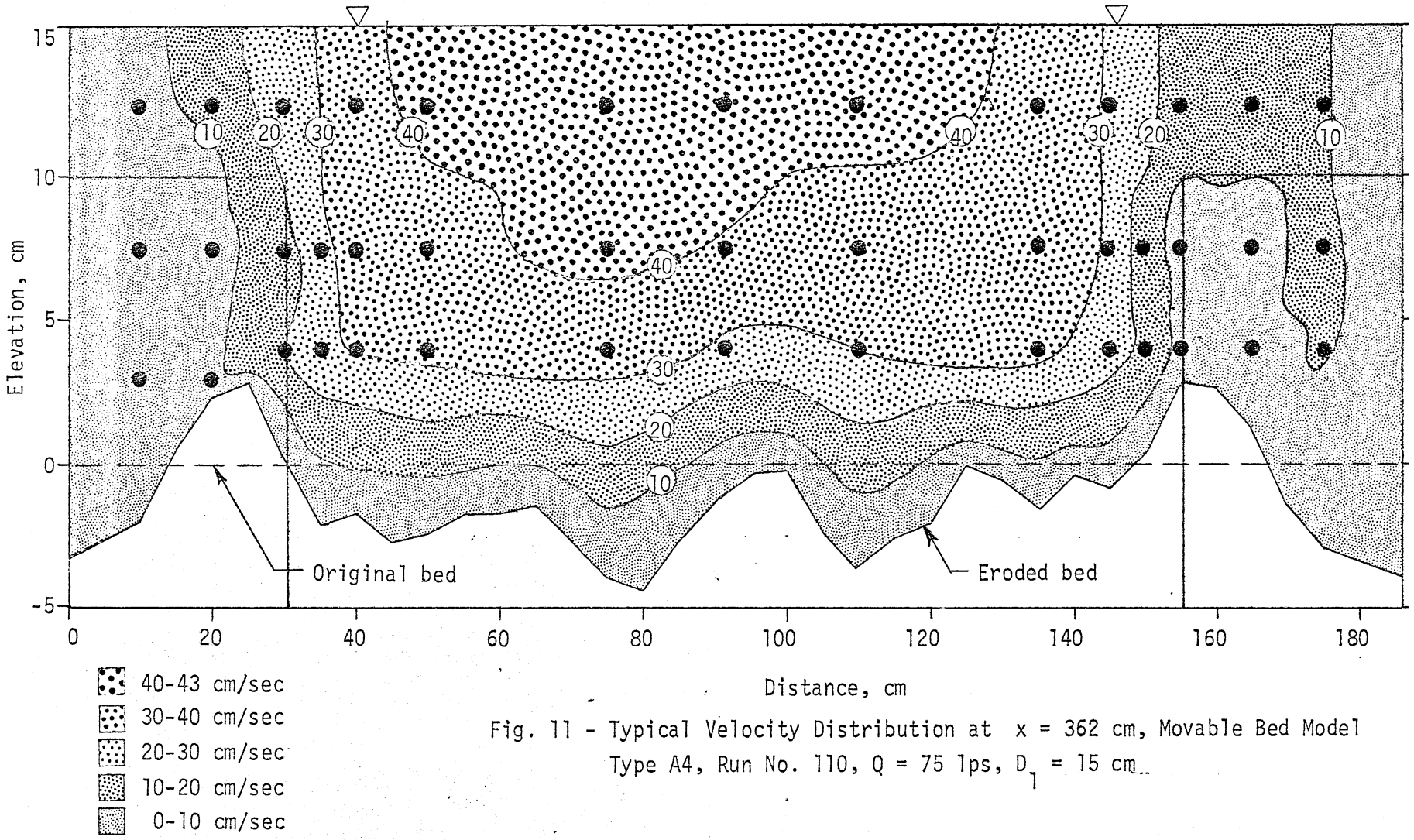

Fig. 11 - Typical Velocity Distribution at x = 362 cm, Movable Bed Model Type A4, Run No. 110, Q = 75 lps, D_1 = 15 cm.

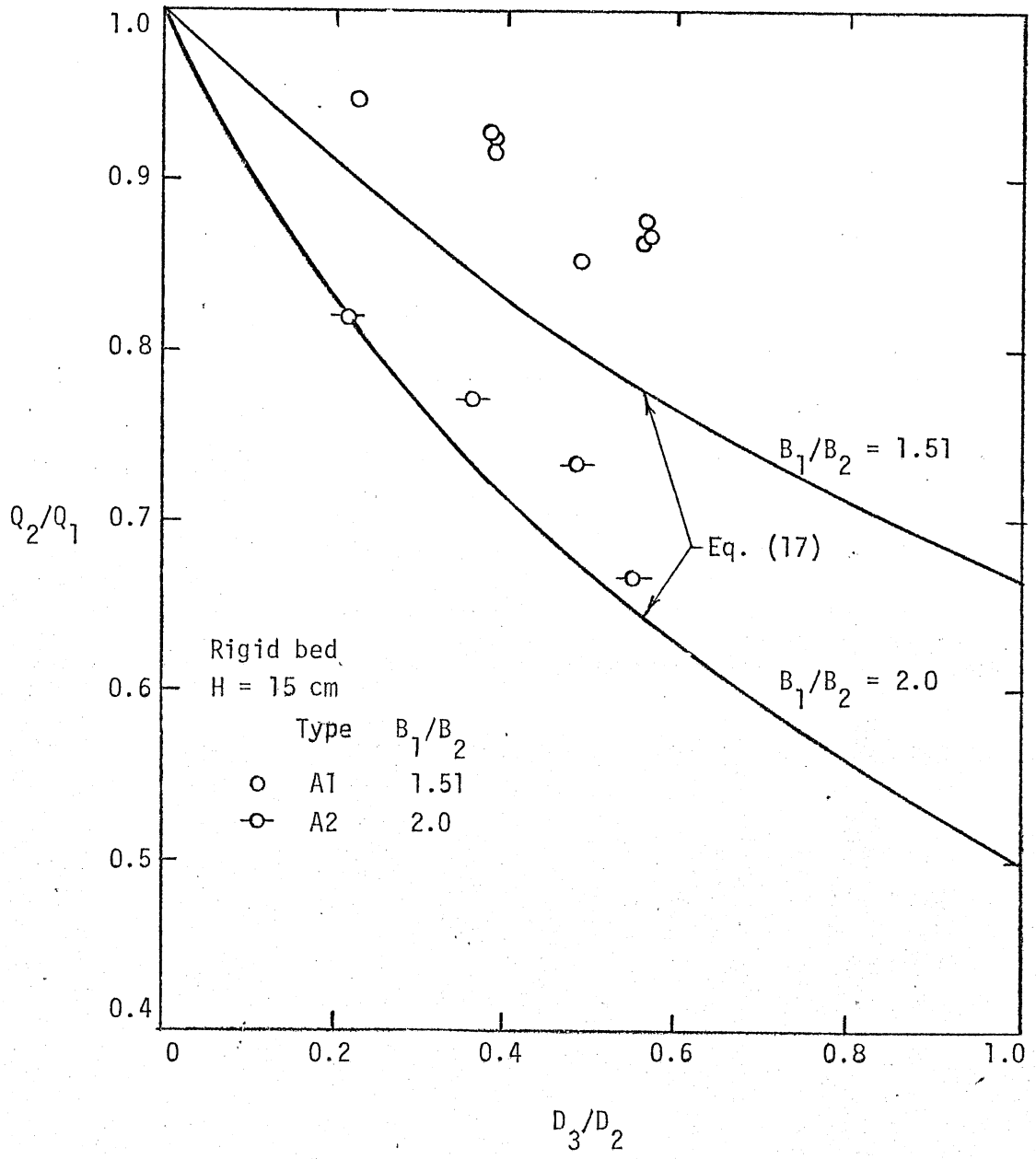

Fig. 12 - Discharge Ratio as a Function of Submergence Ratio Types A1 and A2

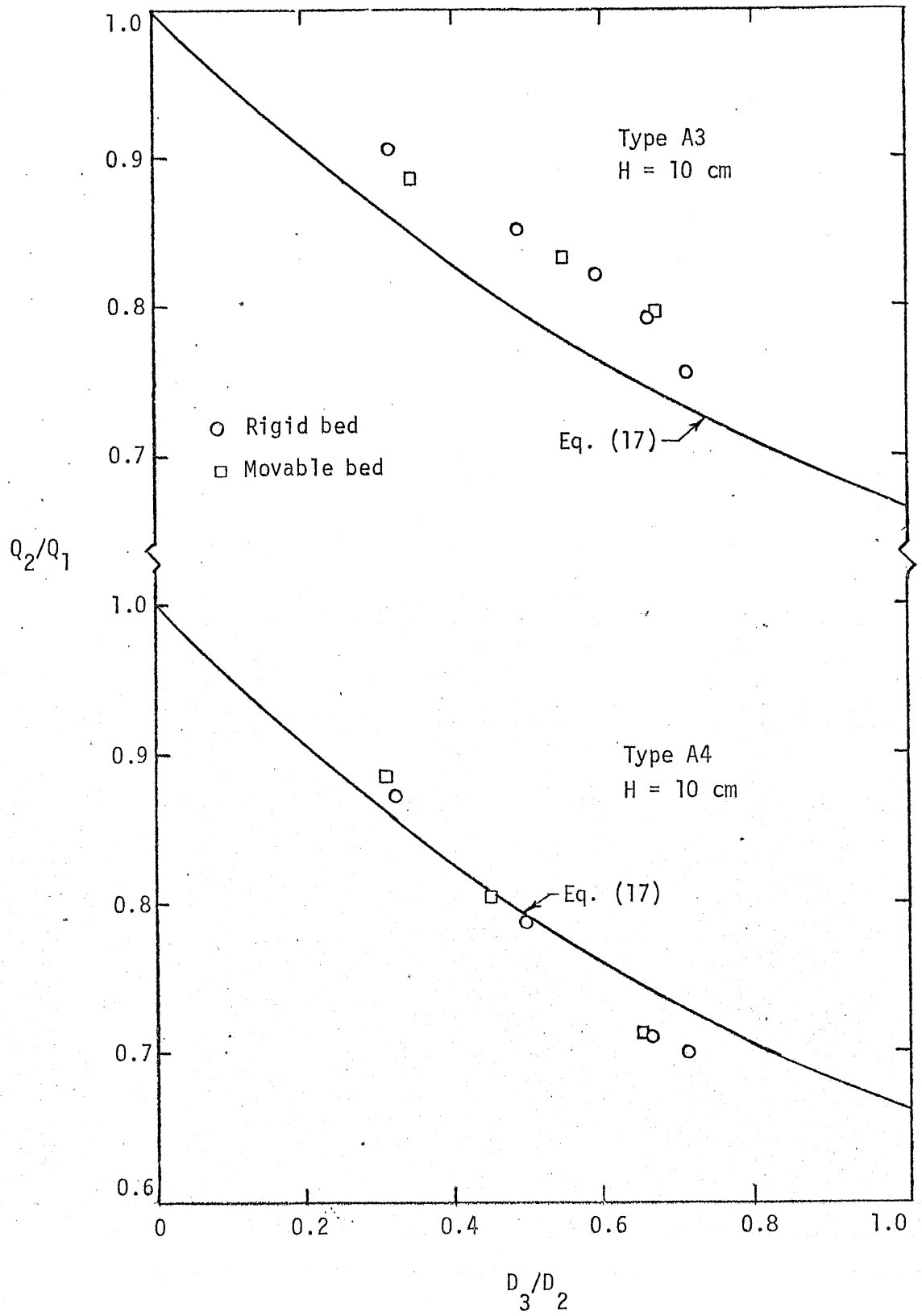

Fig. 13 - Discharge Ratio as a Function of Submergence Ratio
Types A3 and A4

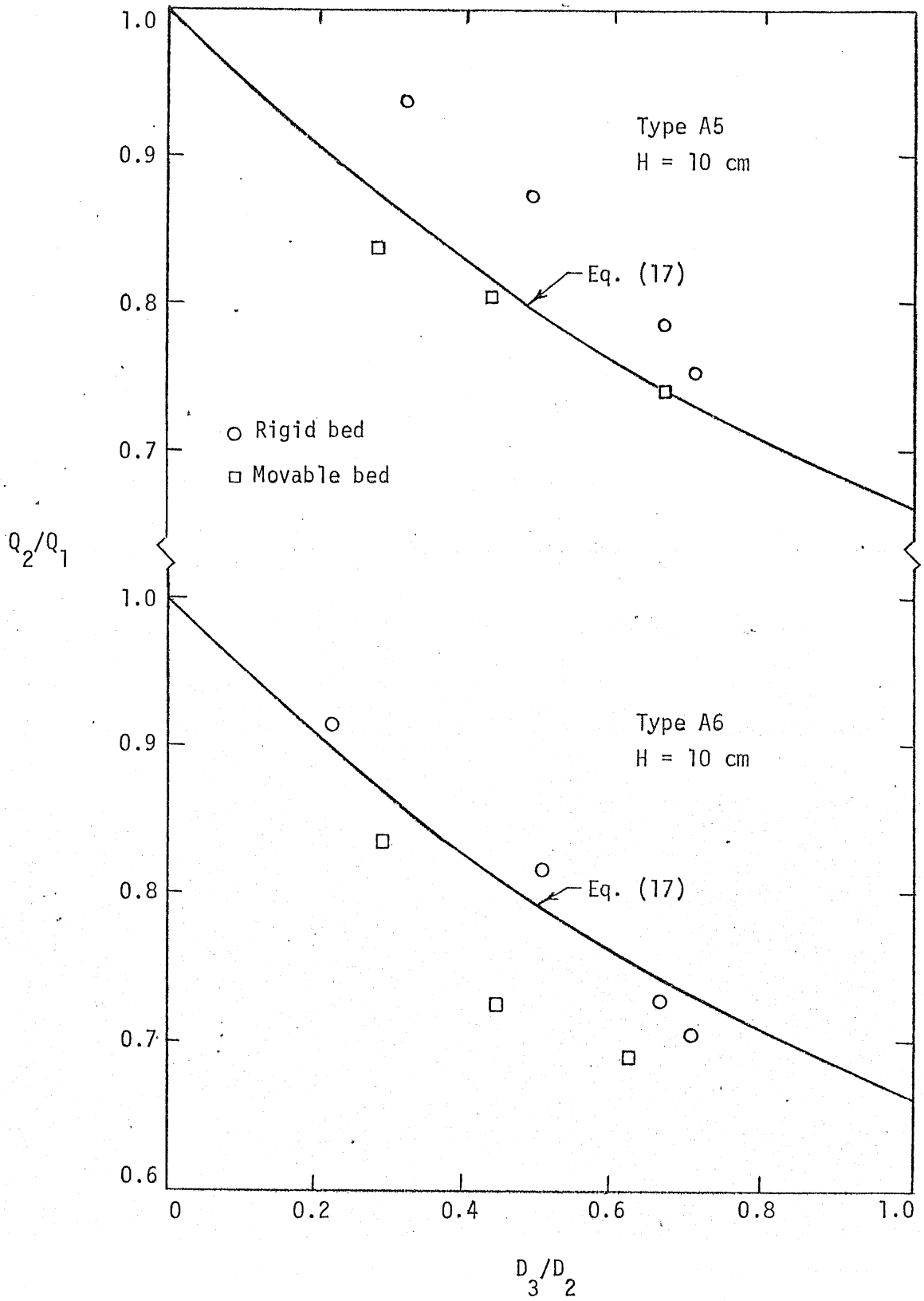

Fig. 14 - Discharge Ratio as a Function of Submergence Ratio
Types A5 and A6

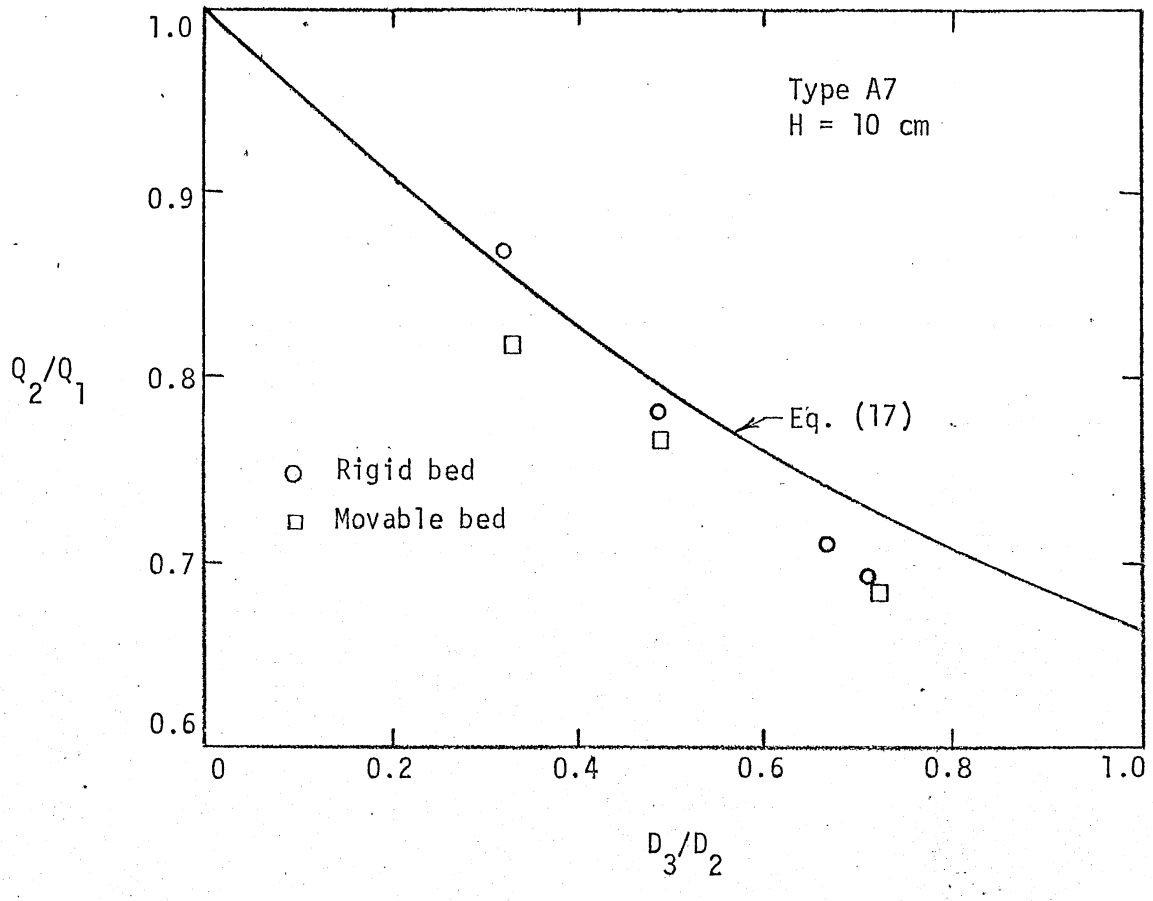

Fig. 15 - Discharge Ratio as a Function of Submergence Ratio Type A7

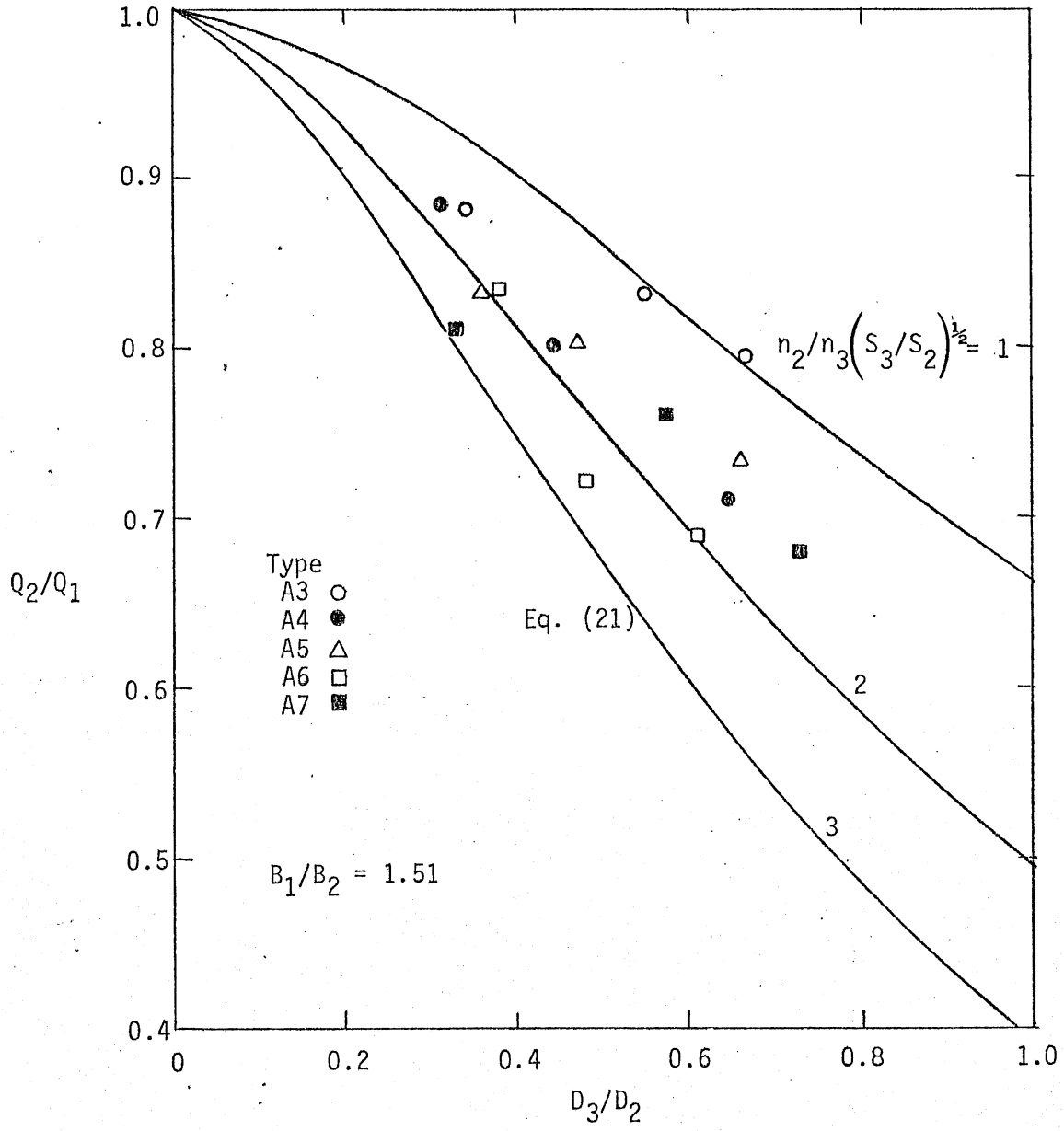

Fig. 16 - Effect of Roughness on Relative Discharge Ratio.

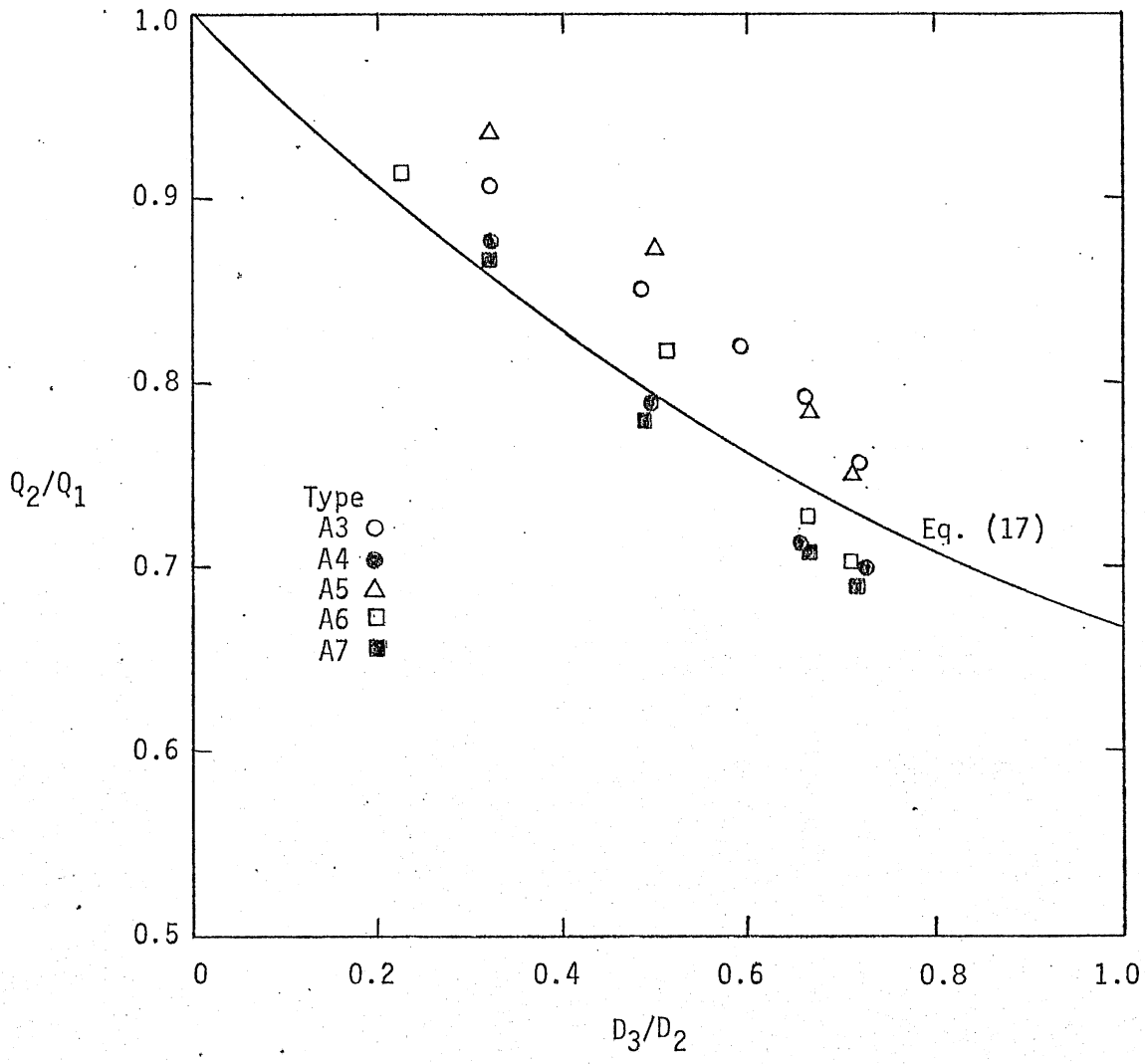

Fig. 17 - Discharge Ratios for Various Groin Geometries
Rigid Bed Model

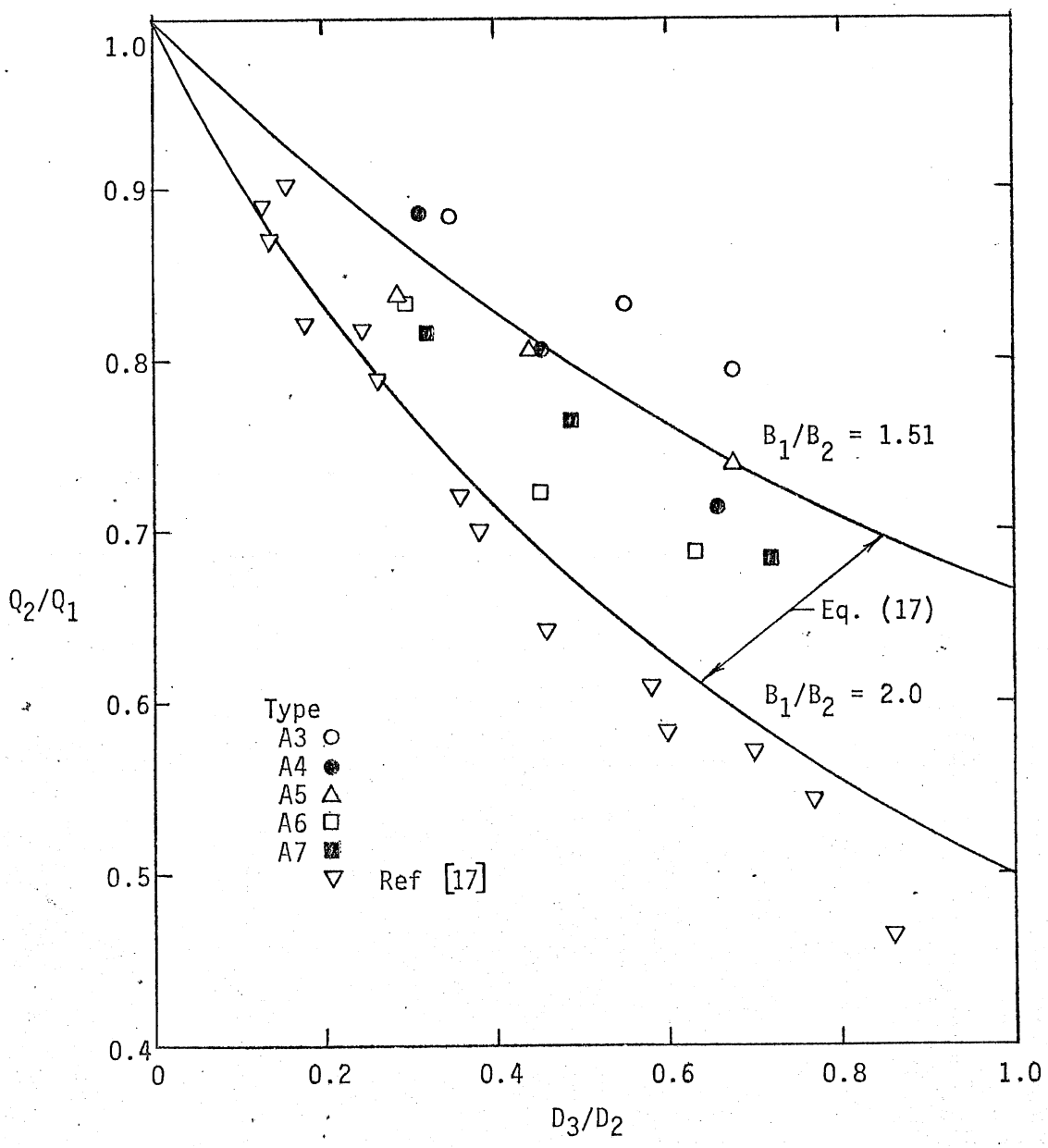

Fig. 18 - Discharge Ratios for Various Groin Geometries. Movable Bed Model

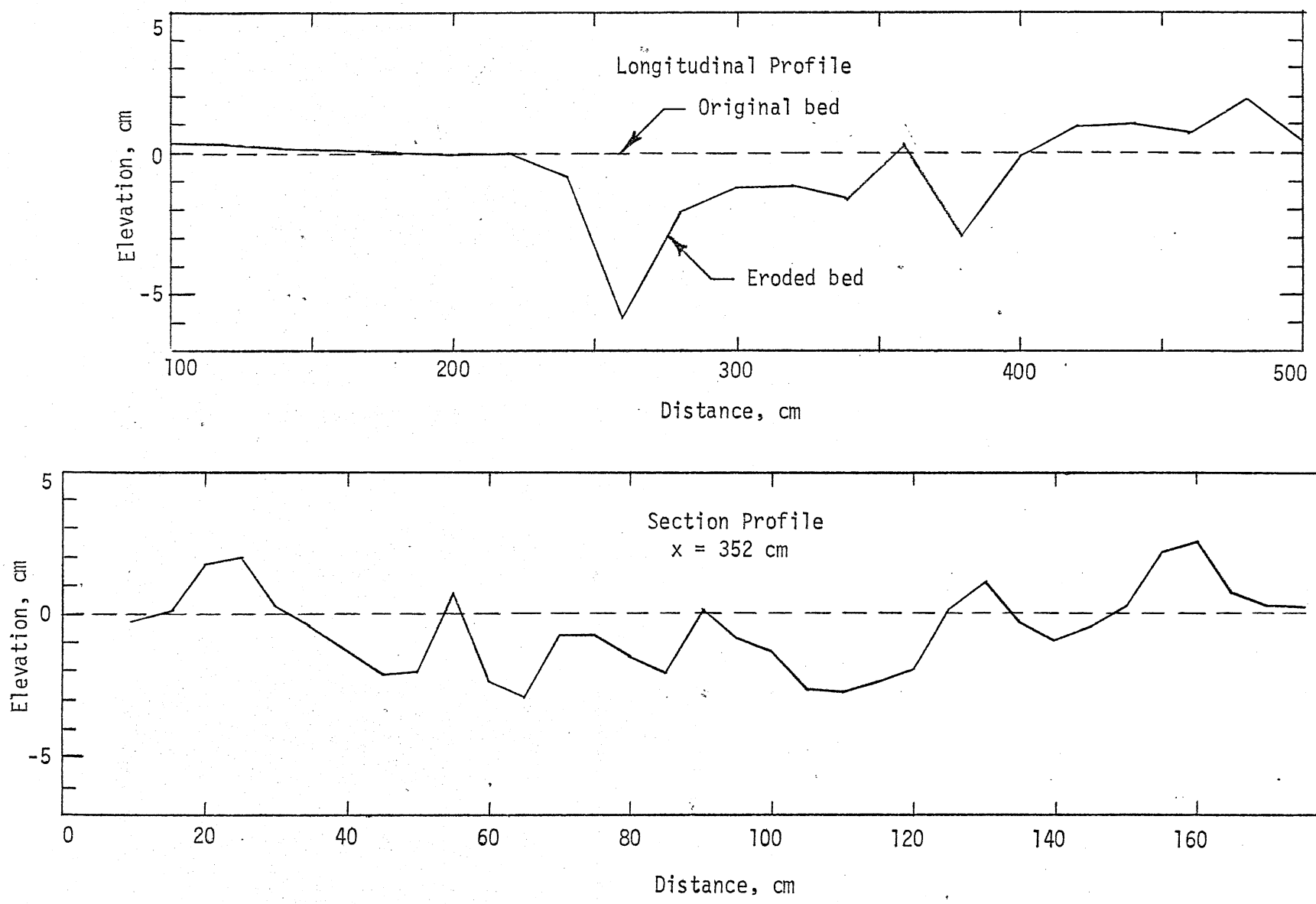

Fig. 19 - Centerline Longitudinal and Section Bed Profiles
Type A3, Run No. 107, $Q_1 \sim 75$ lps, $D_1 \sim 15$ cm

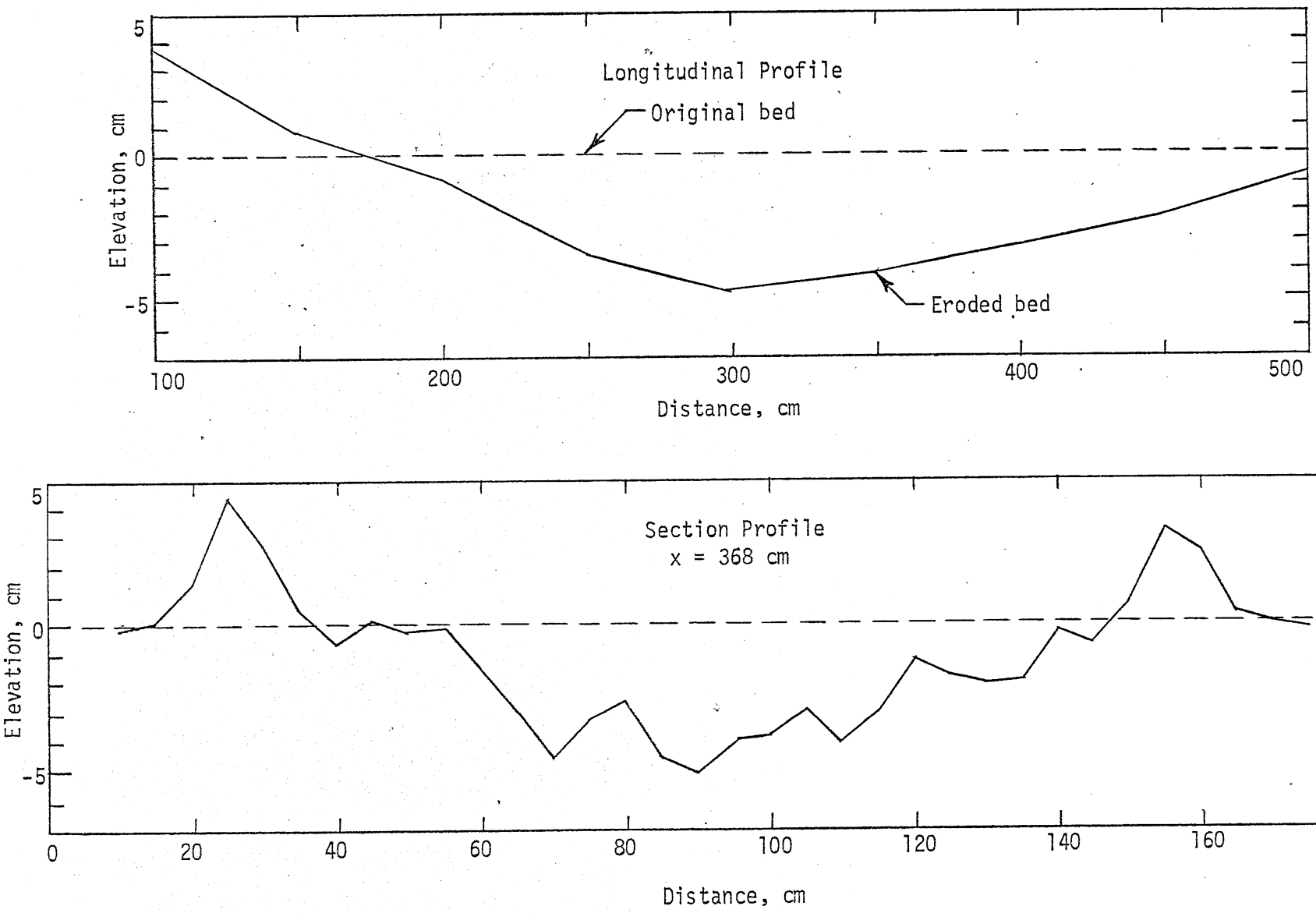

Fig. 20 - Centerline Longitudinal and Section Bed Profiles
Type A4, Run No. 120, $Q_1 \sim 50$ lps, $D_1 \sim 9$ cm

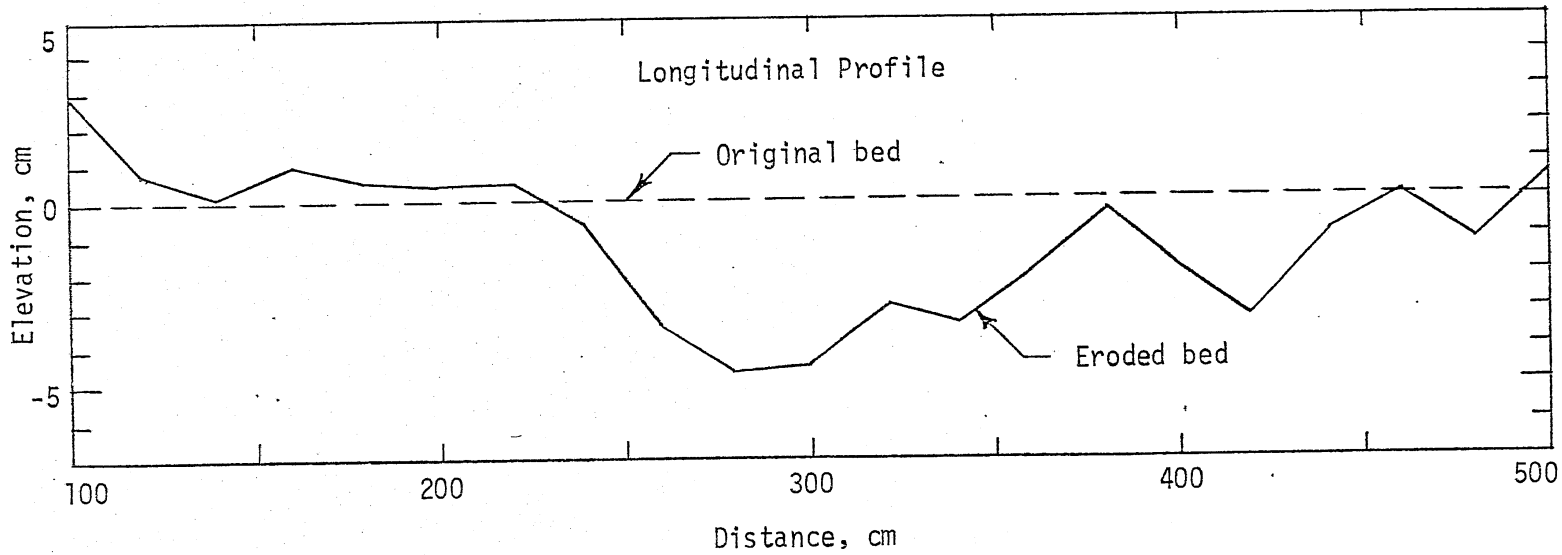

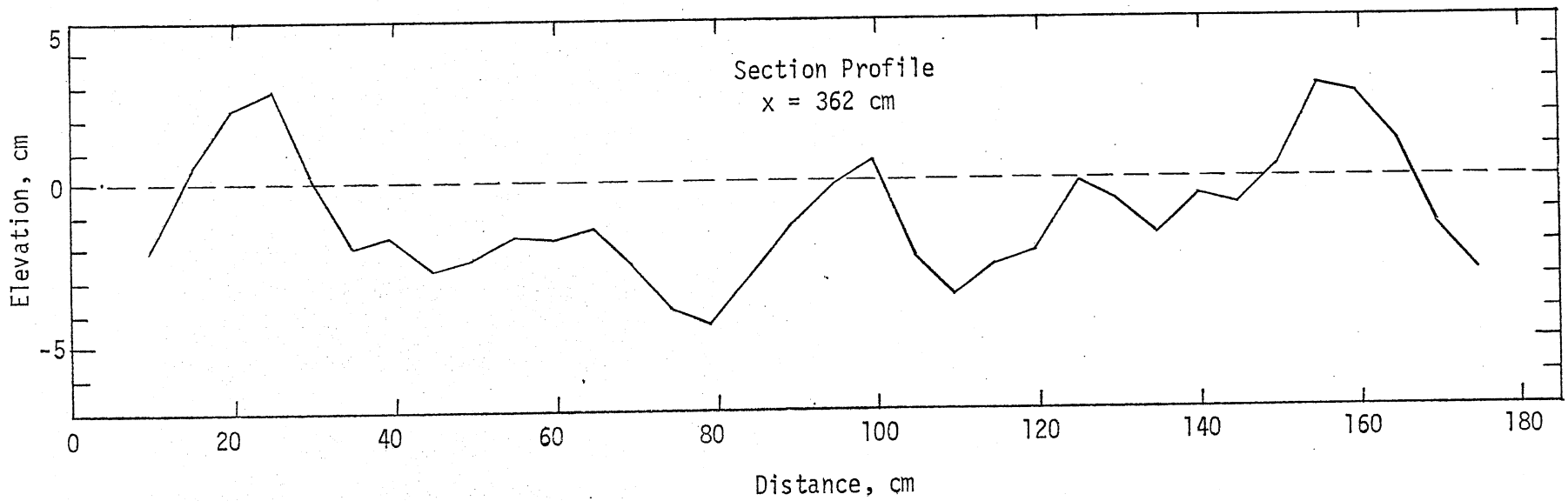

Fig. 21 - Centerline Longitudinal and Section Bed Profiles
Type A4, Run No. 110, $Q_1 \sim 75$ lps, $D_1 \sim 15$ cm

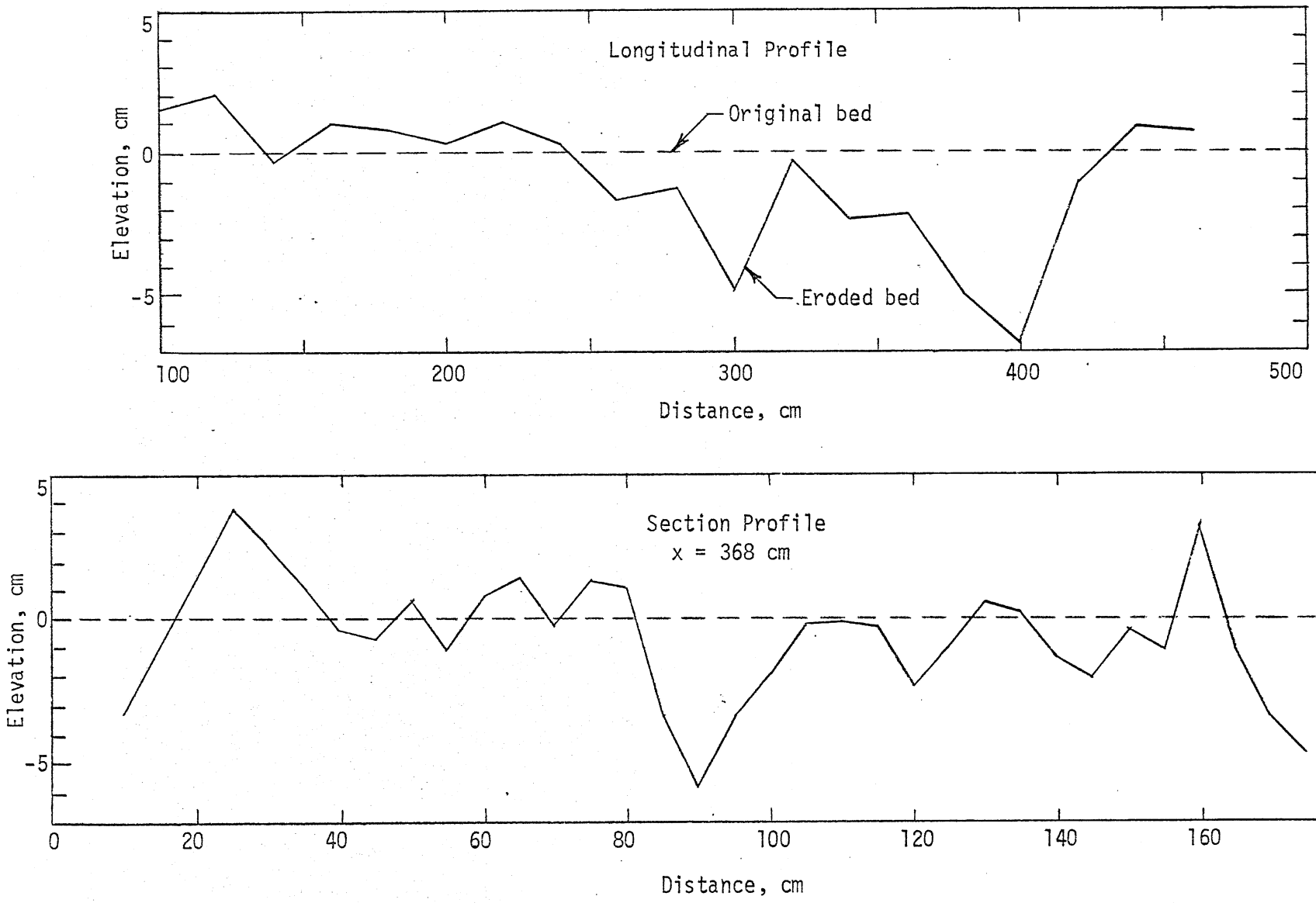

Fig. 22 - Centerline Longitudinal and Section Bed Profiles
Type A4, Run No. 109, $Q_1 \sim 100$ lps, $D_1 \sim 20$ cm

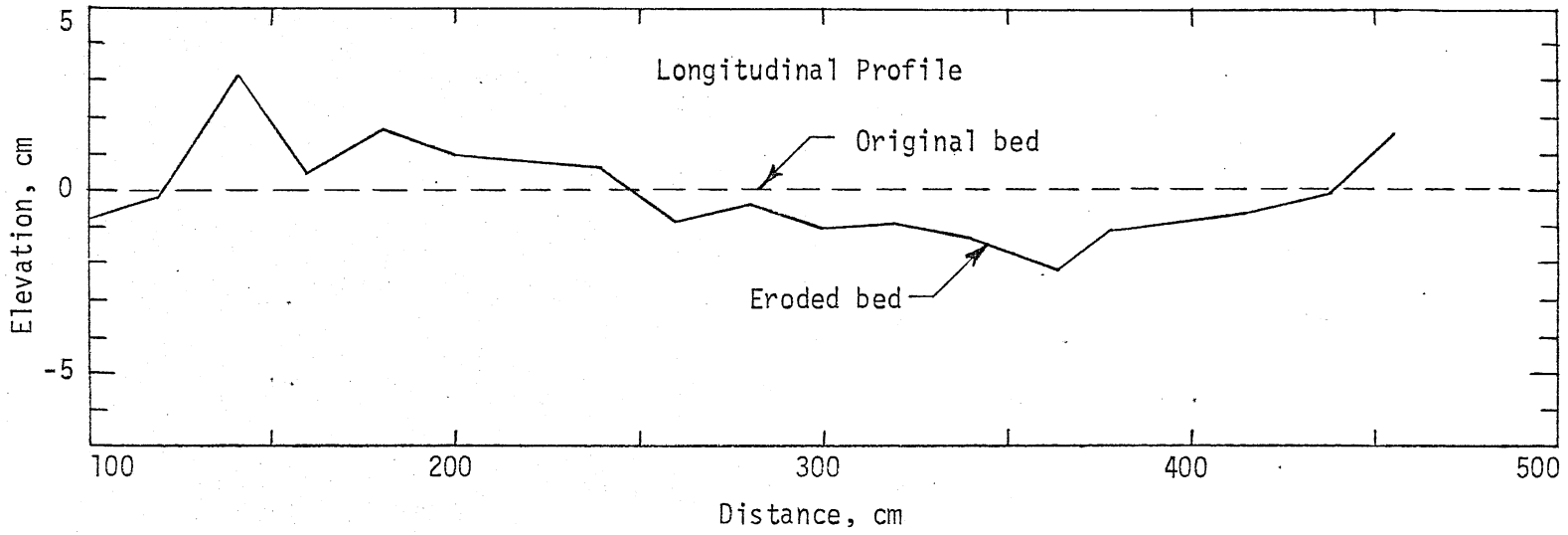

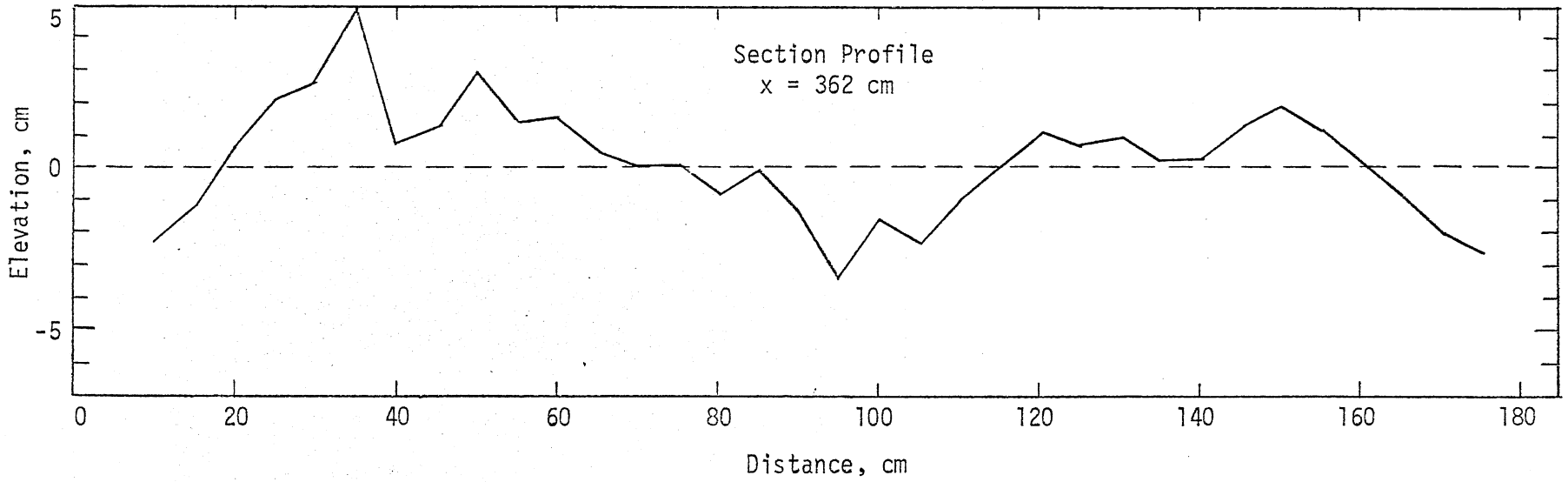

Fig. 23 - Centerline Longitudinal and Section Bed Profiles
Type A4, Run No. 108, $Q_1 \sim 150$ lps, $D_1 \sim 30$ cm

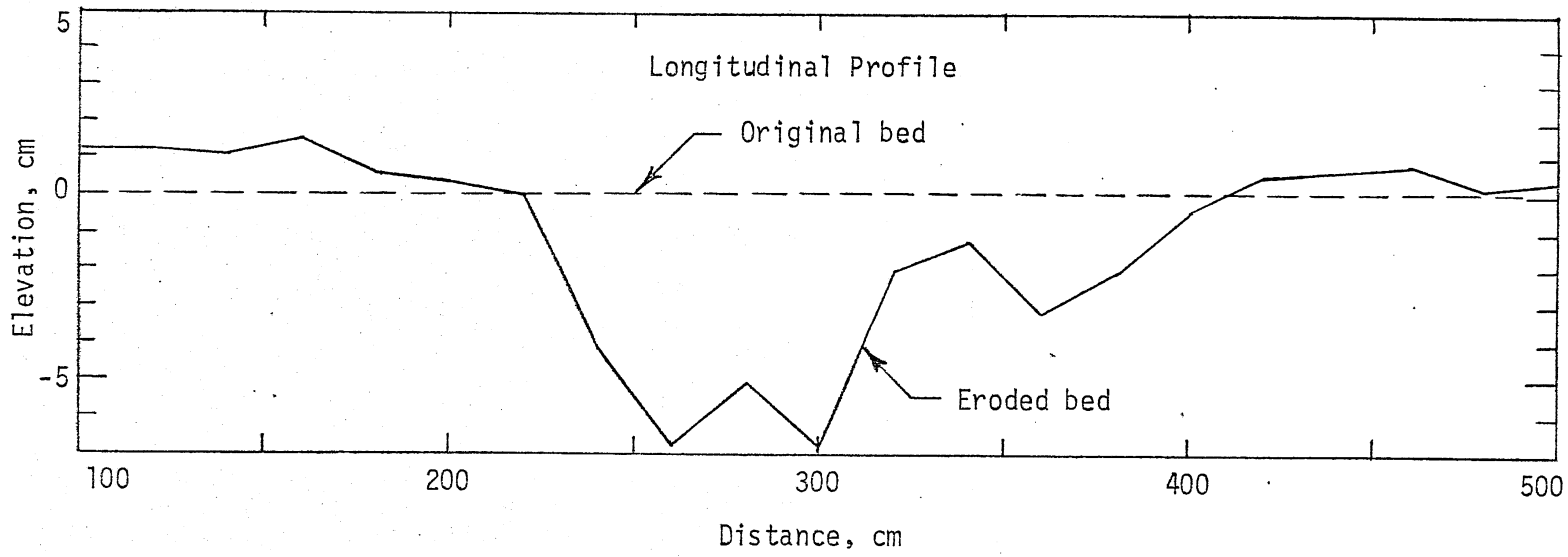

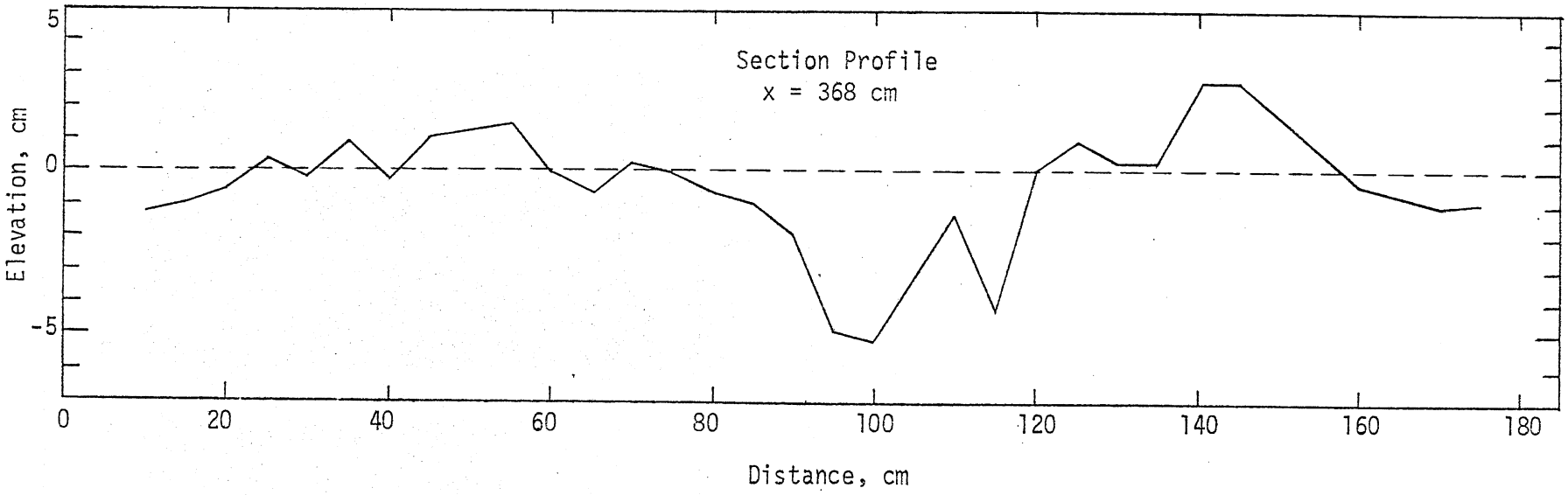

Fig. 24 - Centerline Longitudinal and Section Bed Profiles
Type A5, Run No. 113, $Q_1 \sim 75$ lps, $D_1 \sim 15$ cm

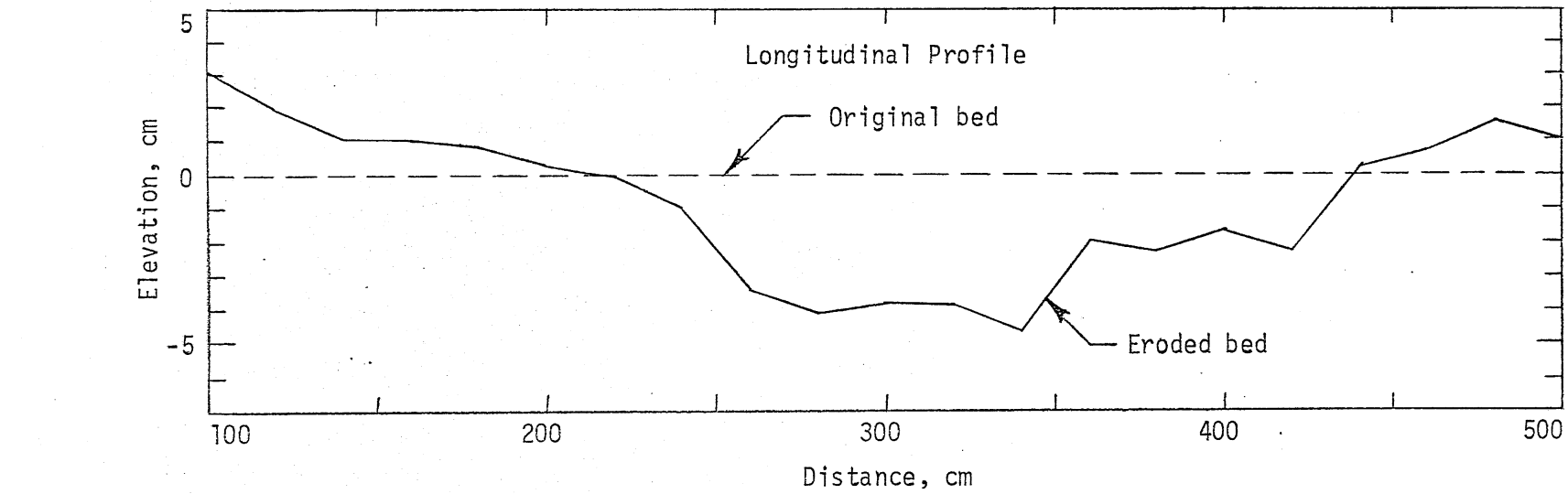

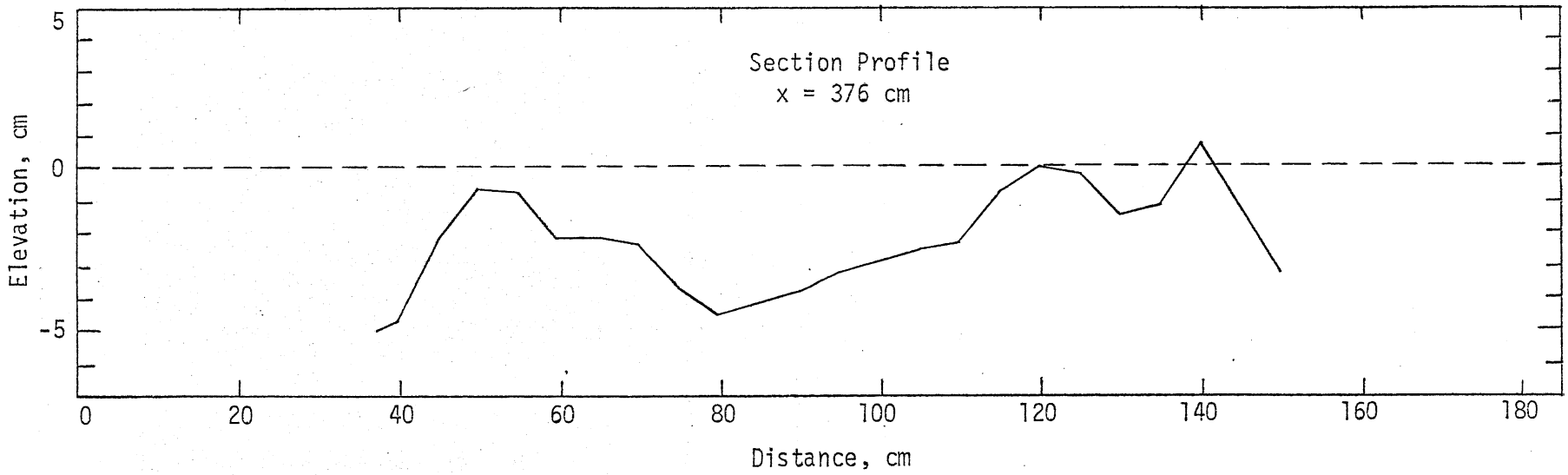

Fig. 25 - Centerline Longitudinal and Section Bed Profiles
Type A6, Run No. 116, $Q_1 \sim 75$ lps, $D_1 \sim 15$ cm

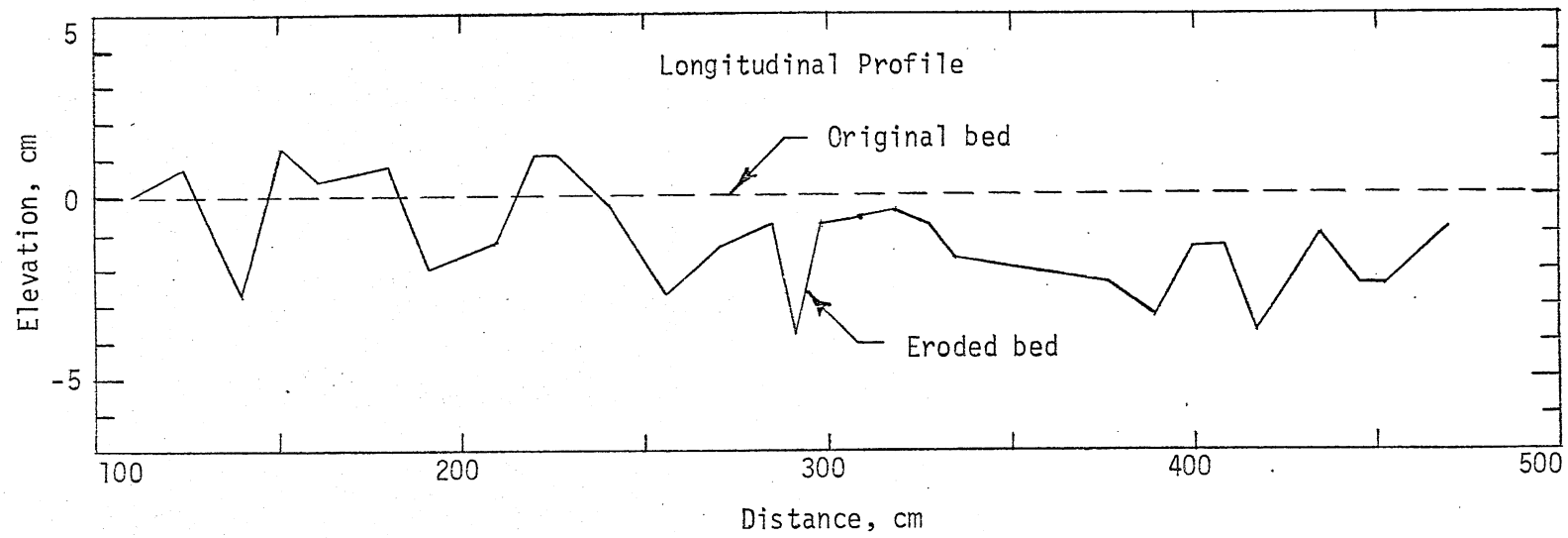

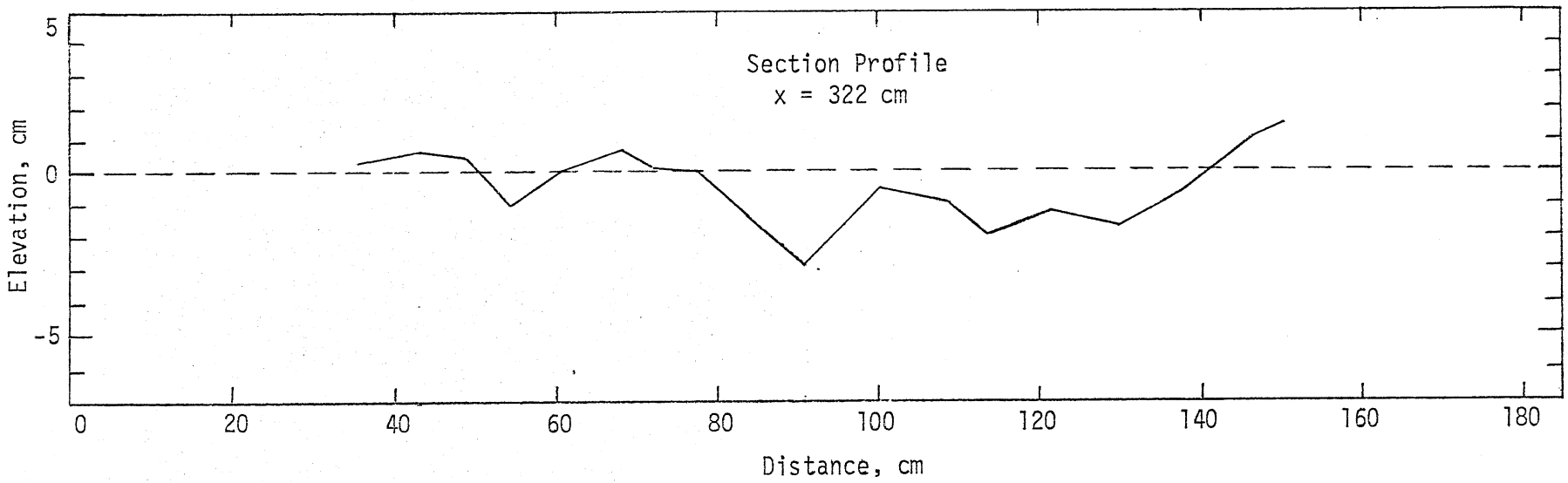

Fig. 26 - Centerline Longitudinal and Section Bed Profiles
Type A7, Run No. 119, $Q_1 \sim 75$ lps, $D_1 \sim 15$ cm

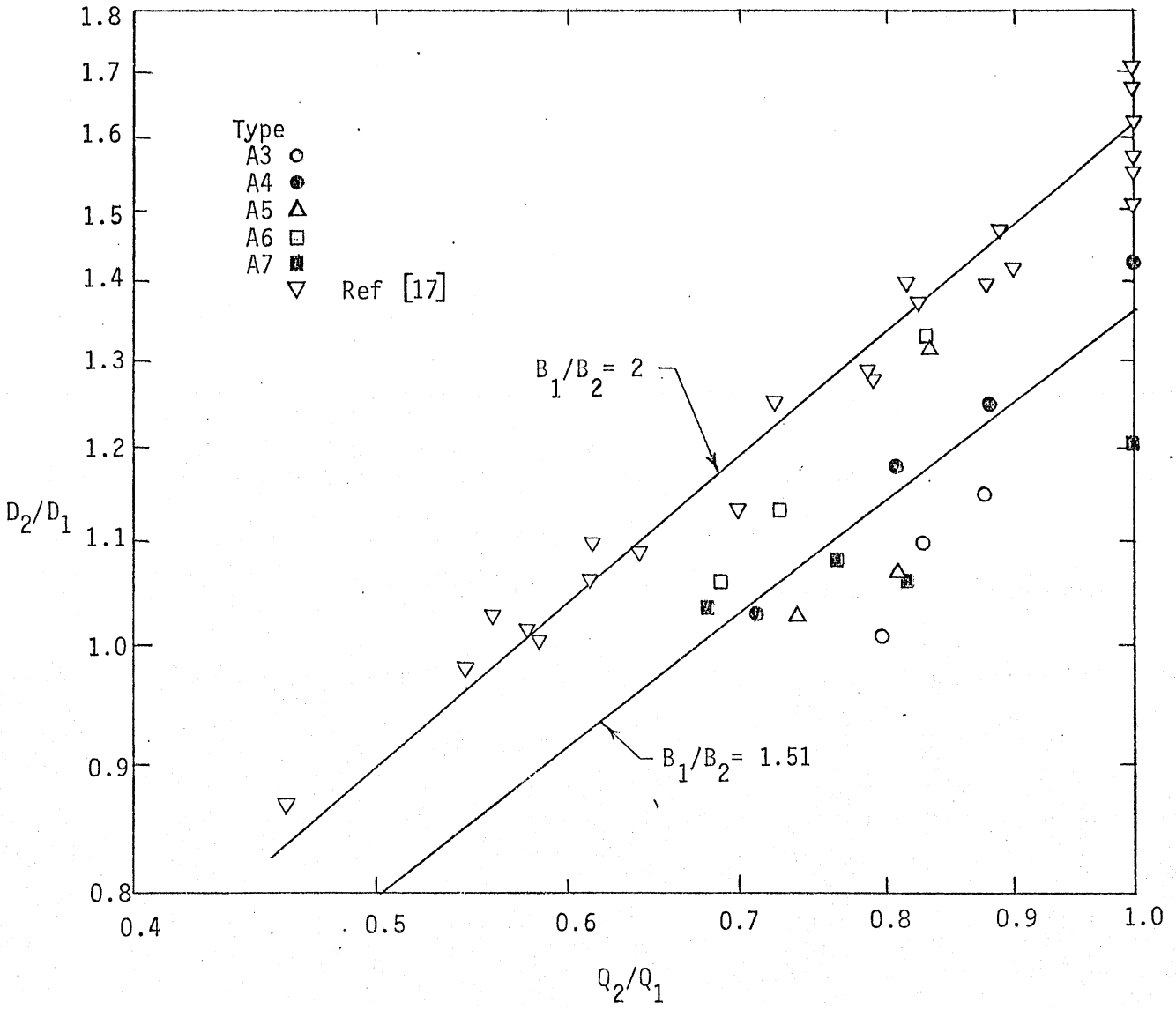

Fig. 27 - Logarithmic Plot of Relative Depth Ratio as a Function of Relative Discharge Ratio.

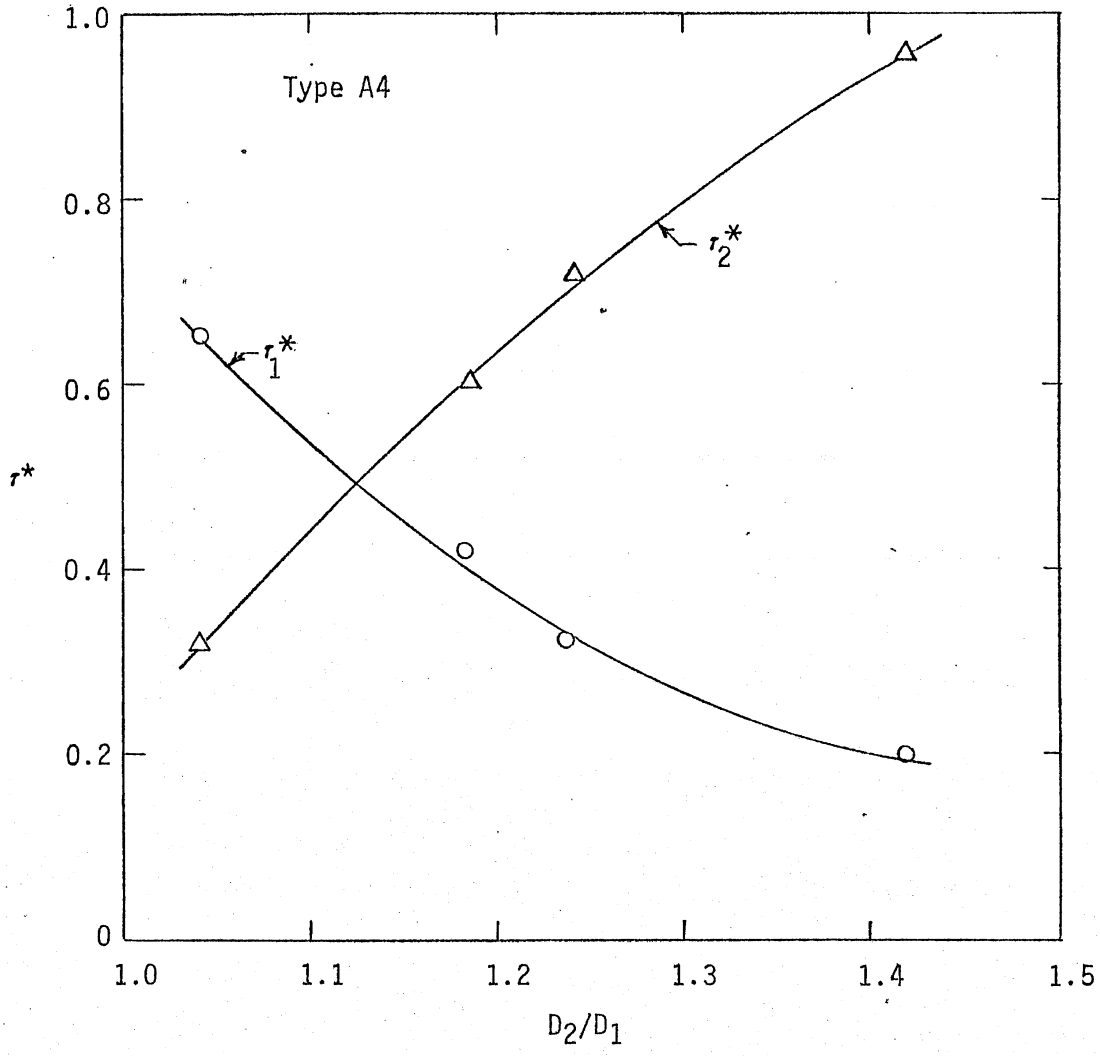

Fig. 28 - Variation of Shields Shear Stress with Relative Depth Ratio.

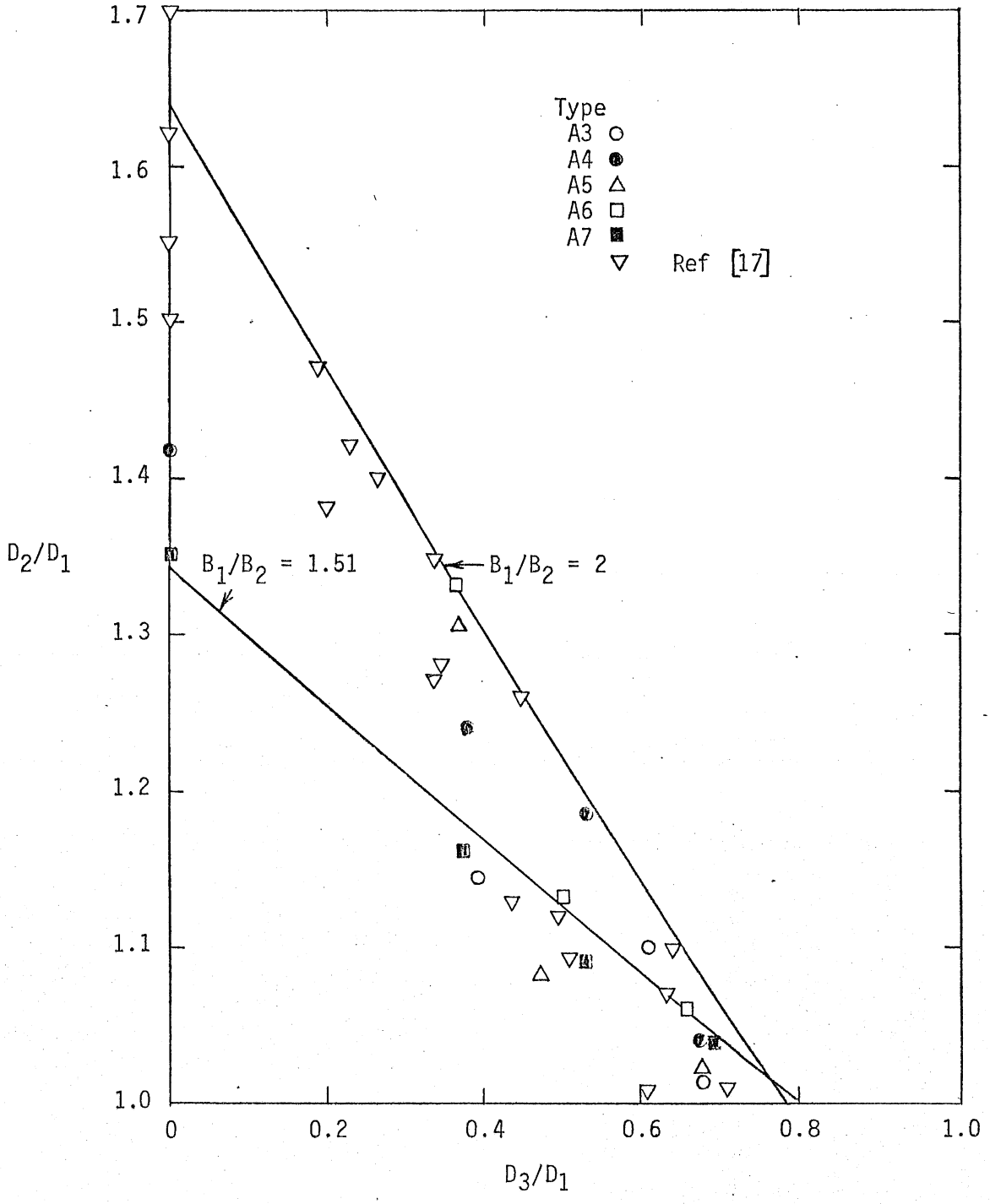

Fig. 29 - Relative Depth Ratio as a Function of Relative Groin Submergence Ratio.

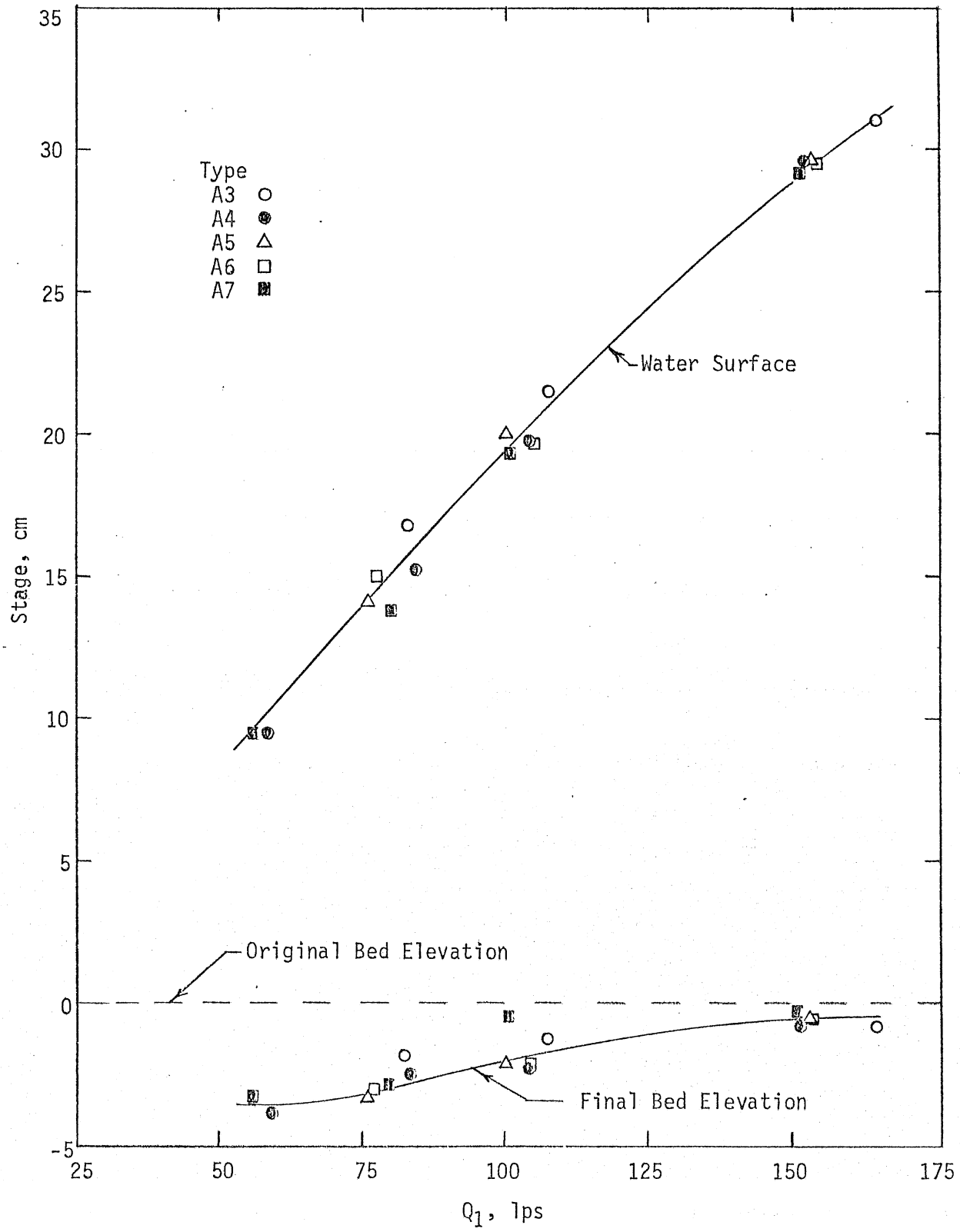

Fig. 30 - Bed Elevation in Contracted Section for Various Discharge and Groin Geometries.

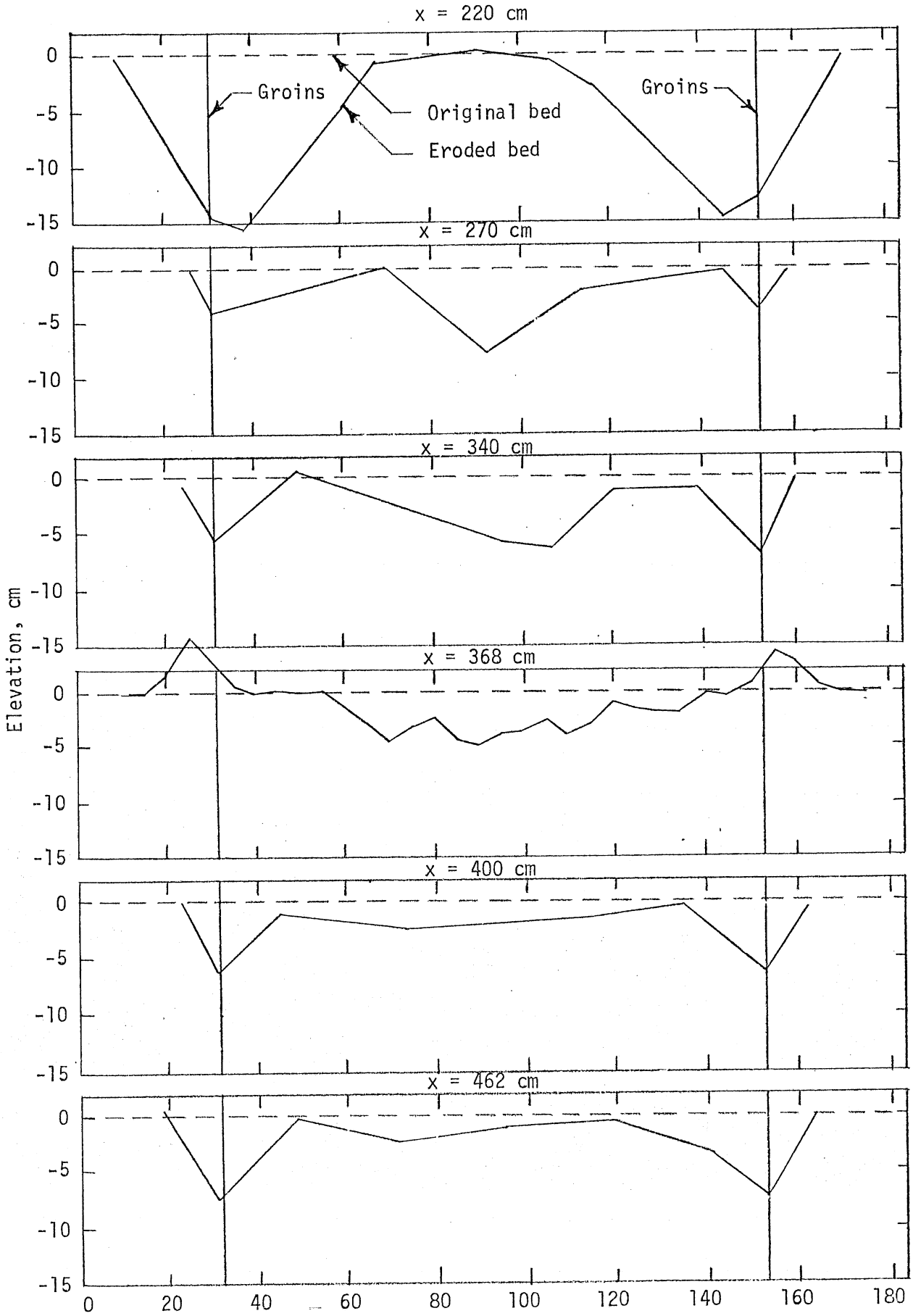

Fig. 31 - Section Bed Profiles at Various Stations
Type A4, Run No. 120, $Q_1 \sim 50$ lps, $D_1 \sim 9$ cm

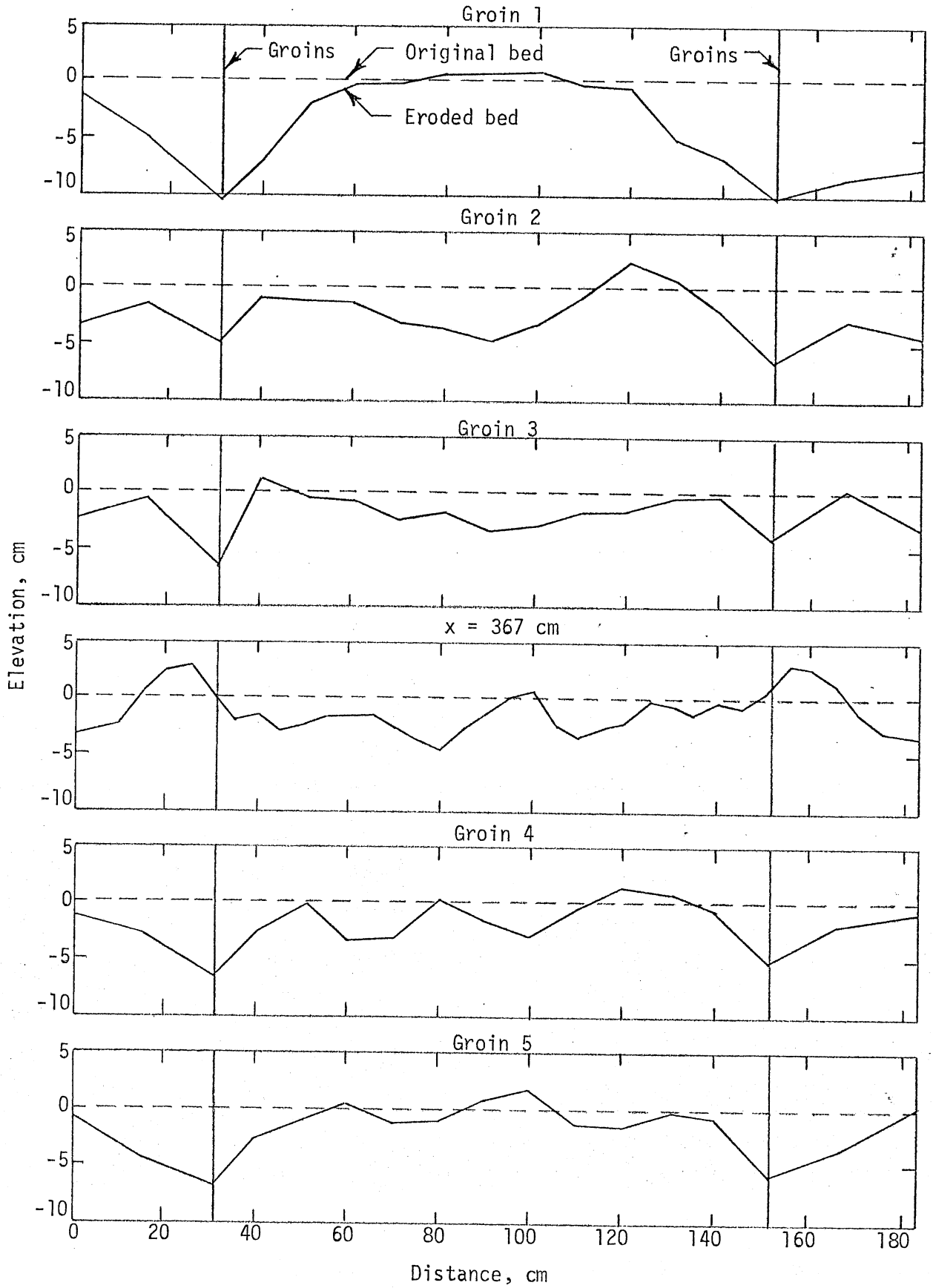

Fig. 32 - Section Bed Profiles at Various Stations
Type A4, Run No. 110, Q_1 ~75 lps, D_1 ~15 cm

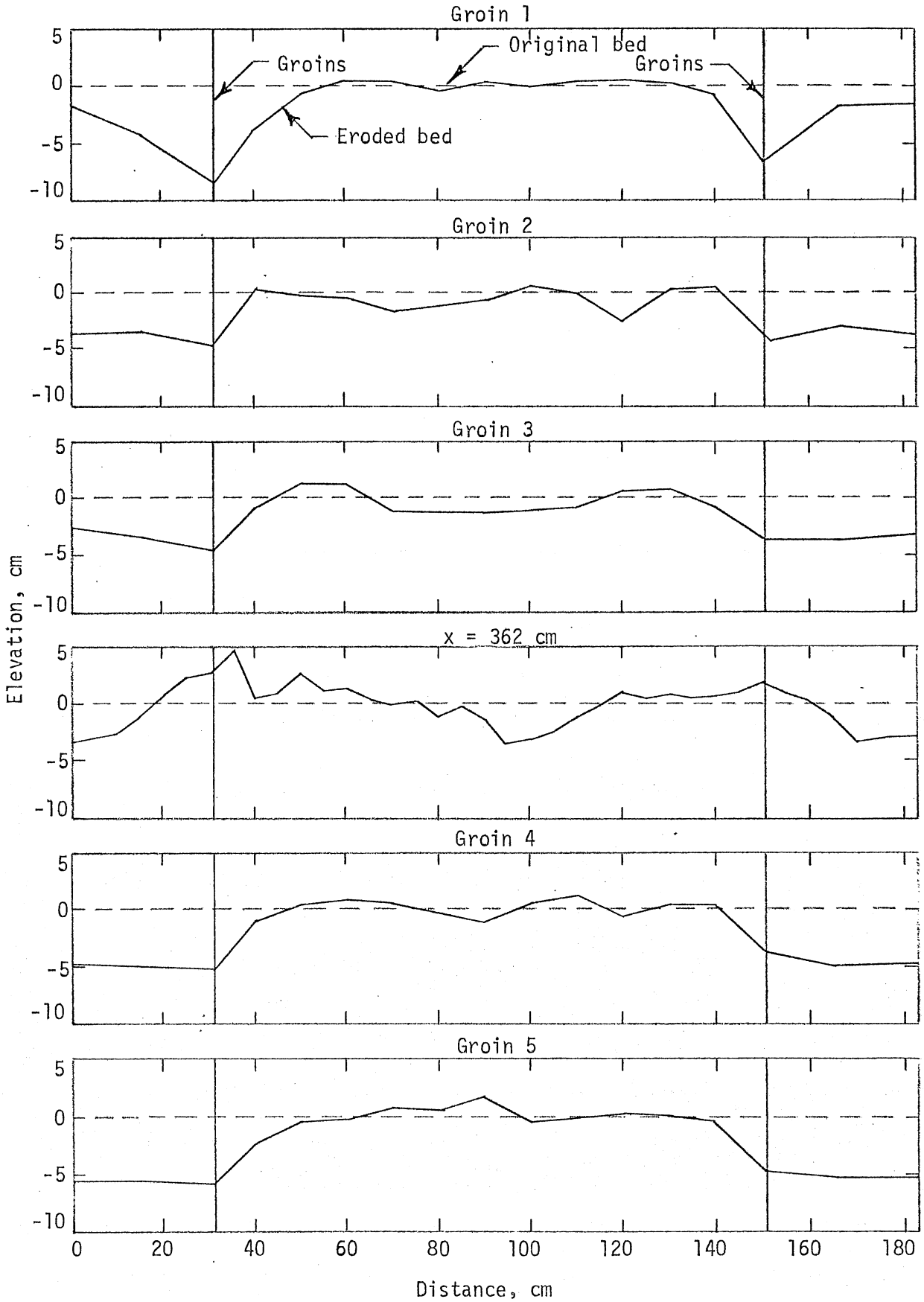

Fig. 33 - Section Bed Profiles at Various Stations
Type A4, Run No. 108, $Q_1 \sim 100$ lps, $D_1 \sim 30$ cm

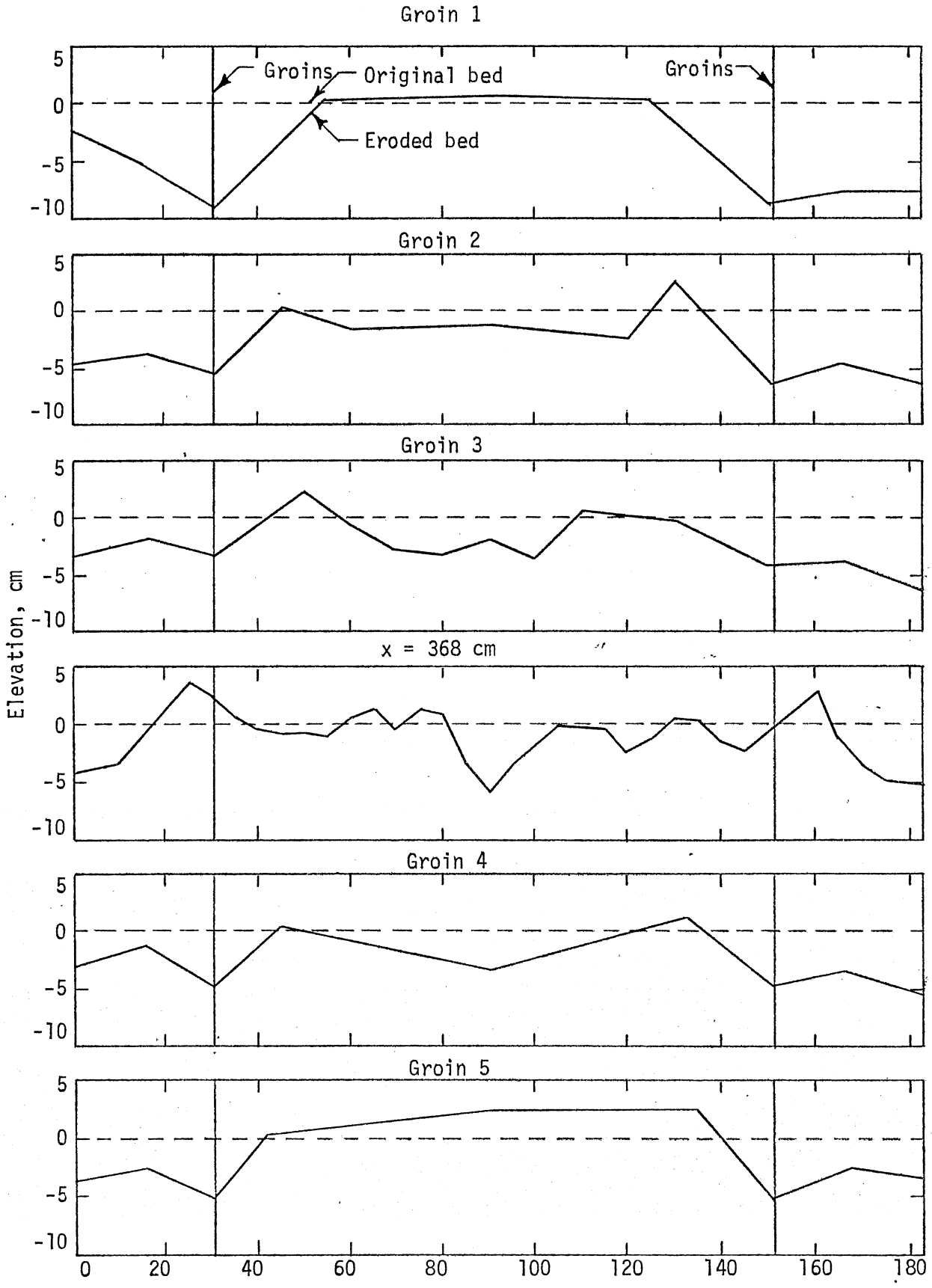

Fig. 34 - Section Bed Profiles at Various Stations
Type A4, Run No. 109, $Q_1 \sim 150$ lps, $D_1 \sim 20$ cm

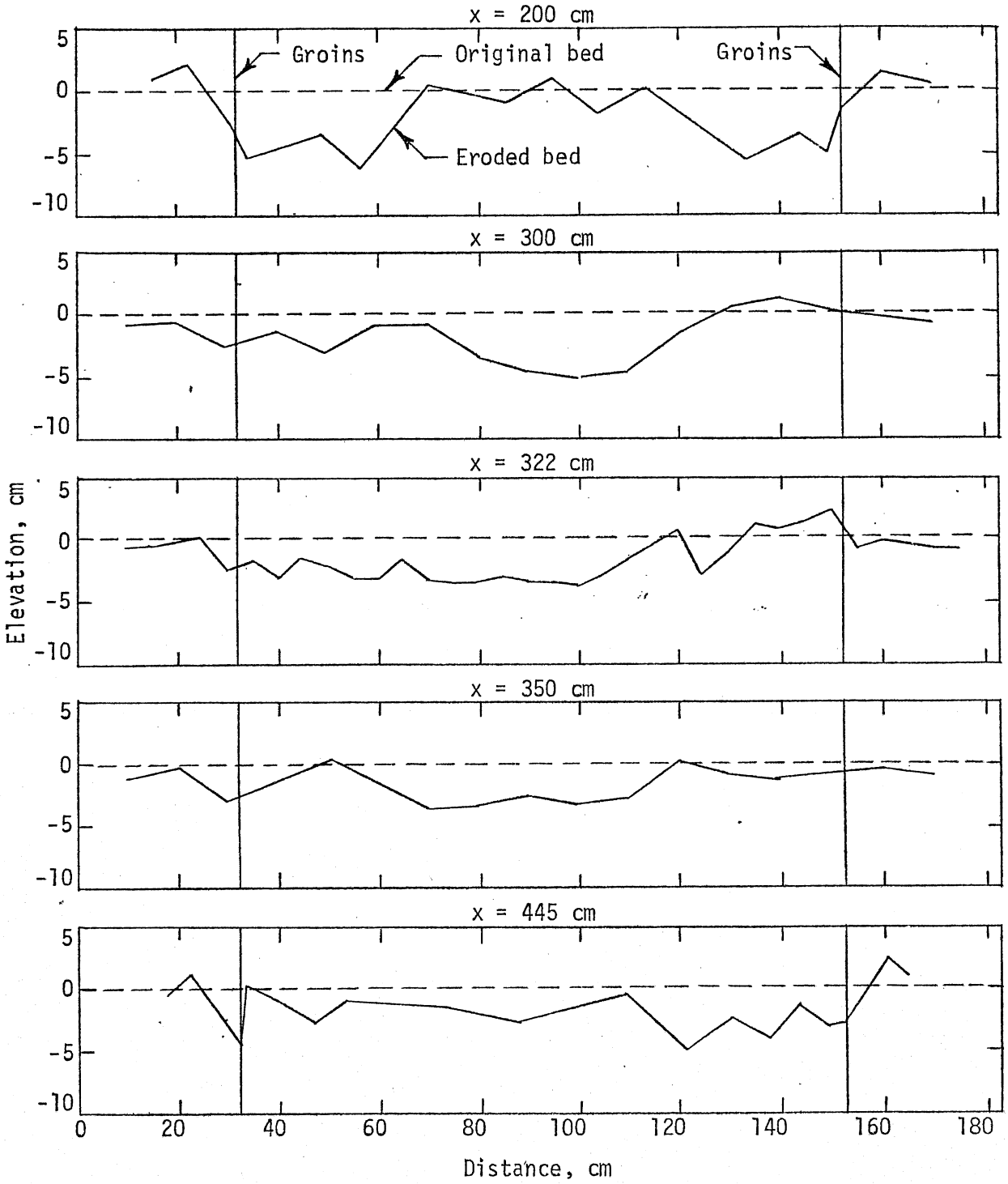

Fig. 35 - Section Bed Profiles at Various Stations
Type A7, Run No. 122, $Q_1 \sim 50$ lps, $D_1 \sim 9$ cm

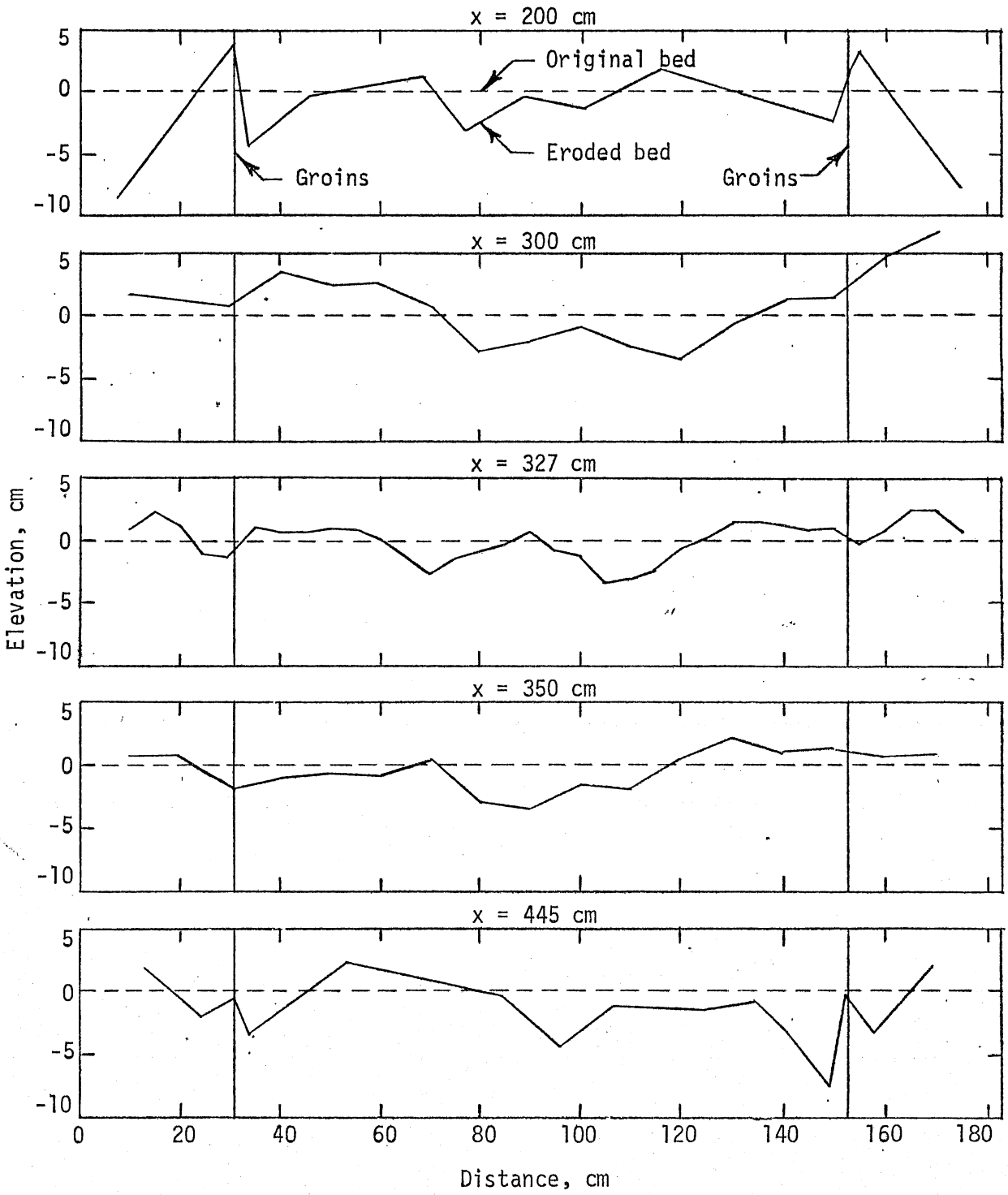

Fig. 36 - Section Bed Profiles at Various Stations
Type A7, Run No. 119, $Q_1 \sim 75$ lps, $D_1 \sim 15$ cm

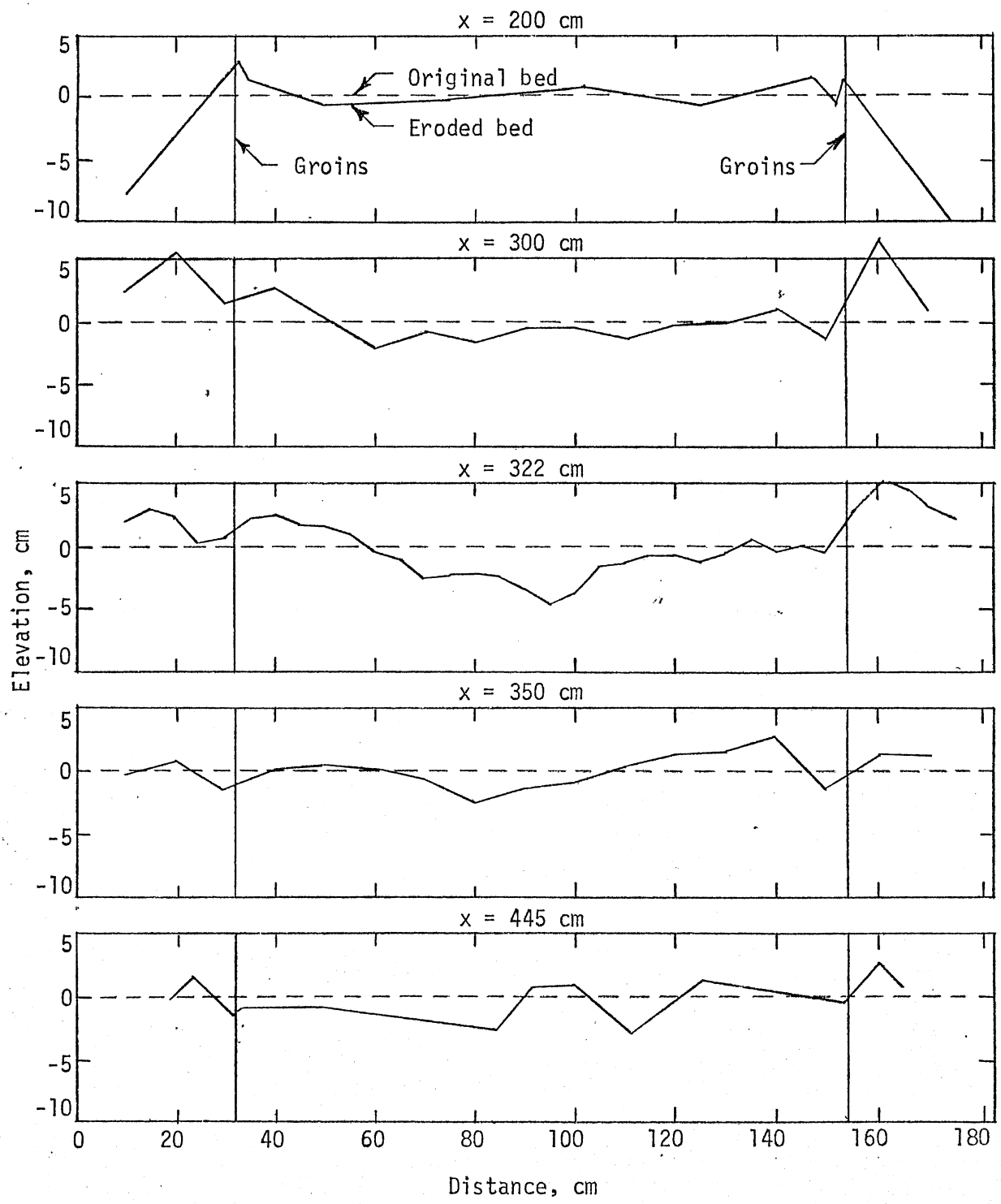

Fig. 37 - Section Bed Profiles at Various Stations
Type A7, Run No. 118, $Q_1 \sim 100$ lps, $D_1 \sim 20$ cm

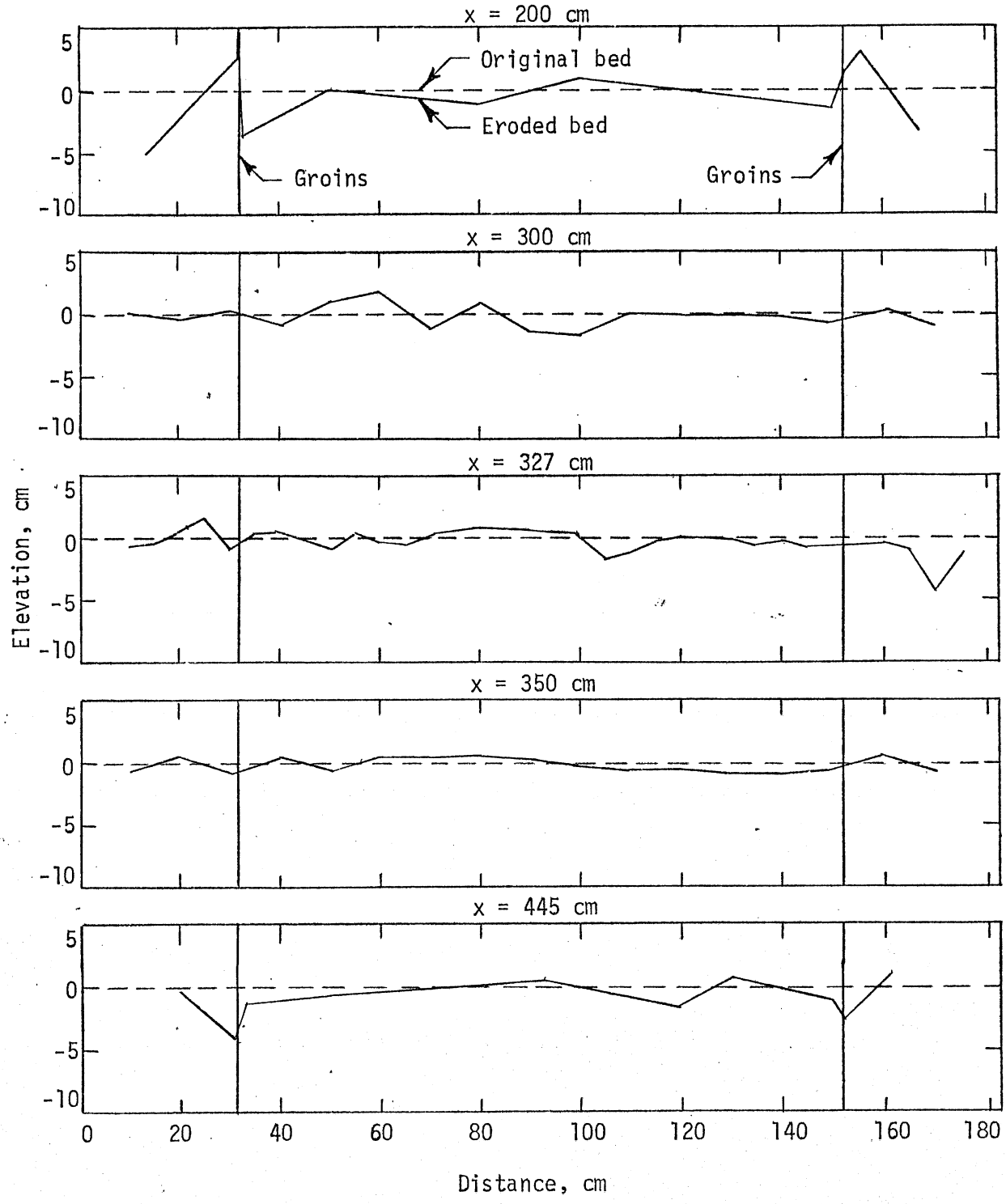

Fig. 38 - Section Bed Profiles at Various Stations
Type A7, Run No. 117, $Q_1 \sim 150$ lps, $D_1 \sim 30$ cm

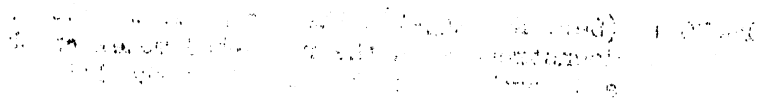

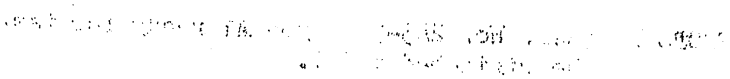

PHOTO 1 (Ser. No. 243-1) The two groin models from downstream with the rigid-bed model on the right and movable sand bed model on the left.

PHOTO 2 (Ser. No. 243-9) Type A1 ready for testing in the rigid-bed model.

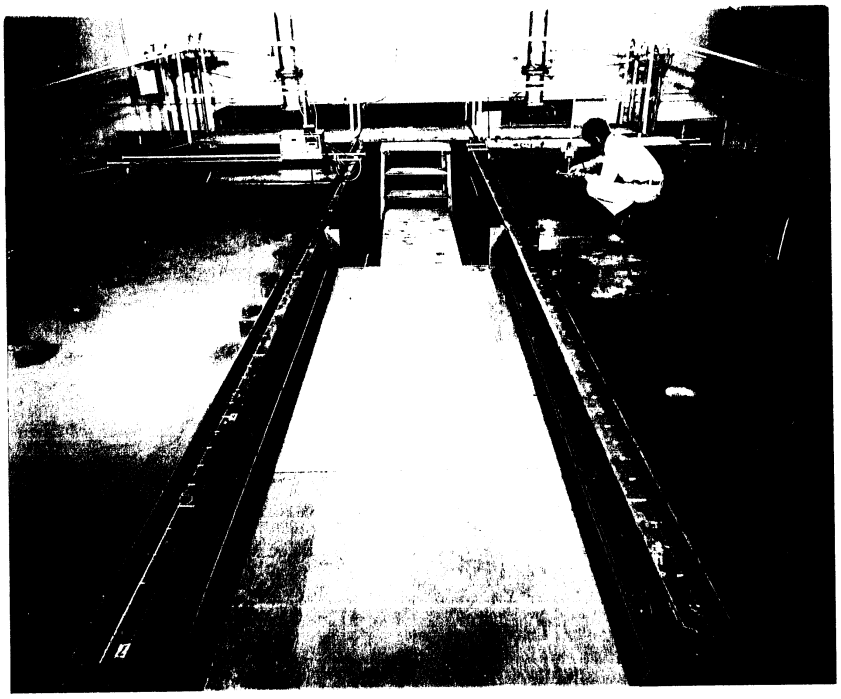


TYPE A1
RUN
DISCH. LPS
U.S.DEP. CM

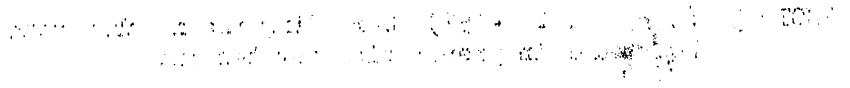

PHOTO 3 (Ser. No. 243-157) Screeding the movable sand bed model in preparation for testing.

PHOTO 4 (Ser. No.243-7) The two groin models in operation, each with a discharge of 50 lps and upstream depth of 20 cm.

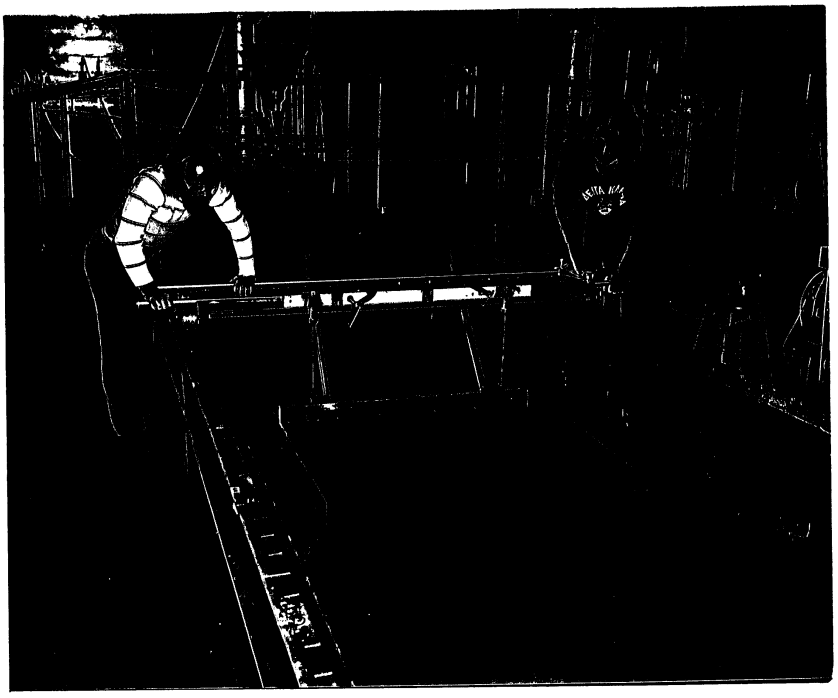

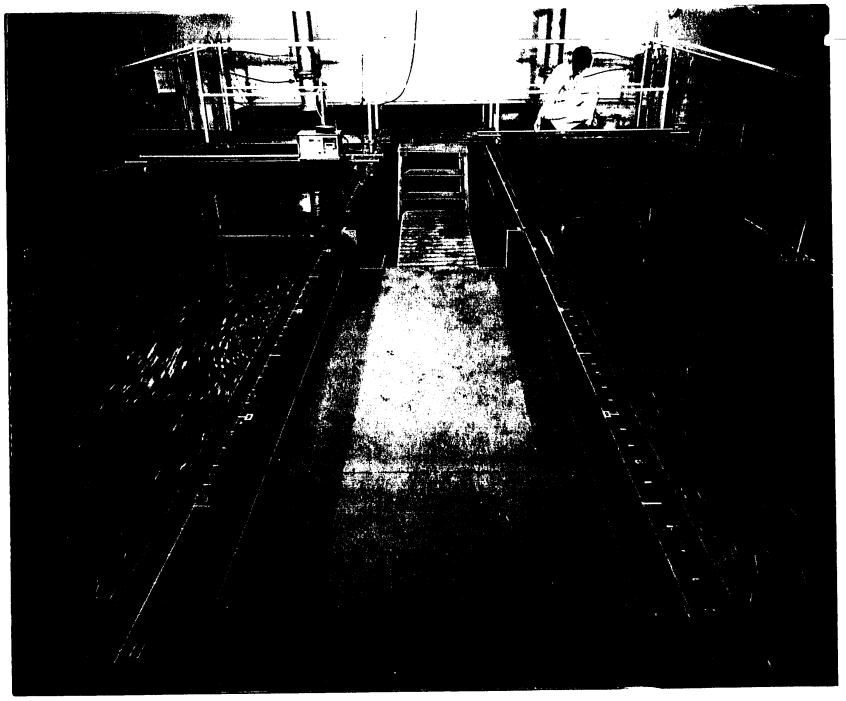

PHOTO 5 (Ser. No. 243-166) Measuring velocities with the Ott meter in the movable sand bed model, the optic probe is also shown.

PHOTO 6 (Ser. No. 243-164) Recording the water surface profile with the optic probe in the movable sand bed model.

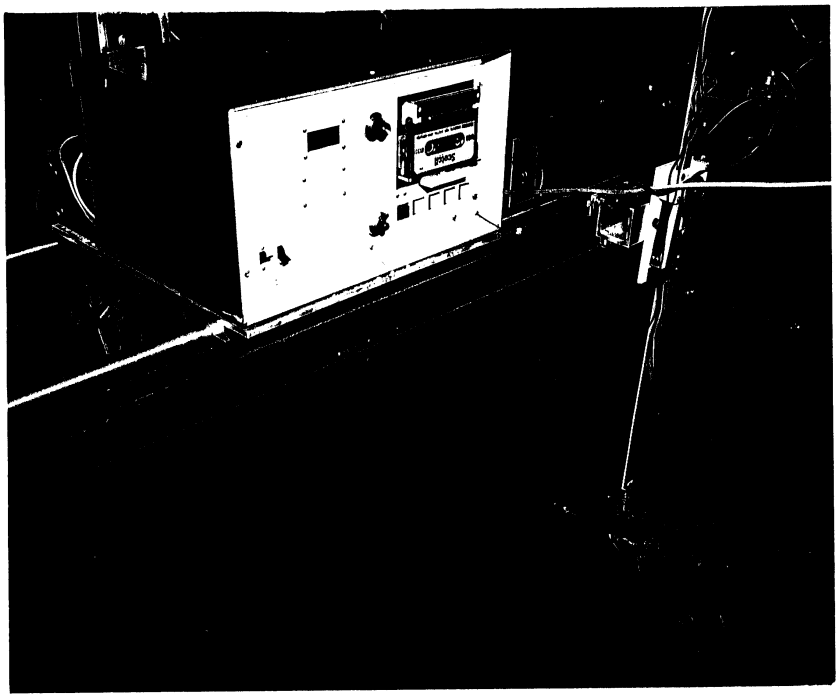

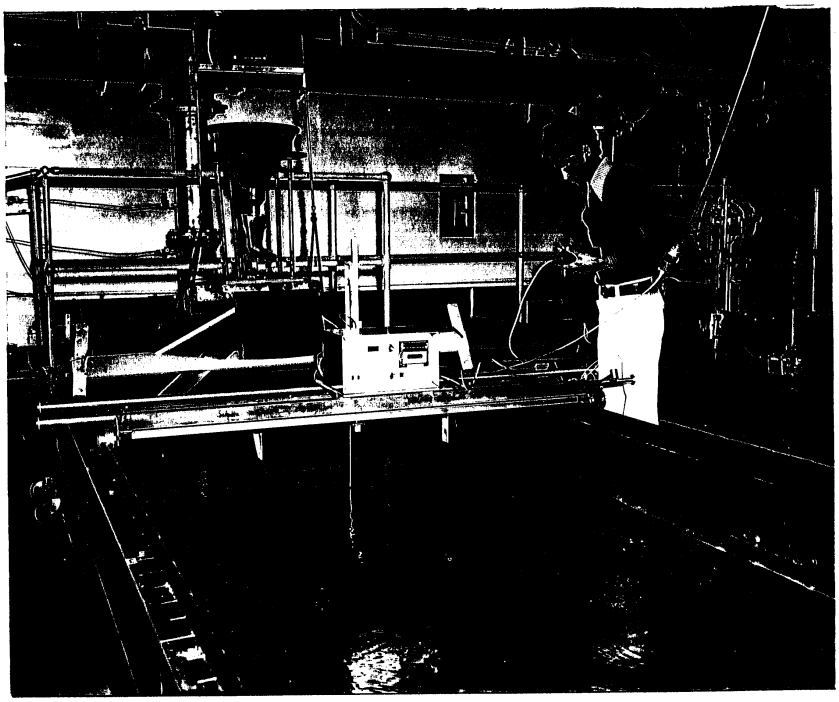

PHOTO 7 (Ser. No. 243-43) Recording the sand bed profile with the optic probe.

PHOTO 8 (Ser. No. 243-162) Collecting a sediment sample at the downstream end of the movable bed model.

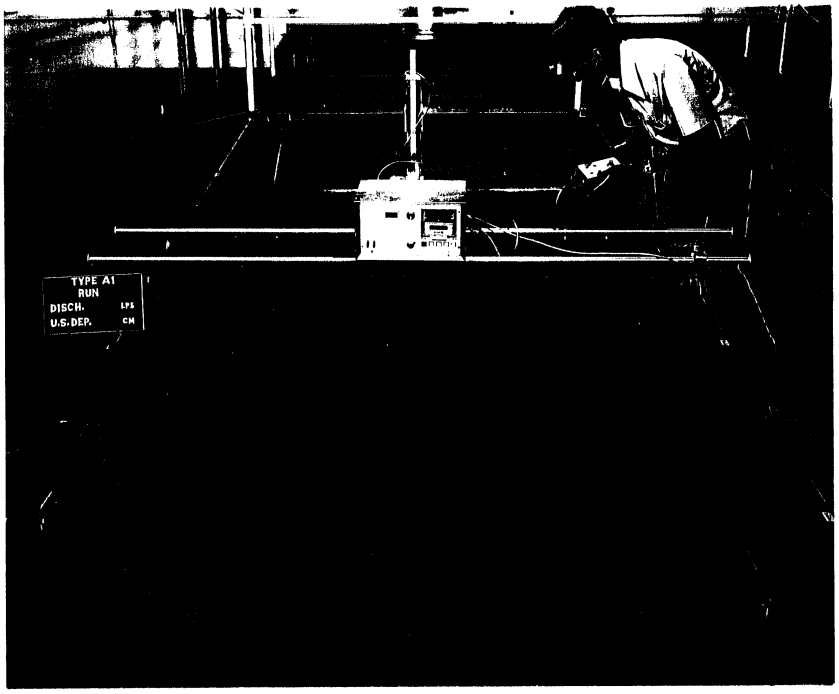
TYPE A1
RUN
DISCH. LPS
U.S.DEP. CM

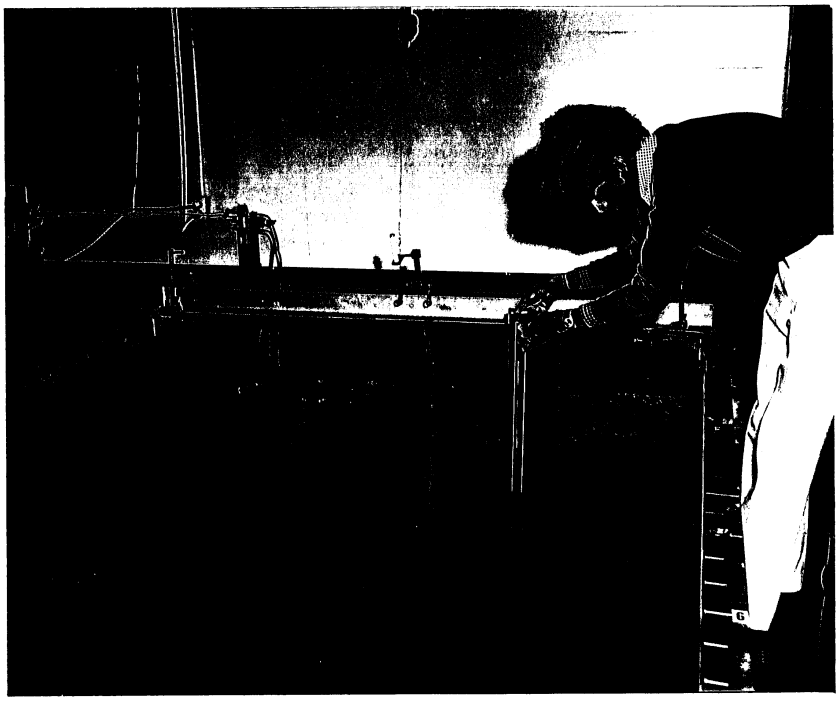

PHOTO 9 (Ser. No. 243-163) Measuring the volume of sand collected in the sampler.

PHOTO 10 (Ser. No. 243-160) Setting the sand feed device at the upstream end of the movable-bed model.

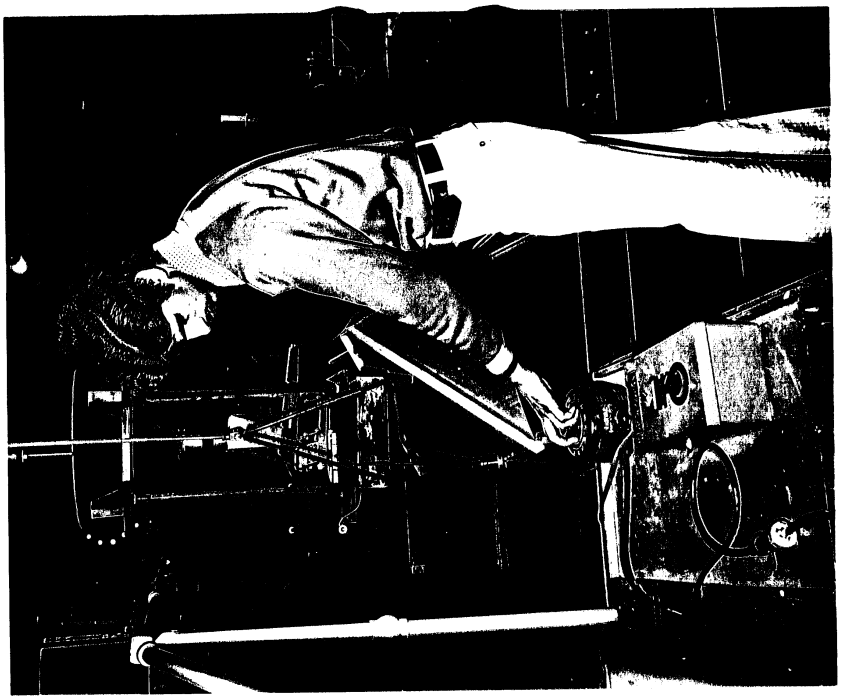

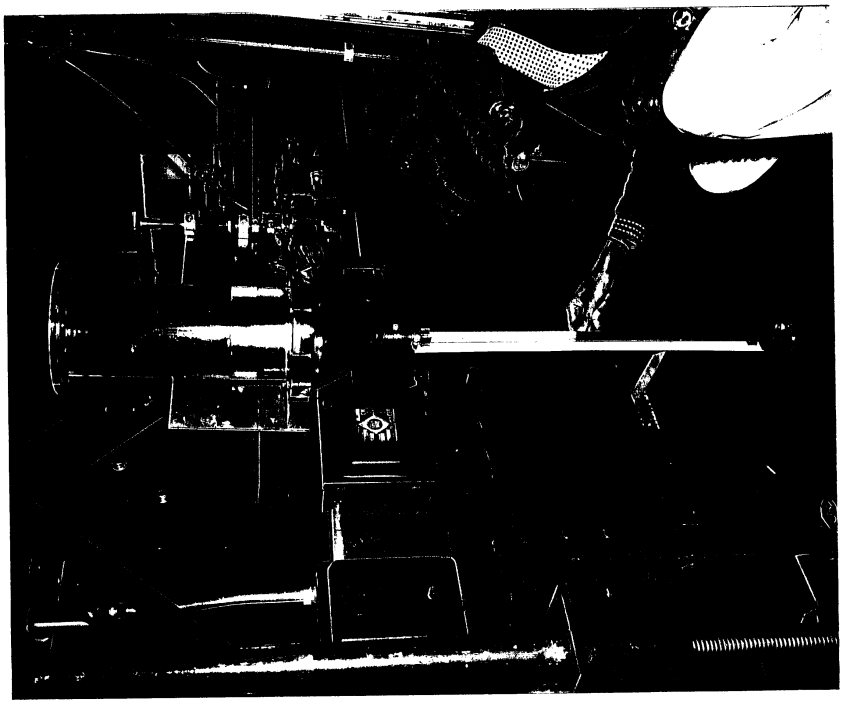

[illegible]

[illegible]

PHOTO 11 (Ser. No. 243-58) Rigid-bed, Type A4, Run No. 23, Q = 40 lps, D_1 = 15 cm, Surface flow pattern.

PHOTO 12 (Ser. No. 243-60) Rigid-bed, Type A4, Run No. 24, Q = 50 lps, D_1 = 20 cm, Surface flow pattern.


TYPE A4
RUN 23
DISCH. 40 LPS
U.S.DEP. 15 CM

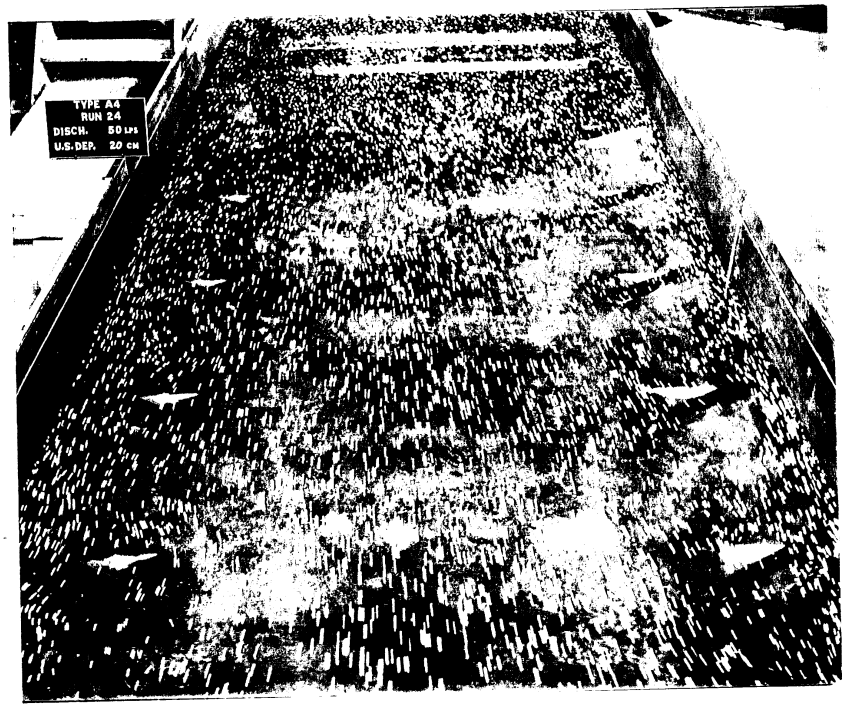
TYPE A4
RUN 24
DISCH. 50 LPS
U.S.DEP. 20 CM

PHOTO 13 (Ser. No. 243-62) Rigid-bed, Type A4, Run No. 25, Q = 100 lps, D_1 = 30 cm, Surface flow pattern.

PHOTO 14 (Ser. No. 243-64) Rigid-bed, Type A4, Run No. 26, Q = 150 lps, D_1 = 35 cm, Surface flow pattern.

PHOTO 15 (Ser. No. 243-55) Rigid-bed, Type A3, Run No. 23, Q = 40 lps, D_1 = 15 cm, Surface flow pattern.

PHOTO 16 (Ser. No. 243-67) Rigid-bed, Type A5, Run No. 28, Q = 40 lps, D_1 = 15 cm, Surface flow pattern.

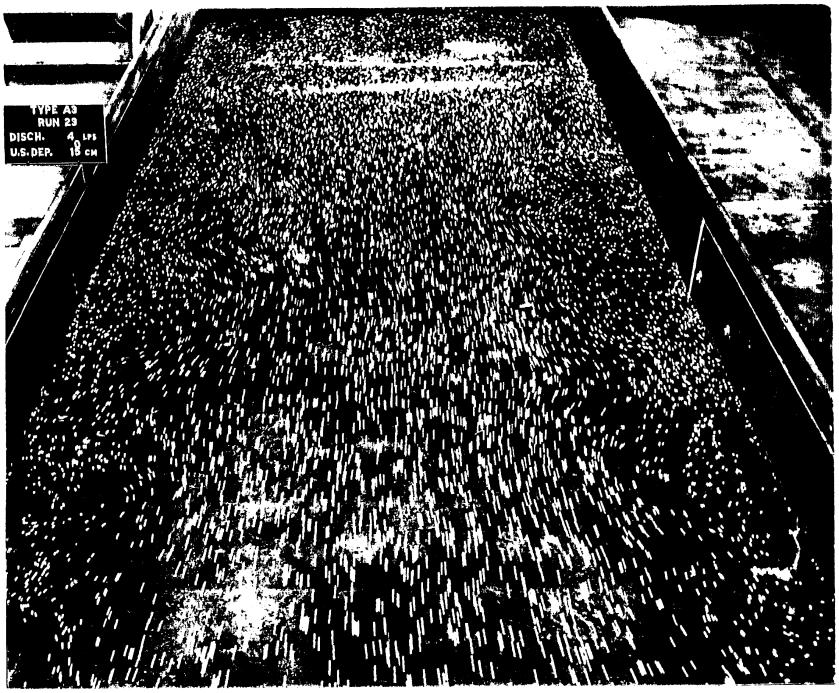
TYPE A3
RUN 23
DISCH. 4 LPS
U.S.DEP. 15 CM

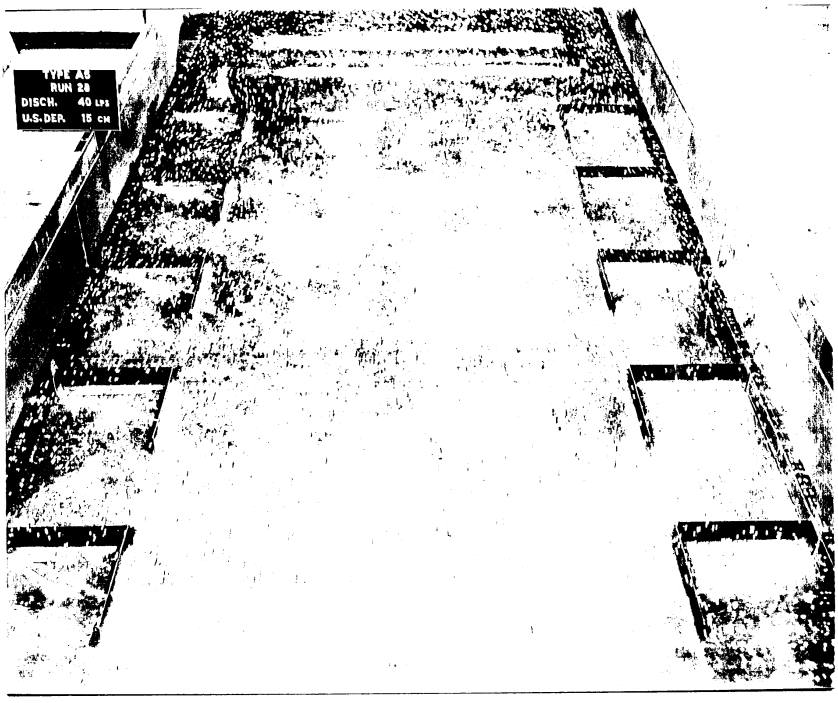
RUN 28
DISCH. 40 LPS
U.S.DEP. 15 CM

PHOTO 17 (Ser. No. 243-76) Rigid-bed, Type A6, Run No. 32, Q = 40 lps, D_1 = 15 cm, Surface flow pattern.

PHOTO 18 (Ser. No. 243-85) Rigid-bed, Type A7, Run No. 36, Q = 40 lps, D_1 = 15 cm, Surface flow pattern.


TYPE A6
RUN 32
DISCH. 40 LPS
U.S.DEP. 15 CM

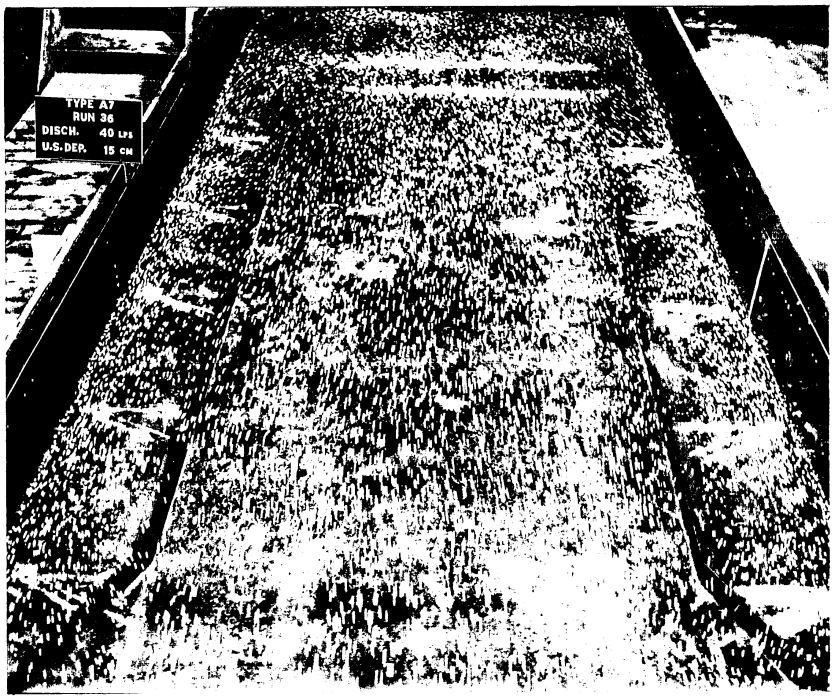
TYPE A7
RUN 36
DISCH. 40 LPS
U.S.DEP. 15 CM

PHOTO 19 (Ser. No. 243-120) Movable-bed, Type A4, Run No. 110, Q = 75 lps, D_1 = 15 cm, Surface flow pattern.

PHOTO 20 (Ser. No. 243-122) Movable bed, Type A4, Run No. 110, Q = 75 lps, D_1 = 15 cm, Final erosion pattern.


TYPE A4
RUN 110
DISCH. .75 LPS
U.S.DEP. .15 CM

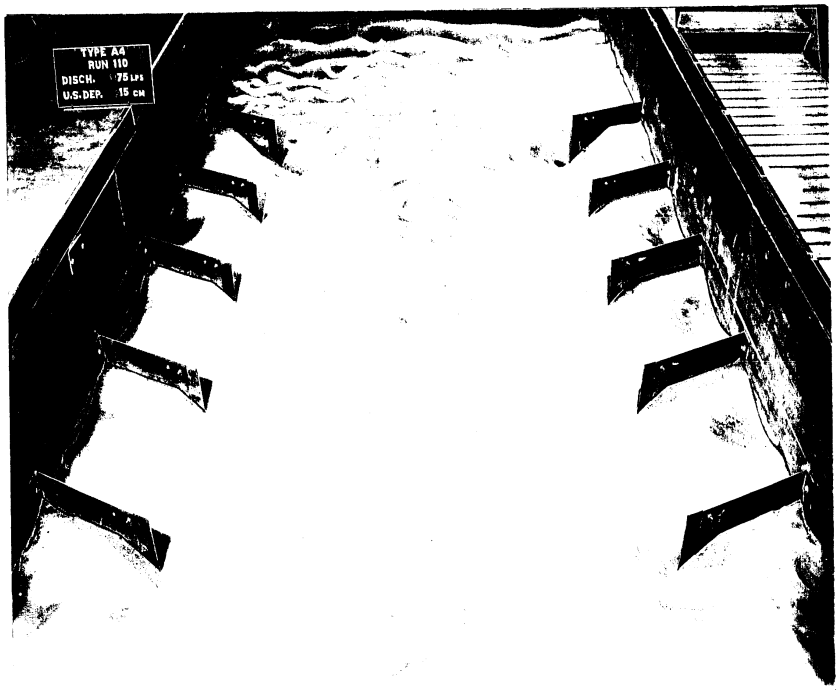
TYPE A4
RUN 110
DISCH. .75 LPS
U.S.DEP. .15 CM

PHOTO 21 (Ser. No. 243-117) Movable-bed, Type A4, Run No. 109, Q = 100 lps, D_1 = 20 cm, Surface flow pattern.

PHOTO 22 (Ser. No. 243-119) Movable-bed, Type A4, Run No. 109, Q = 100 lps, D_1 = 20 cm, Final erosion pattern.

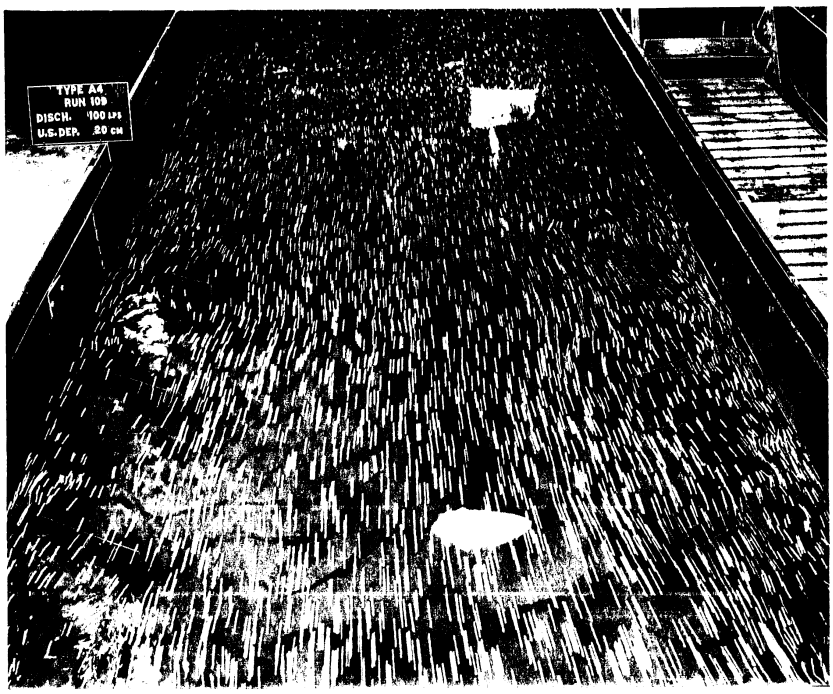
TYPE A4
RUN 109
DISCH. 1100 LPS
U.S.DEP. 20 CM

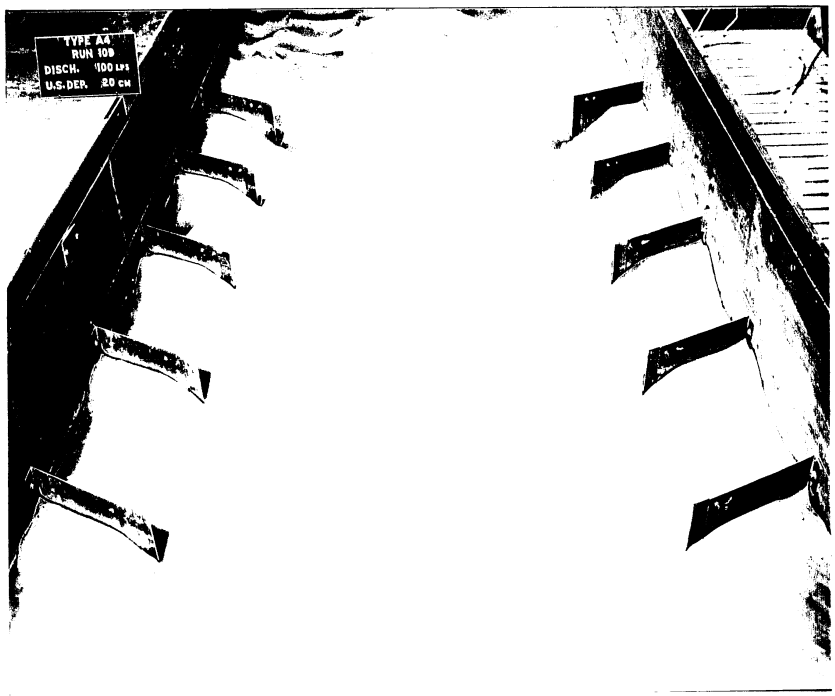
TYPE A4
RUN 109
DISCH. 1100 LPS
U.S.DEP. 20 CM

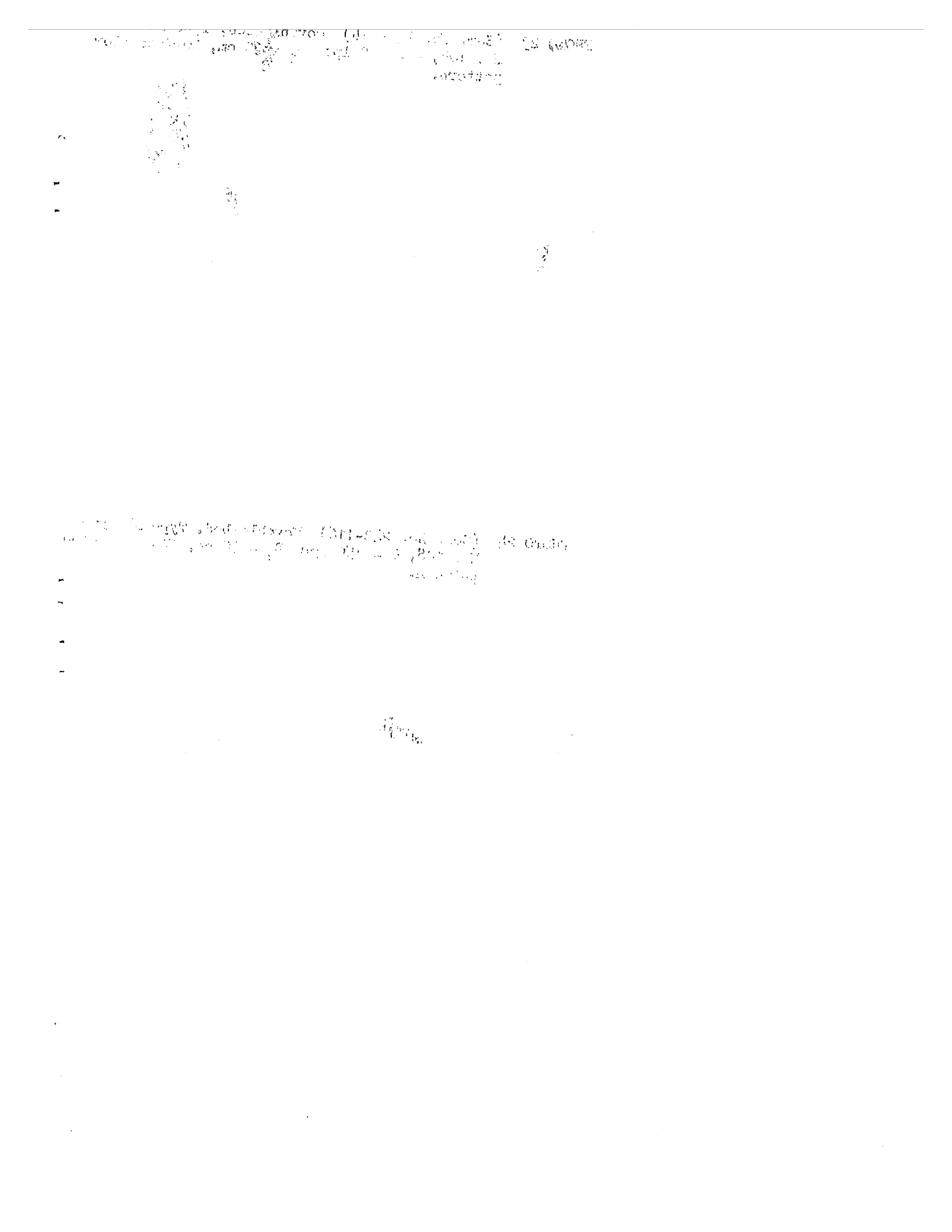

PHOTO 23 (Ser. No. 243-114) Movable-bed, Type A4, Run No. 108, Q = 150 lps, D_1 = 30 cm, Surface flow pattern.

PHOTO 24 (Ser. No. 243-116) Movable-bed, Type A4, Run No. 108, Q = 150 lps, D_1 = 30 cm, Final erosion pattern.

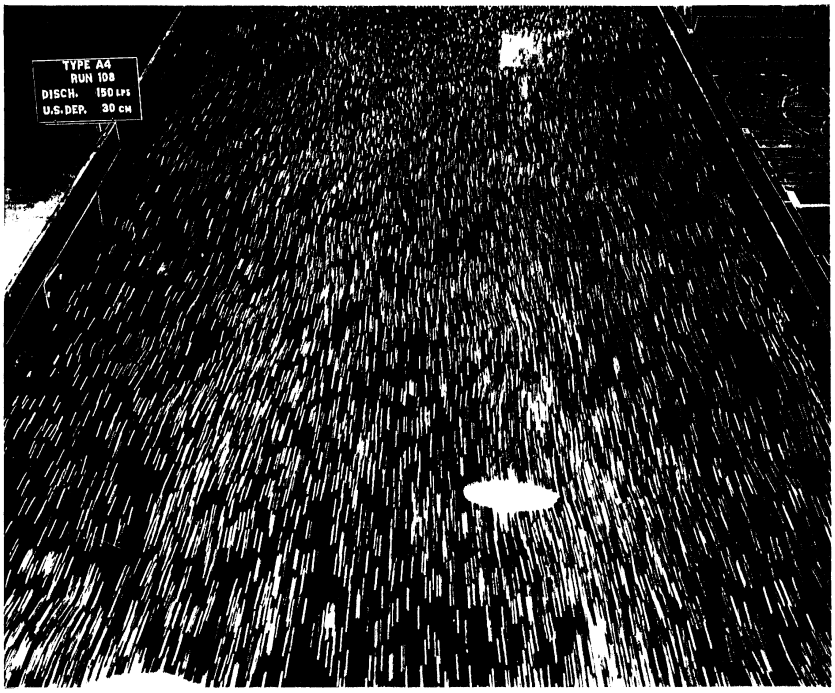
TYPE A4
RUN 108
DISCH. 150 LPS
U.S.DEP. 30 CM

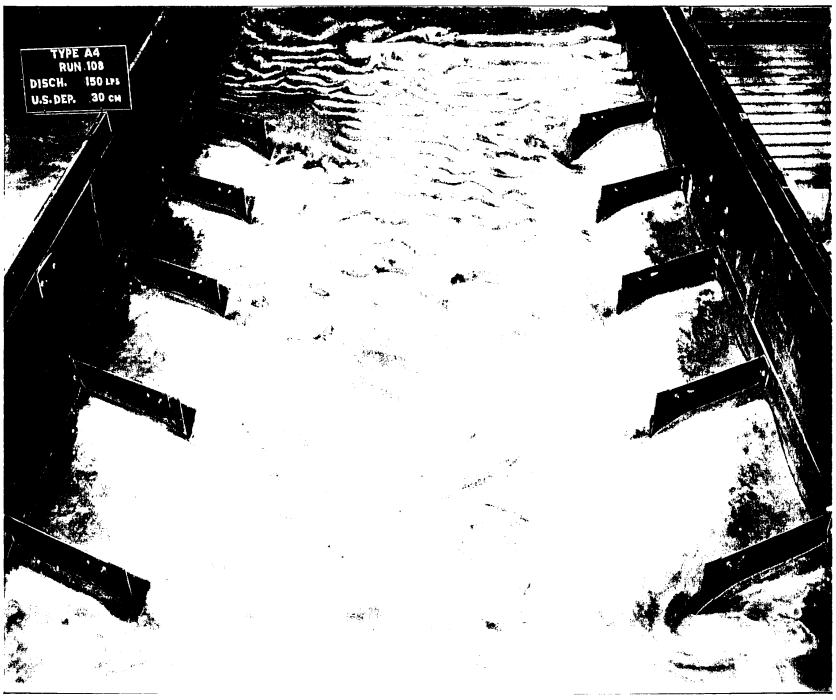
TYPE A4
RUN 108
DISCH. 150 LPS
U.S.DEP. 30 CM

PHOTO 25 (Ser. No. 243-123) Movable-bed, Type A4, Run No. 120, Q = 50 lps, D_1 = 9 cm, Surface flow pattern.

PHOTO 26 (Ser. No. 243-125) Movable-bed, Type A4, Run No. 120, Q = 50 lps, D_1 = 9 cm, Final erosion pattern.


TYPE A4
RUN 120
DISCH. 50 LPS
U.S. DEP. 9 CM

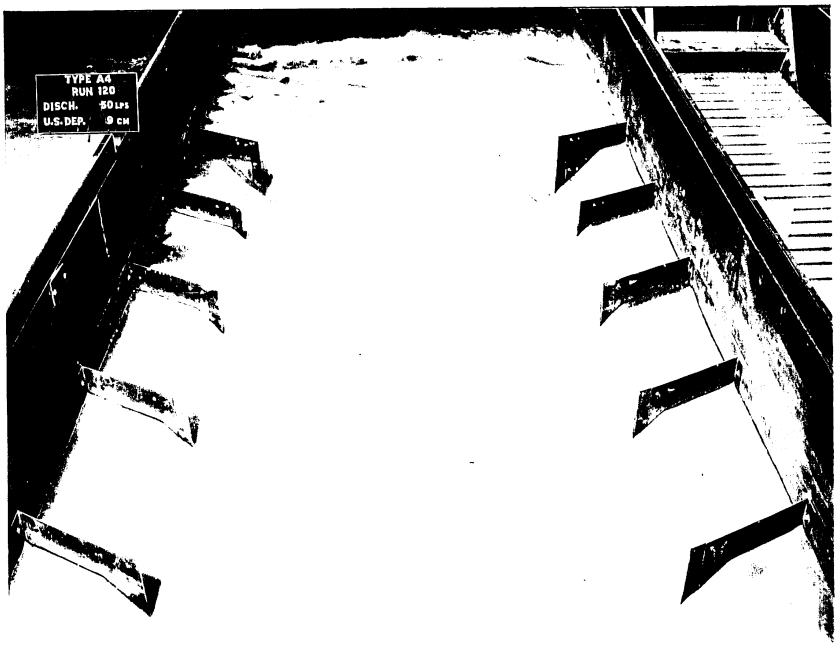
TYPE A4
RUN 120
DISCH. 50 LPS
U.S. DEP. 9 CM

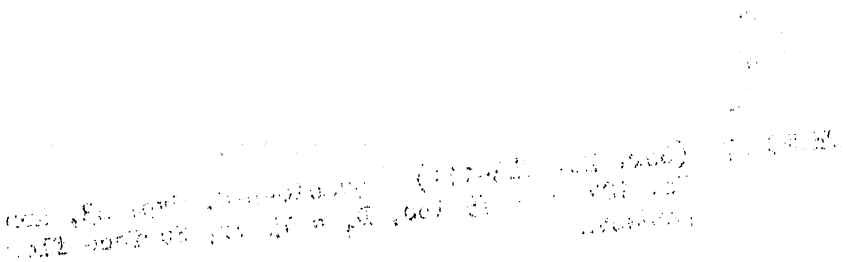

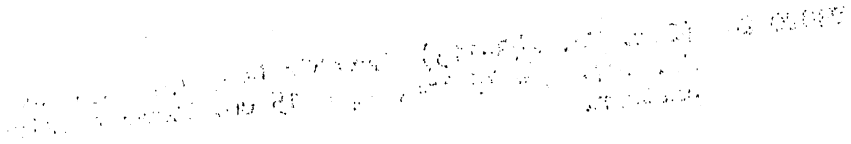

PHOTO 27 (Ser. No. 243-111) Movable-bed, Type A3, Run No. 107, Q = 75 lps, D_1 = 15 cm, Surface flow pattern.

PHOTO 28 (Ser. No. 243-113) Movable bed, Type A3, Run No. 107, Q = 75 lps, D_1 = 15 cm, Final erosion pattern.

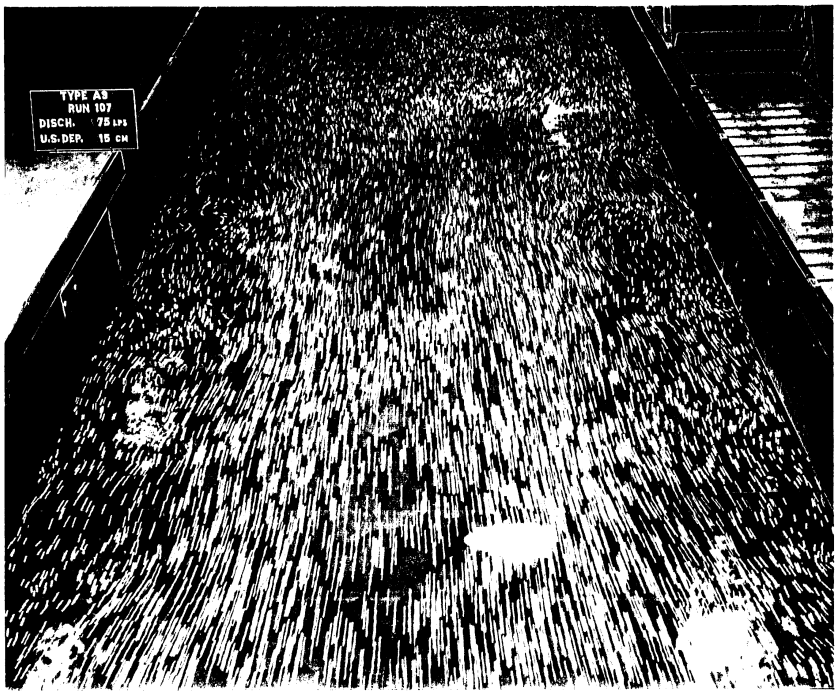
TYPE A3
RUN 107
DISCH. 75 LPS
U.S. DEP. 15 CM

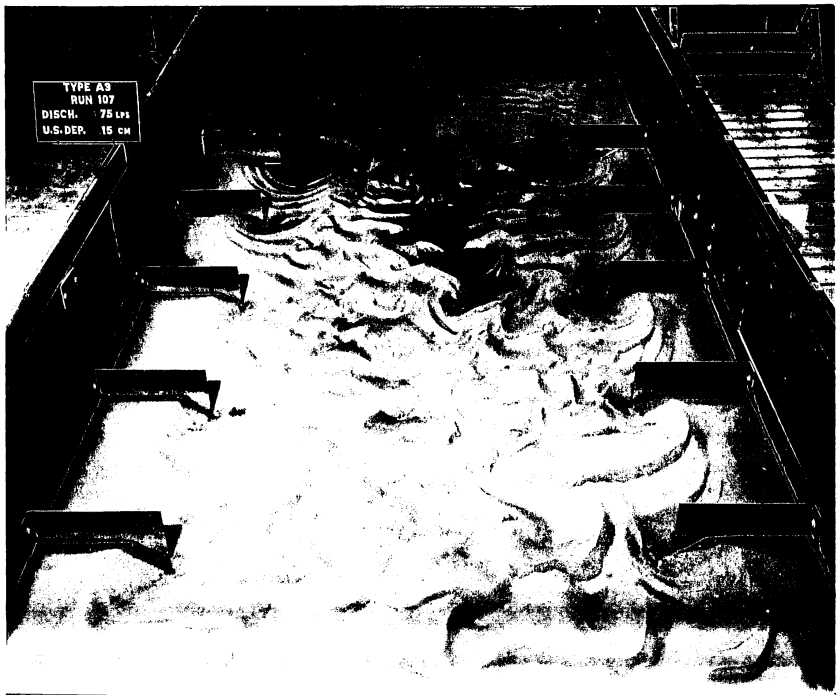
TYPE A3
RUN 107
DISCH. 75 LPS
U.S. DEP. 15 CM

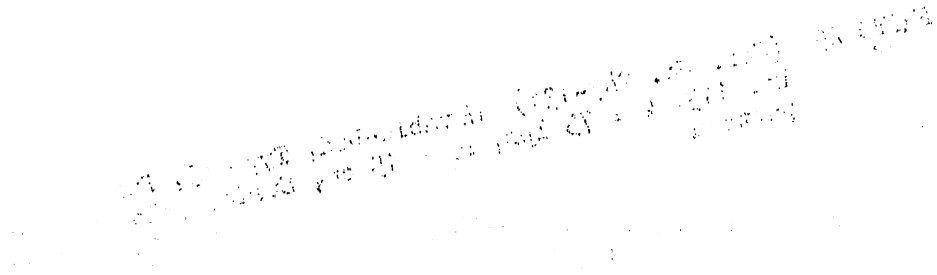

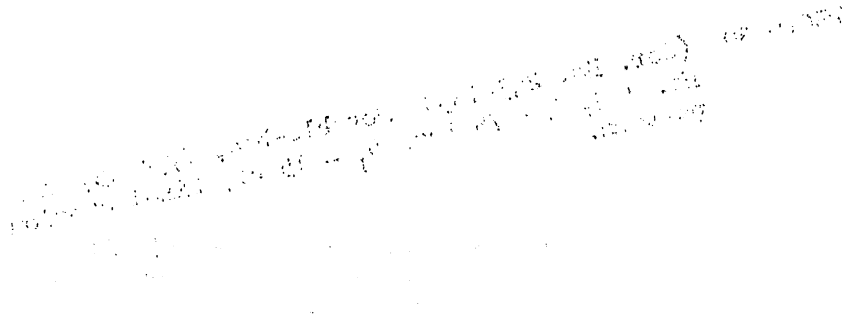

PHOTO 29 (Ser. No. 243-131) Movable-bed, Type A5, Run No. 113, Q = 75 lps, D_1 = 15 cm, Surface flow pattern.

PHOTO 30 (Ser. No. 243-133) Movable-bed, Type A5, Run No. 113, Q = 75 lps, D_1 = 15 cm, Final erosion pattern.

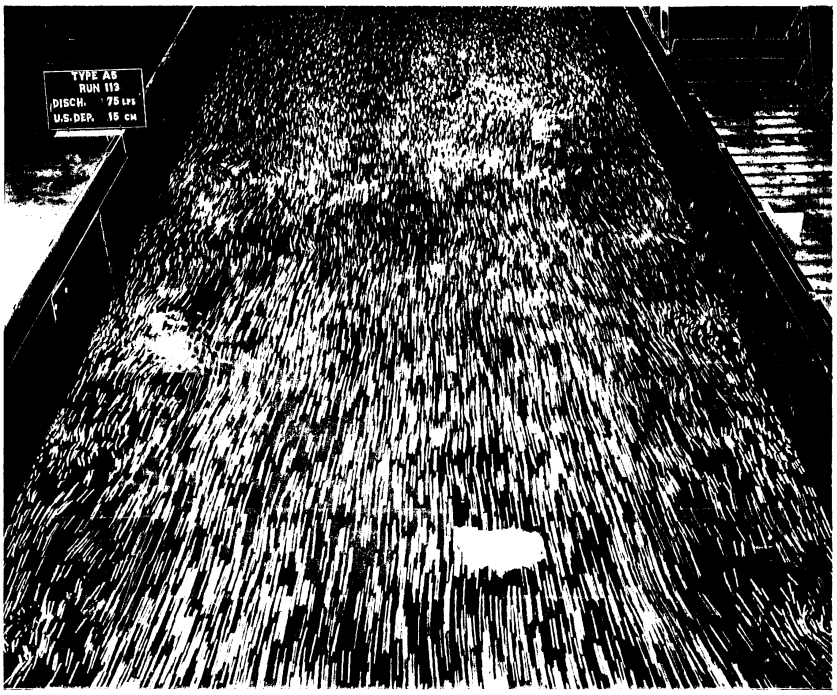
TYPE A6
RUN 113
DISCH. 75 LPS
U.S.DEP. 15 CM

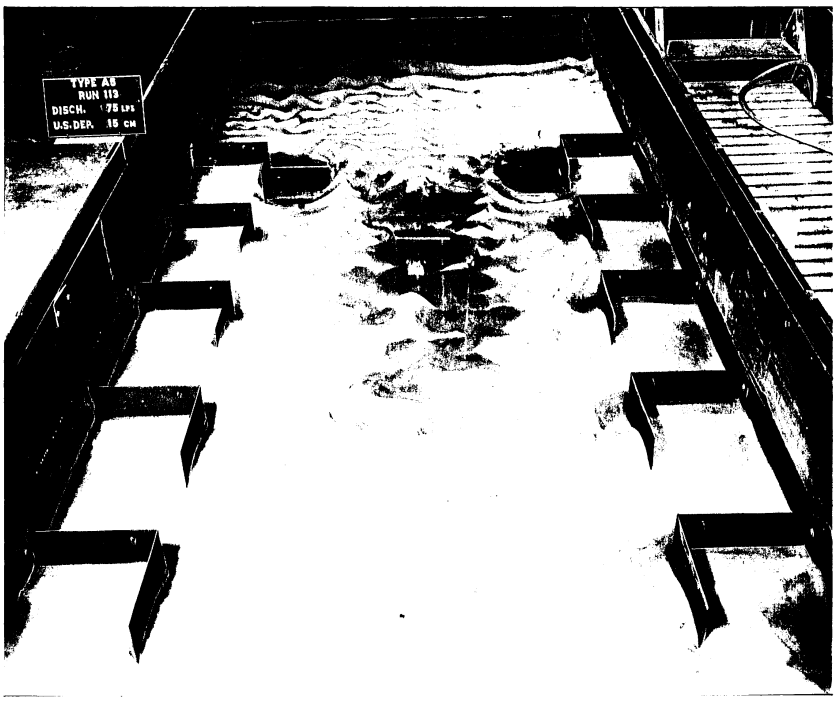
TYPE A6
RUN 113
DISCH. 75 LPS
U.S.DEP. 15 CM

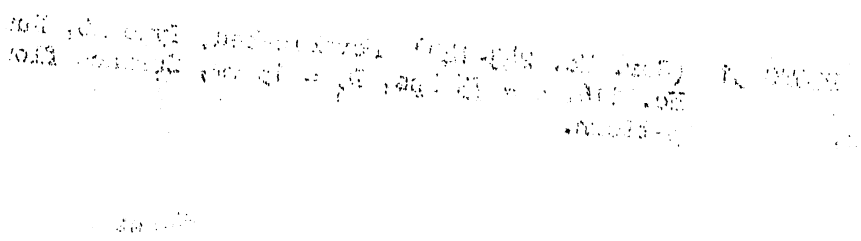

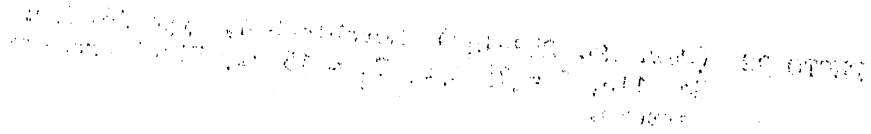

PHOTO 31 (Ser. No. 243-140) Movable-bed, Type A6, Run No. 116, Q = 75 lps, D_1 = 15 cm, Surface flow pattern.

PHOTO 32 (Ser. No. 243-142) Movable-bed, Type A6, Run No. 116, Q = 75 lps, D_1 = 15 cm, Final erosion pattern.

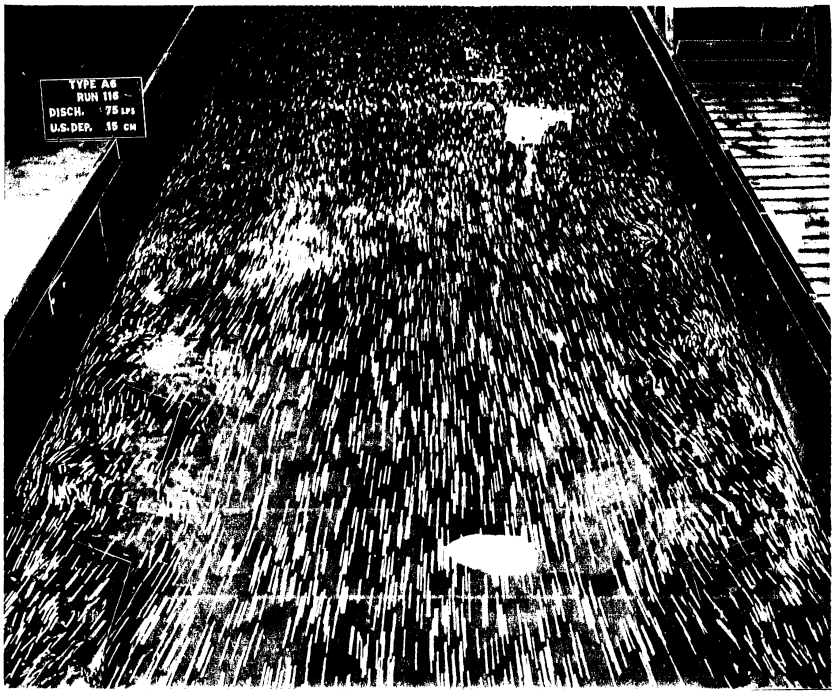
TYPE A6
RUN 116
DISCH. 75 LPS
U.S.DEP. 15 CM


TYPE A6
RUN 116
DISCH. 75 LPS
U.S.DEP. 15 CM

PHOTO 33 (Ser. No. 243-149) Movable-bed, Type A7, Run No. 119, Q = 75 lps, D_1 = 15 cm, Surface flow pattern.

PHOTO 34 (Ser. No. 243-151) Movable-bed, Type A7, Run No. 119, Q = 75 lps, D_1 = 15 cm, Final erosion pattern.

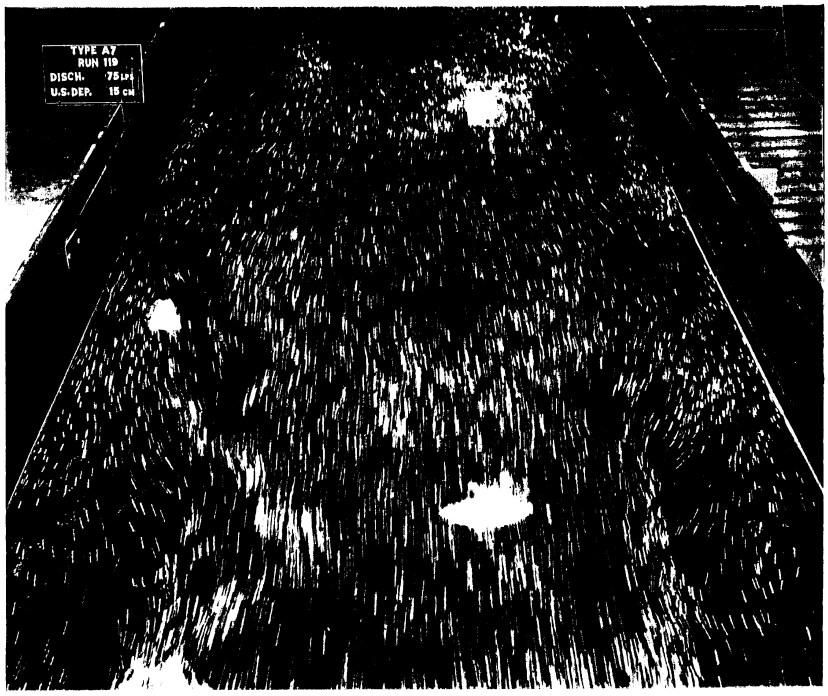
TYPE A7
RUN 119
DISCH. 75 Lps
U.S. DEP. 15 cm

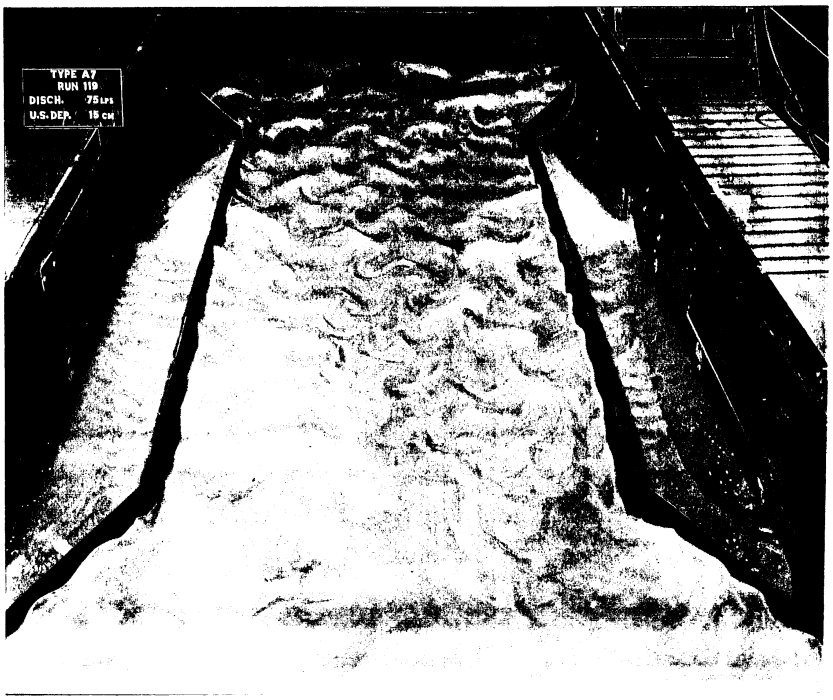
TYPE A7
RUN 119
DISCH. 75 Lps
U.S. DEP. 15 cm

PHOTO 35 (Ser. No. 243-153) Movable-bed, Type A7, Run No. 122, Q = 50 lps, D_1 = 9 cm, Surface flow pattern.

PHOTO 36 (Ser. No. 243-155) Movable-bed, Type A7, Run No. 122, Q = 50 lps, D_1 = 9 cm, Final erosion pattern.

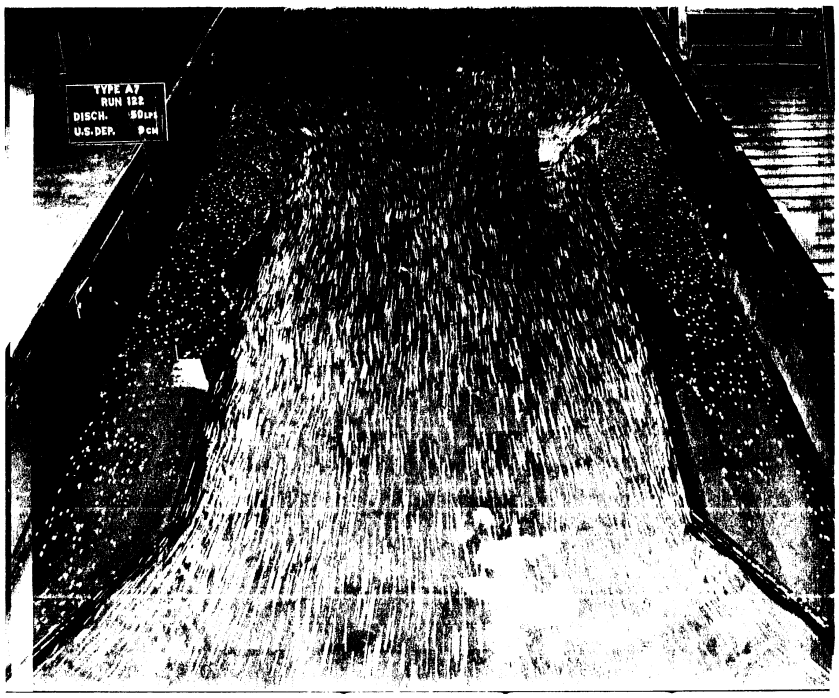
TYPE A7
RUN 122
DISCH. 50 Lps
U.S.DEP. 9 cm


TYPE A7
RUN 106
DISCH. 90 Lps
U.S.DEP. 10 cm

APPENDIX - Tabulated Data

Rigid Bed Model

Run No.	D_1 cm	D_2 cm	D_3 cm	D_3/D_2	Q_1 lbs	Q_2 lbs	Q_2/Q_1	F_1	F_2	T_o C
Groin type A1			H = 15.2 cm,		B_2 = 121.5 cm,		B_1/B_2 = 1.51			
1	25.21	24.84	9.64	0.388	94.60	87.97	0.928	0.130	0.187	20
6	35.08	34.87	19.69	0.564	98.89	85.46	0.864	0.083	0.109	17
9	25.45	24.59	9.39	0.382	152.12	141.45	0.929	0.206	0.305	13
10	35.23	34.99	19.79	0.565	149.55	131.03	0.876	0.124	0.166	13
11	25.02	24.93	9.73	0.390	47.08	43.16	0.916	0.065	0.091	14
12	34.74	34.87	10.62	0.570	45.01	39.01	0.867	0.038	0.050	15
17	19.69	19.59	4.39	0.224	51.02	48.26	0.946	0.101	0.146	11
18	29.81	29.66	14.46	0.487	93.12	79.22	0.851	0.099	0.129	9
Groin Type A2			H = 15.2 cm,		B_2 = 92 cm,		B_1/B_2 = 2.0			
13	24.72	23.96	8.76	0.365	109.59	84.62	0.773	0.155	0.250	9
14	29.63	29.29	14.09	0.481	105.55	77.41	0.733	0.114	0.170	10
15	19.78	19.42	4.22	0.217	52.96	43.37	0.819	0.104	0.176	11
16	34.60	34.20	19.00	0.555	175.72	117.36	0.668	0.150	0.204	11
Groin Type A3			H = 10 cm,		B_2 = 121.5 cm,		B_1/B_2 = 1.51			
19	19.66	19.45	9.45	0.486	75.65	64.45	0.852	0.151	0.198	4
20	24.66	24.45	14.45	0.591	101.25	83.21	0.822	0.144	0.181	8
21	29.57	29.50	19.50	0.661	105.70	83.69	0.792	0.114	0.137	8
22	34.96	34.81	24.81	0.713	145.46	109.94	0.756	0.122	0.141	4
23	14.84	14.69	4.69	0.319	40.97	37.16	0.907	0.124	0.173	2
Groin Type A4			H = 10 cm,		B_2 = 121.5 cm,		B_1/B_2 = 1.51			
24	14.84	14.69	4.69	0.319	39.85	34.92	0.876	0.121	0.163	2
25	19.78	19.75	9.75	0.494	50.20	39.60	0.789	0.099	0.119	1
26	30.57	29.47	19.47	0.661	101.12	71.91	0.711	0.104	0.118	1
27	34.87	34.75	24.75	0.712	146.16	102.36	0.700	0.123	0.131	2
Groin Type A5			H = 10 cm,		B_2 = 121.5 cm		B_1/B_2 = 1.51			
28	14.63	14.72	4.72	0.321	39.33	36.87	0.937	0.122	0.172	3
29	19.63	19.75	9.75	0.494	51.96	45.29	0.872	0.104	0.136	3
30	29.81	29.90	19.90	0.666	101.37	79.61	0.785	0.108	0.128	3
31	34.56	34.66	24.66	0.711	155.01	116.75	0.753	0.132	0.150	2
Groin Type A6			H = 10 cm		B_2 = 121.5 cm,		B_1/B_2 = 1.51			
32	13.29	12.80	2.80	0.219	39.85	36.47	0.915	0.143	0.209	1
33	20.36	20.42	10.42	0.510	47.02	38.41	0.817	0.089	0.109	1
34	29.41	29.78	19.78	0.664	101.75	74.04	0.728	0.111	0.120	0.6
35	33.86	34.32	24.32	0.709	143.61	101.10	0.704	0.127	0.132	1
Groin Type A7			H = 10 cm,		B_2 = 121.5 cm,		B_1/B_2 = 1.51			
36	14.75	14.63	4.63	0.316	37.15	32.30	0.869	0.114	0.152	0.3
37	19.54	19.45	9.45	0.486	45.63	35.59	0.780	0.092	0.109	0.6
38	30.11	30.05	20.05	0.667	97.55	69.19	0.709	0.102	0.110	1
39	34.99	35.05	25.05	0.715	146.95	101.49	0.691	0.123	0.129	1

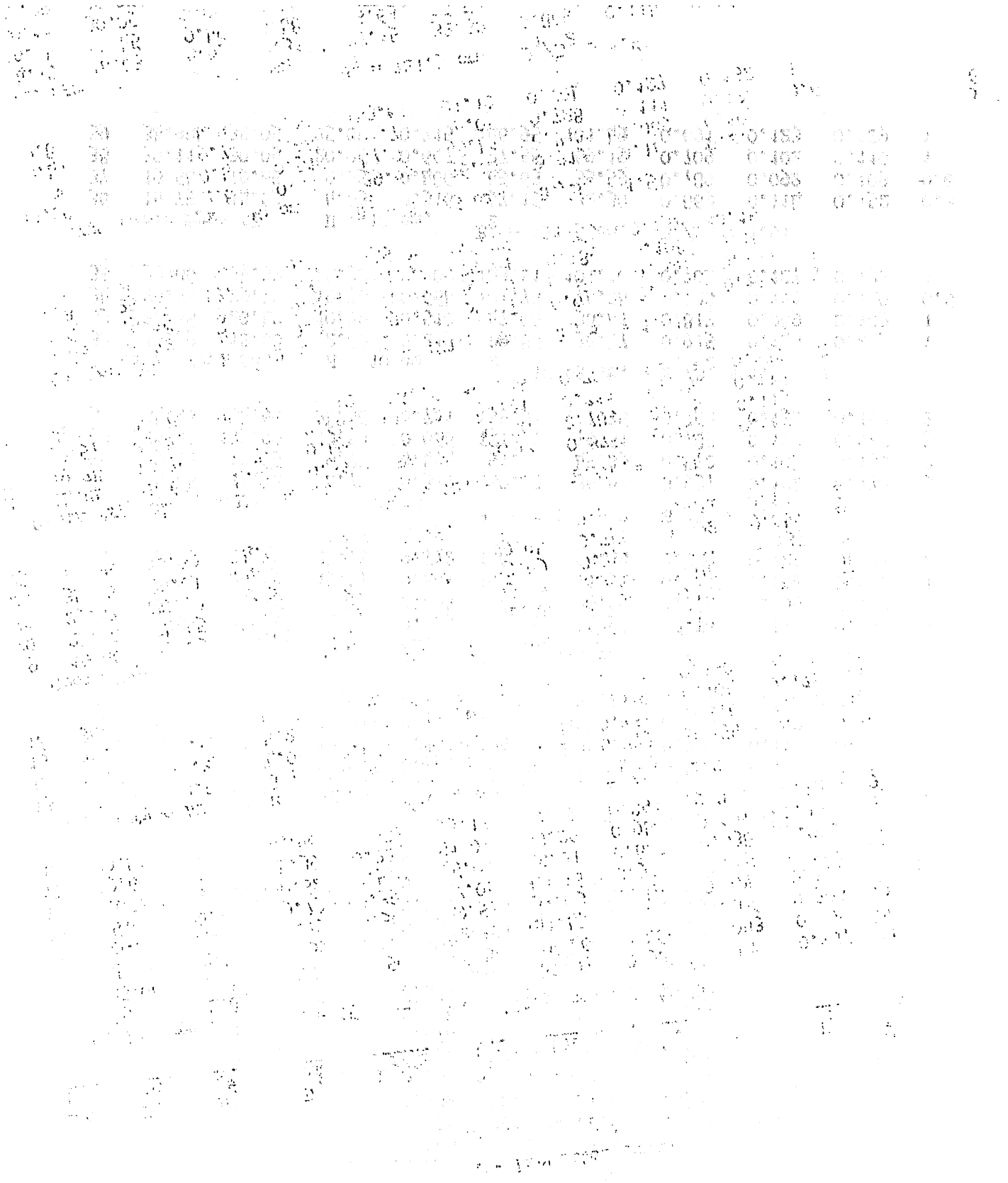

Movable Bed Model

$H = 10$ cm, $B_2 = 120.9$ cm, $B_1/B_2 = 1.51$

Run No.	D_1 cm	D_2 cm	D_3 cm	D_3/D_2	D_2/D_1	Q_1 lps	Q_2 lps	Q_2/Q_1	F_1	F_2	T °C
Groin Type A3											
105	31.36	31.77	21.25	0.669	1.013	163.82	130.94	0.799	0.173	0.161	1
106	20.36	22.40	12.30	0.549	1.100	107.77	89.60	0.831	0.182	0.204	1
107	16.43	18.81	6.45	0.343	1.145	82.87	73.29	0.884	0.234	0.295	1
Groin Type A4											
108	29.18	30.33	19.75	0.651	1.039	151.48	107.69	0.711	0.165	0.179	1
109	18.77	22.29	9.90	0.444	1.187	104.90	84.41	0.805	0.198	0.238	1
110	14.40	17.87	5.50	0.307	1.241	85.13	75.59	0.888	0.224	0.283	1
120	9.03	12.91	0	0	1.42	58.60	58.60	1.00	0.301	0.377	1
Groin Type A5											
111	29.65	30.31	20.10	0.665	1.022	153.49	113.21	0.738	0.162	0.181	3
112	20.15	21.82	9.50	0.435	1.08	100.15	80.53	0.804	0.206	0.260	2
113	14.07	18.42	5.15	0.279	1.309	76.17	63.52	0.834	0.227	0.289	0.3
Groin Type A6											
114	28.38	30.01	18.75	0.625	1.060	154.21	106.31	0.690	0.171	0.184	1
115	19.21	21.77	9.60	0.441	1.133	105.21	76.24	0.725	0.216	0.250	1
116	13.36	17.78	5.15	0.290	1.331	77.49	64.69	0.835	0.214	0.240	1
Groin Type A7											
117	27.78	29.04	19.30	0.665	1.040	150.25	102.13	0.680	0.167	0.173	1
118	17.85	19.52	9.50	0.487	1.090	101.61	77.31	0.761	0.215	0.238	2
119	13.74	15.96	5.20	0.326	1.162	80.38	65.46	0.814	0.248	0.304	2
122	9.35	12.61	0	0	1.350	56.14	56.14	1.000	0.276	0.370	3